Fall 2018

Micro-slotting technique for measurement of local residual stress in metallic materials

Elizabeth Anne Burns

Department: Materials Science and Engineering

MICRO-SLOTTING TECHNIQUE FOR MEASUREMENT OF LOCAL RESIDUAL STRESS IN METALLIC MATERIALS

by

ELIZABETH ANNE BURNS

A DISSERTATION

Presented to the Faculty of the Graduate School of the

MISSOURI UNIVERSITY OF SCIENCE AND TECHNOLOGY

In Partial Fulfillment of the Requirements for the Degree

DOCTOR OF PHILOSOPHY

in

METALLURGICAL ENGINEERING

2018

Approved

Joseph Newkirk, Advisor
Caizhi Zhou
Laura Bartlett
Haiming Wen
James Castle

PUBLICATION DISSERTATION OPTION

This dissertation has been prepared in the form of four manuscripts that have been published or will be submitted for publication as follows:

Paper I: Pages 17-45, “Micro-slotting technique for reliable measurement of sub-surface residual stress in Ti-6Al-4V” was published in *The Journal of Strain Analysis for Engineering Design* volume 53 in 2018.

Paper II: Pages 46-67, “Micro-slotting residual stress measurement technique for understanding fatigue performance of open-hole Ti-6Al-4V samples” has been submitted to *Journal of Materials Engineering and Performance*.

Paper III: Pages 68-97, “Qualitative evaluation of local microstructure effects on micro-slotting residual stress measurements in Ti-6Al-4V” has been prepared for submission to *Materials and Design* journal.

Paper IV: Pages 98-118, “Micro-scale residual stress measurements across interfaces in a LFMT Ti-6Al-4V build” has been prepared for submission to *Additive Manufacturing* journal.

ABSTRACT

Micro-slotting, a micro-scale relaxation residual stress measurement technique, has been shown in recent years to be a reliable method for measuring local residual stresses in metallic materials. This technique employs an SEM-focused ion beam system for milling and imaging, digital image correlation software to track displacements due to residual stress relaxation, and finite element analysis for interpolation of the original local stress state. In this research, a micro-slotting procedure was established using finite element models and was used to obtain sub-surface residual stress measurements on machined and shot peened planar Ti-6Al-4V samples. These measurements were compared to macro-scale XRD residual stress measurements, and discrepancies between the results of the two techniques were discussed. The measurement procedure was then applied to as-drilled and cold-expanded holes for near-edge measurement of residual hoop stresses. Comparison of the measured residual stress distributions with plastic strain data obtained using EBSD allowed for interpretation of fatigue life differences and crack growth behavior. Next, a grid of measurements was performed in a sub-surface region of the shot peened sample, and EBSD was used to acquire microstructure information in the measurement regions. Comparison of the measured displacements and interpolated residual stress values with the local microstructure allowed for novel qualitative observations regarding residual stress orientation and microstructure effects on the measured residual stress relaxation. Last, the use of the micro-slotting technique was demonstrated for measurement of local residual stress in additive manufactured components. Series of measurements were performed across two interfaces in a complex Ti-6Al-4V build, and post-measurement optical microscopy allowed for analysis of the residual stress data at the microstructural level.

ACKNOWLEDGMENTS

The funding support for this work was provided by the Air Force Research Lab-managed Metals Affordability Initiative (MAI) consortium and Boeing Research & Technology.

First and foremost, I would like to thank my PhD advisor, Dr. Joseph Newkirk, and my co-advisor, Dr. James Castle, for their guidance, instruction, and encouragement throughout this process. They are both extraordinarily accomplished engineers and researchers in their fields and have served as the best possible mentors throughout my time as a graduate student and future industry research engineer. It has been an honor to complete my PhD under their counsel, and I very much look forward to working with them in the future.

I would like to thank Dr. Caizhi Zhou, Dr. Haiming Wen, and Dr. Laura Bartlett for serving as members of my PhD committee. I extend my appreciation to the technical research staff of the Materials Research Center, especially Dr. Clarissa Wisner and Dr. Eric Bohannan, for providing me with valuable training and expertise with regards to materials characterization. I would also like to acknowledge the staff members of Missouri S&T's Materials Science & Engineering Department, Teneke Hill and Denise Eddings, for their assistance with managing day-to-day tasks and navigating graduate school procedures.

Finally, I express the utmost gratitude to my family and friends – especially Mom, Dad, Emmy, Jake, and Clayton – for being my support system throughout this whole process, and to the Eta Kappa chapter of Chi Omega Fraternity, which has provided me with a network of amazing women and friends who have helped me to recognize my professional strengths and abilities.

TABLE OF CONTENTS

Page

LIST OF ILLUSTRATIONS

Page

PAPER III

PAPER IV

LIST OF TABLES

Page

PAPER I

1. INTRODUCTION

Reliable residual stress measurement in metallic materials is critical for accurate fatigue life predictions and simulations of material behavior [1]. However, conventional measurement techniques are limited with regards to spatial resolution and accuracy in complex geometry components [2]. Micro-slotting [3], a micro-scale relaxation residual stress measurement technique, has been demonstrated in recent years to be an effective method for providing local residual stress data in a variety of materials. This measurement technique employs a scanning electron microscope-focused ion beam (SEM-FIB) system for milling and imaging, digital image correlation (DIC) software to track displacements due to residual stress relaxation after milling, and finite element (FE) analysis for displacement-stress correlation and calculation of the original local stress state. This research aims to improve the current understanding of the micro-slotting technique and the application of this technique to metallic materials. The objectives of this research all contribute to establishing the micro-slotting technique as a robust and practical approach for measuring local residual stress and providing supplemental data to established macro-scale techniques.

The first objective of this research is to establish and validate a micro-slotting procedure for Ti-6Al-4V that can be used to capture local residual stress in complex-shaped components. Previous works have successfully demonstrated the use of micro-scale relaxation residual stress measurement techniques on thin films [3], bulk metallic glasses [4], and near-isotropic metallic alloys [5]. However, the application of these micro-scale methods to more anisotropic materials presents a source of error when using isotropic assumptions at the micron scale [6]. Previous micro-scale measurements in Ti-6Al-4V [7]

have yet to be compared to results obtained using established macro-scale measurement methods. Thus, this work employs the established micro-slotting procedure for measurement of sub-surface residual stress distributions on machined and shot peened planar Ti-6Al-4V samples and compares the results to measurements obtained using a conventional X-ray diffraction (XRD) depth profiling technique.

The second objective of this research is to apply the established micro-slotting procedure to unique metallic material applications where current techniques are not capable of measuring residual stress. One such application of great importance to the aerospace industry is for obtaining near-edge residual stress data around holes. Reliable measurement of these near-edge residual stresses plays a significant role in successful fatigue life prediction of metallic airframe structures [8]. The process of cold expansion [9] is a widely used method for extending the fatigue life of fastener holes and involves introducing a compressive tangential residual stress region around the hole [10]. The use of this process in the design stage, however, is limited by the ability to accurately measure this resultant residual stress distribution at the hole edge. Therefore, the goal of this work is to use the micro-slotting technique for accurate characterization of near-edge residual stress distributions on both as-drilled and cold-expanded holes in order to interpret differences in fatigue life and crack growth behavior.

The third objective of this research is to evaluate the effects of local microstructure on the micro-slotting measurements. Recent works have demonstrated that micro-scale relaxation residual stress measurement techniques are capable of capturing residual stresses at both the macro- and micro-scales [11-13]. Due to the micron-sized gauge volume of these techniques, measurements of the macroscopic residual stress state are understood to

be significantly affected by the presence of microscopic stresses, and these stresses present themselves as scatter in the measurement results [14]. Yet, studies that aim to identify and quantify the specific sources of these stresses are limited. This work therefore aims to explore the use of the micro-slotting technique for understanding residual stress distribution at the microstructural level.

The fourth and final objective of this research is to demonstrate the use of the micro-slotting technique on additive manufactured (AM) components. Residual stress build-up during AM processes can negatively impact mechanical properties or result in distortion of the finished parts [15]. Prediction of this distortion can be accomplished using computational models, but the accuracy of these models relies on validation using experimental data. Due to the limitations of conventional measurement techniques, previous attempts to quantify residual stresses in AM parts have been confined to simple build geometries and measurement of the macroscopic residual stress state [2, 16, 17]. This work therefore attempts to demonstrate the micro-slotting technique on AM components by capturing local residual stress data across interfaces and analyzing the results at the microstructural level.

2. LITERATURE REVIEW

2.1. RESIDUAL STRESS IN METALLIC COMPONENTS

2.1.1. Residual Stress. Residual stresses are stresses that exist in a material or component when no external load is applied [18]. They are induced by nearly all manufacturing processes and result from the elastic response of the material to inhomogeneous plastic strains, often referred to as eigenstrains [19]. Residual stresses are self-equilibrating, meaning that the tensile and compressive residual stresses present in a component must sum to zero, and they can be categorized by the length scale over which they equilibrate [20]. This concept is schematically illustrated in Figure 2.1. Macroscopic residual stresses, also referred to as Type I stresses, are long-range and equilibrate over the scale of the structure or component [2]. The term "microscopic stresses" is often used to collectively refer to Type II and III residual stresses. Type II stresses vary over grain scale and nearly always exist in polycrystalline materials as a result of phase distribution and differences in neighboring grain orientations. Type III residual stresses occur as a result of inhomogeneity at the nanoscale, such as point defects or dislocations. At any specific location within the material or component, the total residual stress is equal to the sum of these three types of residual stress [21].

2.1.2 Effects of Residual Stress. In life assessment of metallic components, the macroscopic stress state is typically the sole focus of residual stress measurement and analysis [20]. Residual stresses act as an addition to loading stresses and can therefore be either harmful or beneficial, depending upon the sign and where they are located within the part. In terms of fatigue behavior, the effect of residual stress on a cyclically loaded

structure is equivalent to the effect of a static mechanical load [22]. In other words, compressive residual stresses are favorable, while tensile residual stresses are detrimental.

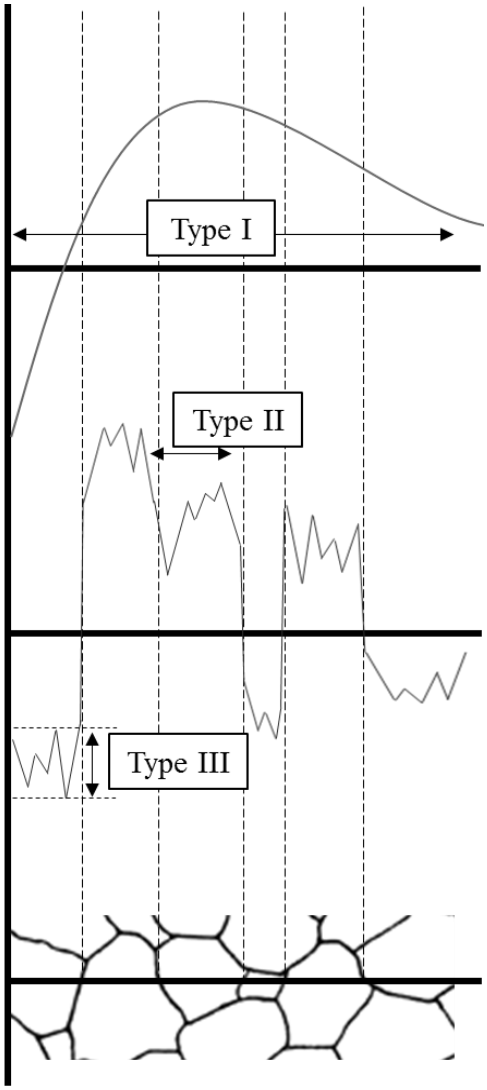

Figure 2.1. Schematic diagram illustrates residual stress classification according to length scales over which they self-equilibrate. Type I occur over scale of component, Type II vary over grain scale, and Type III equilibrate within grains. [20]

Fatigue cracks most often initiate on free surfaces [1]. In order to delay the onset of crack initiation, compressive residual stresses can be engineered in near-surface regions using processes such as shot peening [23] or hole cold-expansion [9]. Shot peening involves bombarding the part surface with small spherical media, or shot, thereby inducing a work hardened layer on the surface of the part. The shot induces local plastic deformation within this layer, and the elastic response of the material in the surrounding region creates a residual stress distribution that consists of a compressive residual stress region below the surface and a balancing tensile residual stress region further into the part [24]. With regards to crack growth, this compressive residual stress region results in a significantly increased ratio of initiation time to propagation time, in comparison to samples that did not undergo shot peening [25].

The process of cold expansion [9] involves generating a large region of compressive residual stress around the hole. The split mandrel process [26] is a widely used technique for performing cold expansion and utilizes a longitudinally slotted, tapered mandrel. The mandrel is inserted into the drilled hole and expanded, thus increasing the hole diameter and creating a region of plastic strain. The surrounding elastic material accommodates this strain, thereby producing a region of high-magnitude residual compressive stress that acts as a crack growth barrier and increases the fatigue life of the component [27, 28].

Both shot peening and cold hole expansion are commonly used to introduce beneficial residual stresses for increased safety margins. However, the associated benefits in fatigue life are rarely used in lifing assessments [18]. Incorporating these processes into design practices requires a thorough understanding of the induced residual stress

distributions, accurate prediction of the residual stress evolution while the parts are in service, and comprehension of residual stress influence on fatigue and failure. Present-day models and simulations are capable of accounting for residual stresses when predicting material properties and behavior, but the reliability of these models is limited by that of the input data. Therefore, reliable measurement of residual stress is critical.

2.2 RESIDUAL STRESS MEASUREMENT

2.2.1. Conventional Measurement Methods. Residual stresses cannot be measured directly. Instead, they are interpreted from measurements of strain or a material property that is subsequently compared to a reference state. The established, standardized techniques for measuring residual stress are generally classified as either destructive methods or non-destructive methods. Destructive methods, also referred to as stress relaxation methods, involve material removal and measuring the subsequent material deformation caused by the residual stress redistribution [29, 30]. Cutting of the material is required for each of these methods, thereby destroying the measured specimen. Non-destructive methods involve measuring a material property and comparing that property to a stress-free standard [2]. No material removal is typically required for these methods, and the components can therefore remain intact and be returned to service after the measurements are performed.

Commonly used destructive techniques include the slitting method, the hole drilling method, and the contour method. The slitting method, also known as the crack compliance method [31, 32], measures only one stress component and involves incrementally milling a long slit using a thin saw or wire electrical discharge machining (EDM). Strain gages

attached to the surfaces of the part measure the incrementally relieved strains, which allow for calculation of the residual stress component normal to the slit as a function of the slit depth. Hole drilling [33-36] employs a similar concept and involves incrementally drilling a shallow hole while surrounding strain gauges measure the resultant stress relaxation. This technique therefore provides measurement of the two in-plane stress components as a function of depth below the sample surface. The contour method [37] provides capability of residual stress measurement as a two-dimensional cross-sectional map. The method involves sectioning the part using wire EDM, and the measured topography of the cross-sectioned surface is used to back-calculate the original residual stress state within the part. This technique, combined with superposition-based theory, allows for measurement of multiple stress components [38].

The non-destructive methods most commonly used for metallic materials are the diffraction techniques, which include laboratory X-ray diffraction (XRD), synchrotron X-ray diffraction, and neutron diffraction. These techniques effectively measure the distance between atomic planes, and this distance can then be related to the magnitude and direction of the residual stress present within the material. Laboratory XRD is the most widely used non-destructive technique and employs X-ray wavelengths that are typically capable of penetrating a few microns into the material. As a result, XRD becomes a semi-destructive technique when used to measure residual stress as a function of depth below the sample surface, since material removal is required to expose the sub-surface layers [39]. Synchrotron X-ray diffraction employs X-rays of higher energy than laboratory XRD. These X-rays are capable of penetrating deeper into the sample, on the order of millimeters, to measure bulk residual stresses [35]. Neutron diffraction [40, 41] employs high-energy

neutrons that can diffract through a depth of several tens of millimeters, thereby measuring bulk residual stresses at greater depths into the sample.

2.2.2. Measurement Method Selection. The different residual stress measurement methods vary with regard to measurement volume, spatial resolution, and sample geometry limitations. Proper method selection requires a balance of these factors combined with an understanding of the residual stress component to be measured and the length scale over which the residual stress will equilibrate.

Destructive residual stress measurement techniques tend to measure the macroscopic residual stress state. These techniques remove macroscopic-sized regions of material in which microscopic residual stresses average to zero and are therefore not detected [30]. Measurement techniques that are capable of measuring microscopic stresses are limited since they require micron-scale gauge volumes and high spatial resolution. Because the spacing of lattice planes is extremely small, diffraction methods are affected by both macroscopic and microscopic residual stresses. However, only macroscopic residual stresses can generally be measured due to the large irradiated area of the beam, which is typically on the order of millimeters, relative to the micron-scale grain size of the material. The use of micro-focus synchrotron X-rays attempts to overcome this limitation [42, 43], along with high resolution-electron backscatter diffraction [44]. Yet both of these techniques can be considered highly complex and require specialized equipment. The recently established micro-scale stress relaxation measurement methods [45] offer an alternative solution.

2.3. MICRO-SCALE RELAXATION RESIDUAL STRESS MEASUREMENT TECHNIQUES

In recent years, micro-scale residual stress measurement techniques have been used to capture local residual stresses in materials where more conventional measurement methods are incapable of measuring residual stress. These techniques are based on established stress relaxation measurement methods that have been scaled down to micron-size using the combined imaging and milling capabilities of a scanning electron microscope-focused ion beam (SEM-FIB) dual-beam system. They are classified as semi-destructive techniques, as they can be used to quantify local residual stress without introducing significant disturbance to the overall stress state of the sample [19]. Selection of appropriate micro-scale milling geometry is primarily dependent on the desired stress components. Micro-hole drilling [46] and the micro-scale ring-core method [47, 48] allow for calculation of the full in-plane stress tensor, while micro-slotting allows for determination of the single stress component perpendicular to the milled slot.

2.3.1. Micro-Slotting Technique. Micro-slotting was first proposed by Kang et al. for measuring residual stresses in thin films [3]. It is a micro-scale version of the crack compliance method [31] and involves using the FIB to mill a single, narrow, rectangular slot, creating two traction-free surfaces. The material surrounding the slot relaxes and displaces as a result of the local residual stress relief, as illustrated in Figure 2.2. Electron beam images of the local region are taken before and after the slot is milled, and digital image correlation (DIC) is used to measure the displacement of the material on either side of the slot. The residual stress in the local region can then be interpolated using analytic or finite element solutions and assuming pure elastic relaxation.

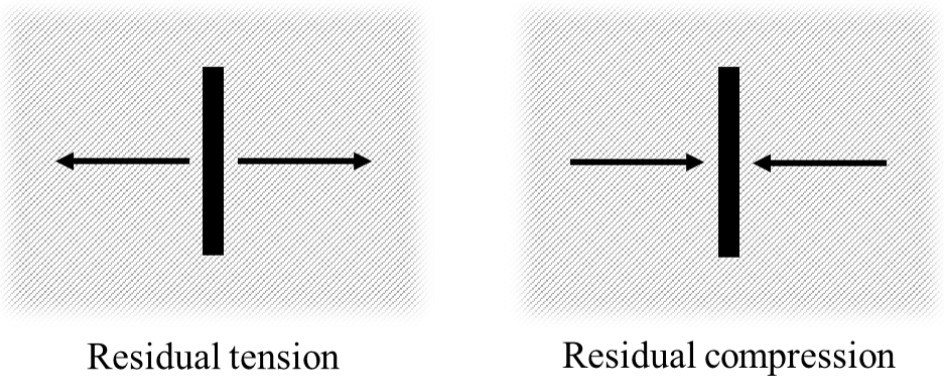

Figure 2.2. Schematic diagrams of residual stress relaxation that occurs after micro-slot milling. Material around the slot displaces either away (residual tension) or toward the slot (residual compression), depending on the sign of the residual stress present in the local region.

Many previous studies have employed slot geometries that simulate an infinite surface crack. Such slots are long and narrow with shallow depths, and the resulting displacements can be related to the original stress state in the local region using two-dimensional elasticity analysis [3, 49-51]. Shorter slots result in more complex displacement fields and require finite element analysis (FEA) for interpolation of the original stress state in the measurement regions [7].

Over the years, improvements in the micro-slotting approach have allowed for more complex residual stress evaluation, including residual stress variations with slot depth [52] and along the length of the slot [50, 53]. The assumption of a homogeneous stress state further simplifies the micro-slotting approach by allowing the residual stress to be averaged over the local measurement area. Under this assumption, a shorter slot is more ideal for obtaining local residual stress data, since the residual stress is consequently averaged over a smaller area.

Due to the micron-sized sampling volume and localized stress relief, the micro-slotting method has been successfully used to obtain spatially resolved residual stress profiles below shot peened surfaces [5, 50] and around drilled holes [7]. Sequential milling [43] is a common approach for acquiring such data and involves milling micro-scale geometries at regular intervals in order to capture the residual stress gradient. The spacing between subsequent measurements is strongly dependent upon the slot length [45]. Thus, shorter slots can be used to improve spatial resolution.

2.3.2. Effects of Local Anisotropy. A major limitation of micro-scale residual stress measurement techniques is that they are significantly affected by local microstructure and anisotropy in polycrystalline, multi-phase alloys. Spatially resolved micro-slotting measurements have been shown to agree well with micro-XRD measurements obtained in similar measurement locations on a near-isotropic aluminum alloy [5]. However, the application of the micro-scale methods to more anisotropic materials presents a source of error when using isotropic assumptions.

A study by E. Salvati et al. [6] involved performing a statistical analysis of the uncertainty in micro-scale residual stress measurements due to unknown grain orientation in the measurement regions. This analysis was performed for materials displaying cubic symmetry, and experimental validation of the analysis was performed on a nickel-base superalloy sample. By experimentally performing micro-scale measurements and using electron backscatter diffraction (EBSD) to acquire local grain orientation data at the measurement locations, the authors were able to obtain results consistent with the statistical evaluation.

2.3.3. Effect of Microscopic Residual Stresses. Other recent works employing micro-scale measurement methods have investigated the ability of these techniques to capture both the macroscopic and microscopic residual stress states. A study by J. Everaerts et al. involved using the micro ring-core technique in combination with eigenstrain modeling to separate the macroscopic and microscopic stresses in a bimodal Ti-6Al-4V bar following plastic four-point bending [11]. However, when the separate contributions of the macroscopic and microscopic residual stresses are unknown, a significant amount of scatter can be observed in the micro-scale measurement results [6, 54]. A separate study by J. Everaerts et al. [12] saw good agreement between micro ring-core measurements and high-energy synchrotron X-ray data on a laser shock-peened Ti-6Al-4V sample, yet decreasing the gauge volume of the micro ring-core measurements resulted in strong deviations from the X-ray results due to the increased contribution of microscopic residual stresses.

While these recent works aimed to quantify microscopic residual stresses, studies that serve to identify the specific sources of these stresses are limited. One such study performed by I. Basu et al. [13] employed a micro-slotting methodology to measure spatially resolved residual stress profiles in the vicinity of grain boundaries in commercially pure titanium, and the observed stress profiles indicated mechanisms of local stress relaxation near grain boundaries.

2.4 POTENTIAL APPLICATIONS FOR THE MICRO-SLOTTING TECHNIQUE

2.4.1. Fastener Holes. A unique application for micro-scale residual stress measurement techniques is the measurement of residual stress around holes. Reliable

measurement of near-edge residual stresses around fastener holes plays a significant role in successful fatigue life prediction of metallic airframe structures. Fastener holes act as sites of stress concentration and are prone to fatigue cracking in aging aircraft [8]. Furthermore, the complexity of the drilling process results in numerous parameters that can affect fatigue performance [55].

The process of cold expansion [9] is a widely used method for extending the fatigue life of fastener holes. The improvement in fatigue life is a result of the compressive tangential residual stress region around the hole that is introduced by the cold expansion process [10, 56]. The use of this process in the design stage, however, is limited by the ability to accurately measure this resultant residual stress distribution. Therefore, the fatigue improvements that result from cold expansion are not generally applied to the design life of structural parts due to difficulties in reliably predicting such improvements.

Established residual stress measurement techniques are limited with regards to measuring residual stress around holes. Laboratory XRD and neutron diffraction are non-destructive methods that can measure residual stress in two dimensions [57], yet both techniques are unable to resolve steep stress gradients close to the hole edge since resolution is limited by the averaging effect of the beam [58-61]. The contour method [37] is the most commonly used destructive technique for measuring residual stress around holes and can provide two-dimensional maps of the tangential residual stress distributions [62]. However, contour method results are understood to be uncertain near the edges of the cut, and this region of uncertainty can extend up to 0.500 mm from the part or hole edge [2].

Supplemental residual stress data obtained via micro-scale measurement techniques shows promise for obtaining increased accuracy in fatigue life prediction. A previous study by Ioannis et al. [7] used the micro-slotting technique and EBSD to evaluate the elastic and plastic strain gradients, respectively, around drilled holes in Ti-6Al-4V plates. This analysis allowed for interpretation of fatigue life differences as a result of different drilling parameters. The peak compressive residual stresses measured by the micro-slotting technique were consistently observed to be within 10 μm of the plastic deformation depth for the analyzed drilling conditions.

2.4.2. Additive Manufactured Components. Another novel application for micro-scale residual stress measurement techniques is measurement of residual stresses in metallic additive manufactured (AM) components. Additive manufacturing is based on incremental layer-by-layer manufacturing and allows for deposition of complex near-net-shape metal components [63]. Movement of the laser causes repeated localized melting and rapid cooling, which leads to thermal expansion and contraction of the material during the build process. The resultant permanent inelastic strains [64] can give rise to significant residual stresses in the finished builds.

Residual stress in AM parts can have a negative impact on mechanical properties and may result in distortion upon part removal from the baseplate or during subsequent machining processes. Moreover, residual stress accumulation during deposition of large parts can result in significant distortion prior to completion of the build [65, 66]. Accurate estimation of residual stress accumulation during additive manufacturing processes is accomplished using computational models [67-69], which allow for design-based

approaches to residual stress mitigation. However, the accuracy of these models relies on validation using experimental data.

Numerous attempts have been made in recent years to quantify residual stresses in AM parts, and a variety of measurement techniques have been used, including x-ray diffraction [57], neutron diffraction [41], and the contour method [37]. These techniques, however, are limited with regards to spatial resolution and measurement accuracy in complex geometry components [2]. As a result, many previous studies have focused on characterizing the distribution of residual stress in simple build geometries [16, 17, 70] and using simple build geometries to investigate effects of process parameters on the residual stress state. Such process parameters include dwell time [71], exposure strategy [72], and laser power and travel speed [73, 74].

While the data provided by macroscopic residual stress measurement techniques is ideal for validating distortion predictions, the micron-scale gauge volume of the micro-slotting technique can allow for targeted residual stress measurements in AM parts [75]. Such local analysis of residual stress may provide improved understanding of residual stress origins in AM parts on a layer-by-layer basis [76] or as a function of process parameters.

PAPER

I. MICRO-SLOTTING TECHNIQUE FOR RELIABLE MEASUREMENT OF SUB-SURFACE RESIDUAL STRESS IN Ti-6Al-4V

Elizabeth Burns[1,2], Joseph Newkirk[1] and James Castle[2]

[1]Department of Materials Science and Engineering

Missouri University of Science and Technology

Rolla, MO, USA

[2]Boeing Research and Technology

St. Louis, MO, USA

Published in *The Journal of Strain Analysis for Engineering Design,*

Vol. 53, Issue 6, 2018

ABSTRACT

Micro-slotting, a relaxation residual stress measurement technique, has recently been shown to be an effective method for measuring local residual stresses in a variety of materials. The micro-slotting method relies on a scanning electron microscope-focused ion beam system for milling and imaging, digital image correlation software to track displacements due to residual stress relaxation after milling, and finite element analysis for displacement-stress correlation and calculation of the original stress state in the imaged region. The high spatial resolution of the micro-slotting method makes it a promising technique for obtaining near-surface residual stress data in Ti-6Al-4V components for input into fatigue life models and crack growth simulations. However, use of the micro-slotting method on this alloy has yet to be evaluated against more established measurement techniques. In this study, spatially resolved sub-surface residual stress measurements were obtained on shot peened and low-stress surface-machined Ti-6Al-4V planar coupons using the micro-slotting method and were compared to measurements obtained using the conventional X-ray diffraction depth profiling technique. The sub-surface measurements were in good agreement for the shot peened ample. Observed differences in the measured near-surface residual stresses on the surface-machined sample were attributed to the larger measurement volume of the X-ray diffraction method, suggesting that the micron-sized measurement volume of the micro-slotting method may be more suitable for capturing shallow stress profiles and steep stress gradients. Prior to performing the micro-slotting measurements, finite element modeled displacements were used to verify the measurement procedure and to address uncertainties in the milled slot geometries. The results of this

study demonstrated the validity of the micro-slotting procedure and established the technique as a reliable method for measuring sub-surface residual stresses in Ti-6Al-4V.

1. INTRODUCTION

Residual stresses are stresses that remain in a material or component when no external load is applied [1]. Induced by nearly all manufacturing processes, residual stresses can have a significant effect on the performance of metal components [2] and must be taken into account during design, material processing, and fatigue life assessment. Present-day models and simulations are capable of accounting for residual stresses when predicting material properties and behavior, but the reliability of these models is limited by that of the input data. Therefore, reliable measurement of residual stress is critical.

The established techniques for measuring residual stresses are generally classified as either destructive methods or non-destructive methods. Destructive methods involve material removal and measurement of the subsequent stress relaxation, while non-destructive methods involve measuring a material property and comparing that property to a stress-free standard [3]. X-ray diffraction (XRD) is the most widely used non-destructive technique and involves measuring the change in lattice spacing relative to the unstressed lattice spacing of the material [4]. XRD becomes a semi-destructive technique when used to measure a residual stress distribution as a function of depth below the sample surface, since material removal is required to expose the sub-surface layers [5]. The different residual stress measurement methods vary with regard to measurement volume, spatial resolution, and sample geometry limitations. Proper method selection requires a balance of these factors [3].

In recent years, micro-scale residual stress measurement methods have been used to capture local residual stresses in materials where established measurement methods are incapable of measuring residual stress. These techniques are based on established stress relaxation measurement techniques that have been scaled down to micron-size using the combined imaging and milling capabilities of a scanning electron microscope-focused ion beam (SEM-FIB) dual-beam system. Selection of appropriate micro-scale milling geometry is dependent on the desired stress components. Micro-hole drilling [6] and the micro-scale ring-core method [7, 8] allow for calculation of the full in-plane stress tensor, while micro-slotting solely allows for determination of the stress component perpendicular to the milled slot.

The micro-slotting approach was chosen for this study, since only one stress component is of interest. Micro-slotting was first proposed by Kang et al. for measuring residual stresses in thin films [9]. It is a micro-scale version of the crack compliance method [10] and involves using the FIB to mill a single, narrow, rectangular slot, creating two traction-free surfaces. The material surrounding the slot relaxes and displaces as a result of the local residual stress relief. Electron beam images of the local region are taken before and after the slot is milled, and digital image correlation (DIC) is used to measure the displacement of the material on either side of the slot. The residual stress in the local region can then be interpolated using analytic or finite element solutions and assuming pure elastic relaxation.

Many previous studies have employed slot geometries that simulate an infinite surface crack. Such slots are long and narrow with shallow depths, and the resulting displacements can be related to the original stress state in the local region using two-

dimensional elasticity analysis [9, 11-13]. Shorter slots result in more complex displacement fields and require finite element analysis (FEA) for interpolation of the original stress state in the measurement regions [14].

Recent improvements in the micro-slotting approach have allowed for more complex residual stress evaluation, including residual stress variations with slot depth [15] and along the length of the slot [12, 16]. The assumption of a homogeneous stress state simplifies the micro-slotting approach by allowing the residual stress to be averaged over the local measurement area and may be sufficient for some experiments. Under this assumption, a shorter slot is more ideal for obtaining local residual stress data, since the residual stress is consequently averaged over a smaller area.

Due to the micron-sized sampling volume and localized stress relief, the micro-slotting method has been successfully used to obtain spatially resolved residual stress profiles below shot peened surfaces [12] and around drilled holes [14]. Sequential milling [17] is a common approach for acquiring such data and involves milling micro-scale geometries at regular intervals in order to capture the residual stress gradient. One limitation of this approach is the spacing between subsequent measurements [18]. Since this distance is strongly dependent upon the slot length, shorter slots can be used to improve spatial resolution.

Spatially resolved micro-slotting measurements have been shown to agree well with micro-XRD measurements obtained in similar measurement locations on a near-isotropic aluminum alloy [19]. However, the application of the micro-scale methods to more anisotropic materials presents a source of error when using isotropic assumptions at the micro-scale. A recent study by Salvati et al. [20] evaluated residual stresses in a Ni-

base superalloy using electron backscatter diffraction (EBSD) to acquire local grain orientation data at the micro-scale measurement locations. Another study employed a combination of EBSD and micro-slotting to determine stress profiles near grain boundaries in commercially pure titanium [21]. Such advances in the micro-slotting method make it a promising choice for obtaining reliable near-surface and near-feature residual stress data in Ti-6Al-4V components for input into fatigue life models and crack growth simulations. However, micro-scale measurements on this alloy have yet to be compared to results obtained using established macro-scale measurement techniques.

The work presented here builds on previous work [14] of developing and refining a micro-slotting residual stress measurement procedure that can be applied for measuring residual hoop stresses around drilled holes in Ti-6Al-4V. For this study, the authors chose to use a homogeneous stress field assumption in combination with a short slot geometry of $5 \times 1 \times 7\ \mu m^3$ in order to decrease the required spacing between the micro-slots and reduce the local measurement area over which the residual stress is averaged. FE displacement outputs were used to determine the appropriate spacing between sequential micro-slotting measurements, and slot geometry uncertainties were addressed using FEA to perform a virtual sensitivity analysis. In order to validate the technique and procedure against more conventional stress measurement methods, both micro-slotting and an XRD depth profiling technique were used to measure sub-surface residual stresses on shot peened and surface-machined planar coupons. Due to the complex microstructure of the Ti-6Al-4V alloy used in this study, the authors chose to use isotropic properties and will address the effect of local anisotropy in a future paper.

2. MATERIALS AND METHODS

Mill-annealed Ti-6Al-4V (ASTM Grade 5 [22]) plates of 3.4-4.0 mm thickness were stress relief annealed and chem-milled prior to surface processing. The resulting bulk microstructure was equiaxed α-phase with intergranular β-phase (Figure 1).

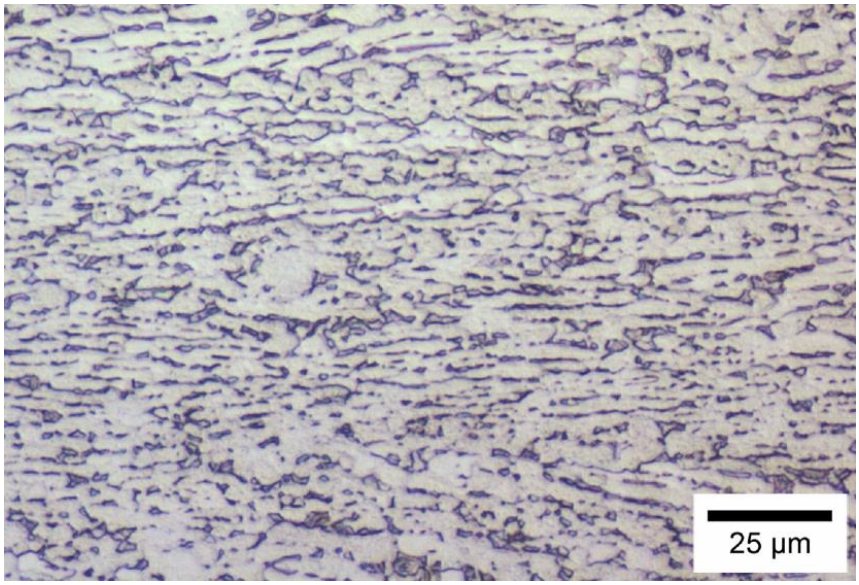

Figure 1. Optical micrograph of mill-annealed Ti-6Al-4V shows equiaxed α phase with intergranular β phase. Sample was etched with Kroll's reagent.

A low-stress machining process was used on the surfaces of two coupons, and one of the coupons was then shot peened. The low-stress machining process used a 10-flute cutter with a 25.4 mm diameter and a 3.05 mm corner radius to minimize stress input. Machining was performed at a spindle speed of 1146 r/min and a feed rate of 14.4 mm/s. Shot peening was performed using a robotic shot peening setup and cast steel shot of size S230 [23] to an Almen intensity of 0.32 mm A with 200% coverage. Samples with

dimensions of approximately 75 mm × 100 mm were sectioned from each plate for XRD residual stress measurements using a band saw, while 20 mm × 10 mm pieces were sectioned using a water jet cutter and set aside for micro-slotting residual stress measurements.

2.1 XRD

XRD residual stress measurements were carried out with a Philips X'Pert Materials Research Diffractometer using the diffraction of Cu Kα radiation from the {213} lattice planes of the α-phase. The $\sin^2\Psi$ method was applied, and measurements were taken in ϕ directions of 0°, 45°, and 90° on the sample to identify any directional dependence of the residual stress induced by the shot peening and surface machining processes. The size of the measurement region was limited by a collimator to a 2 mm × 2 mm area. Measurements were taken on the surfaces of the samples and in increments of 10-35 μm below the surface. Electrolytic polishing was used for localized material removal on a region approximately 15 mm in diameter, and micrometers were used to take measurements of the sample thickness in the polished region before and after each polishing step. All measurements were taken in the middle of the coupons in order to avoid effects of sectioning on the residual stress state. After data were collected on each sample, the measurements were corrected according to SAE J784a [24] in order to account for the presence of steep stress gradients. Electropolishing was performed in a small, confined area on the samples in order to minimize the effects of material removal on the sub-surface residual stress distribution. A StressCheck® FE model was created in order to estimate the stress relief due to the local

removal of material during each electropolishing step, and the stress relaxation was determined to be negligible.

2.2 MICRO-SLOTTING METHOD

The 20 mm × 10 mm pieces sectioned from the plates were mounted in a thermosetting bakelite resin with carbon filler for use in the SEM. The surfaces of the sample cross-sections were prepared by grinding to a 9 μm finish with a diamond suspension and polishing with colloidal silica. Samples were polished for at least 30 minutes using the lowest force setting in order to minimize any deformation induced during the grinding steps. This polishing procedure was also chosen in order to allow for future EBSD analysis in the micro-slot measurement regions.

A Helios NanoLab 600 focused ion beam/field emission scanning electron microscope (FIB/FESEM) was used for performing the micro-slotting procedure. The electron beam was used to navigate and image regions of interest on the sample while the ion beam was used for milling. In order to view the same local region with both beams, the sample was positioned at the eucentric height for this system, resulting in a working distance of ~4.0 mm for the electron beam and ~16.5 mm for the ion beam. The colloidal silica polishing procedure used in this study resulted in a scratch-free surface finish that lacked sufficient surface features required for reliable DIC. Therefore, artificial patterns of small surface dots, approximately 70 nm in depth, were created on the sample using the FIB. Series of patterns were milled using a voltage of 30 kV and a current of 28 pA, and the corresponding series of 5 × 1 × 7 μm^3 micro-slots were milled using a current of 0.92 nA. Electron beam images of the patterned regions were taken at 0° stage tilt before and

after milling the micro-slots using a voltage of 5 kV and a beam current of 43 pA (Figure 2). Imaging was performed with the integration filter using a scan speed of 3 µs on eight frames. These imaging conditions were shown in a previous study [25] to reduce the standard deviation of DIC displacement measurements. Image resolution was 1024 × 884 pixels.

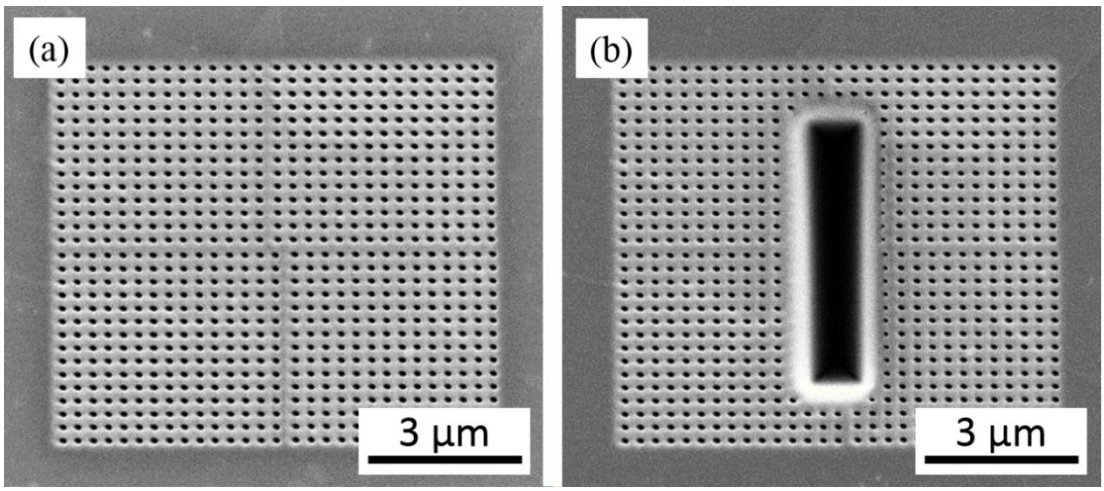

Figure 2. Electron images of FIB-milled pattern (a) before and (b) after milling 5 × 1 × 7 μm^3 slot. Images were imported into MATLAB DIC program to measure milled grid point displacements resulting from residual stress relaxation.

2.3 DIC AND FEA

DIC was performed with an in-house MATLAB code that uses the cpcorr function to resolve the displacements of the grid points between the two electron images. DIC analysis used 20 × 20 pixel patches at 25 pixel spacing. The MATLAB code linearly interpolates a residual stress value from the displacement of each grid point using the surface displacements from a reference stress FE model. The in-house DIC code was

validated against Ncorr [26], an open-source 2D DIC MATLAB program. The reference displacement field was calculated using a 3D FE model of a 5 × 1 × 7 μm^3 slot in a finite body created in StressCheck. The 3D FE model employed quarter symmetry, fixed boundary conditions, and a uniform compressive stress of 1000 MPa perpendicular to the slot length. Isotropic elastic properties for the finite body were chosen in order to agree with the elastic constant used in the XRD analysis. The dimensions of the finite body were validated by increasing the body dimensions and comparing the displacement values in the area of the patterned region. Convergence of the solution was observed, and any error due to the chosen body dimensions was determined to be negligible. A rectangular grid of points was created on the surface of the body, and a text file of the grid point coordinates and corresponding displacement values was extracted from the FE results for input into the MATLAB DIC software. The rectangular grid of points and the corresponding displacements are shown in Figure 3.

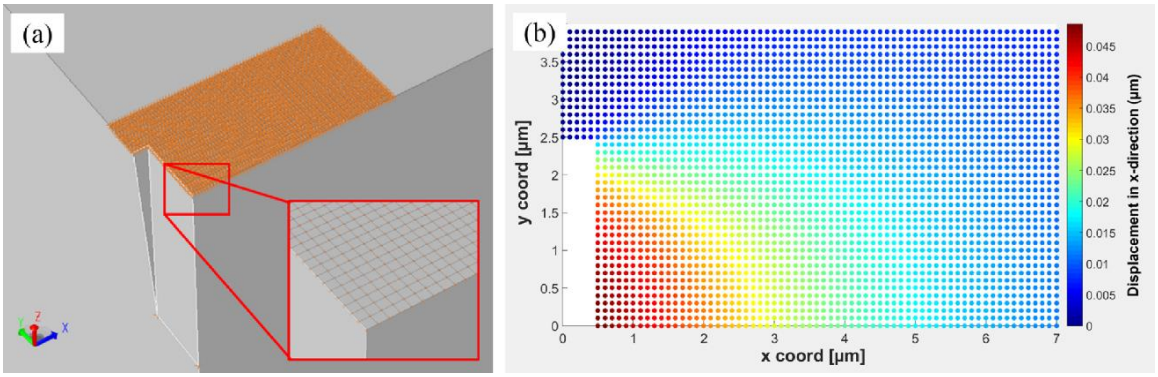

Figure 3. (a) Quarter symmetry FE model of 5 × 1 × 7 μm^3 slot with surface point-grid and (b) text file of corresponding displacement values due to uniform stress field of 1000 MPa for input into MATLAB DIC program.

For each micro-slot, a residual stress value was interpolated for each milled grid point on either side of the slot. The average of these values was determined to be the average residual stress in the local region. Therefore, a residual stress value and a standard deviation were reported for each measurement location. Grid points in close proximity to the milled slot were removed. Extremely large displacements were observed in these areas, most likely due to the re-deposition of the milled material. Points above and below the slot ends were also removed due to the small displacements in these regions and to increase consistency between measurements. In order to remove outlier points from the calculation, all points outside of the standard deviation were removed, and a new average residual stress and standard deviation were calculated. Each reported measurement was determined using at least 60% of the grid points.

2.4 USE OF FEA TO DETERMINE SLOT SPACING

To reduce the amount of time required for the micro-slotting procedure, it was desired to complete the milling and imaging steps for each series of measurements in the following sequential order: (1) mill all patterns, (2) obtain first electron images, (3) mill all slots, and (4) obtain second electron images. However, this procedure allows for any milled slot to affect the displacements around the previously milled slot.

In order to determine the necessary spacing between sequentially milled slots for < 1% change in any grid point displacement, the FE surface displacement outputs were acquired for slots of various lengths, widths, and depths. This allowed for observation of the maximum displacements in the x- and y- directions relative to the slot center. The x-

and y-directions respectively refer to the directions perpendicular and parallel to the slot length.

To determine the necessary spacing between sequential slots in a series, it was necessary to look at the maximum displacement values in the area of the DIC point-grid as a function of distance from the slot center in the y-direction. From observations of the FE output of the surface displacements (Figure 3(b)), the displacement magnitudes increase in the y-direction as the distance from the slot center in the x-direction increases. Consequently, the size of the area over which DIC is performed affects the required spacing between slots. For this analysis, the patterned area was assumed to extend to a distance of x = L and y = L/2 from the slot center, where L is the slot length. Therefore, the necessary spacing between the slots was determined by looking at the magnitudes of the displacements at a distance of x = L as a function of distance from the slot center in the y-direction (Figure 4).

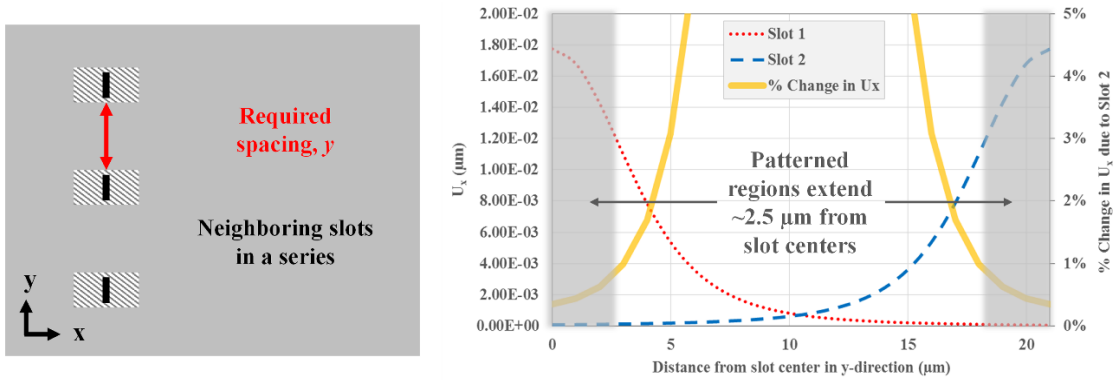

Figure 4. Required spacing, y, was determined by overlaying two maximum displacements (U_x) profiles obtained at a distance of 5 µm from the slot center in the x-direction so that addition of the two displacements resulted in < 1% change in patterned regions. Resulting y was estimated at 22 µm for the slot size used in this study.

The displacement profile of a second slot was then overlaid so that addition of the two displacements in the regions of the milled patterns experience a change of < 1%. The distance between the two profiles was determined to be the required spacing, y, between slots. By calculating this distance for slots of various sizes, the required spacing could be determined as a function of the slot parameters. Thus, the required spacing, y, could be estimated by the function 3L + D, where L is slot length and D is slot depth. This distance equates to 22 µm for the 5 × 1 × 7 μm^3 slot size used in this study.

The required distance between neighboring series of slots was also determined, as multiple series of slots were milled on each sample. To determine this spacing, the maximum displacements in the x-direction were plotted as a function of distance from the slot center (Figure 5).

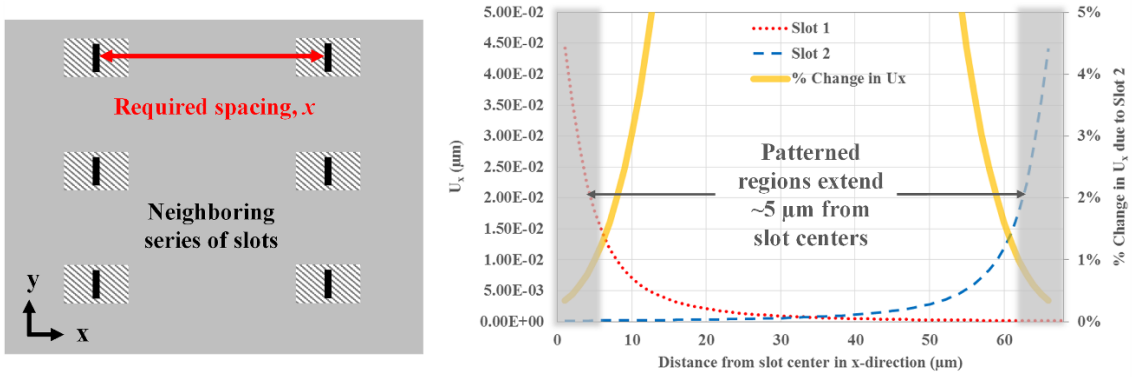

Figure 5. Required spacing, x, between neighboring series of slots was determined by overlaying two maximum displacement (U_x) profiles so that addition of the two displacements resulted in < 1% change in patterned regions. Resulting x was estimated at 68 µm for the slot size used in this study.

Again, a second displacement profile was overlaid so that addition of the two displacements in the regions of the milled patterns experienced a change of < 1%. The distance between the two profiles was estimated to be the required spacing, x, between neighboring series and could be estimated by the function 8L + 4D. For the 5 × 1 × 7 μm^3 slot size used in this study, this distance is equal to 68 µm.

After creating a valid measurement procedure, the micro-slotting measurements were performed in order to map the sub-surface residual stress distributions for the two samples. Each series of 5 × 1 × 7 μm^3 slots was milled as a function of distance below the processed surface of each sample (Figure 6). The spacing between sequential measurements in a series was set at approximately 25 µm.

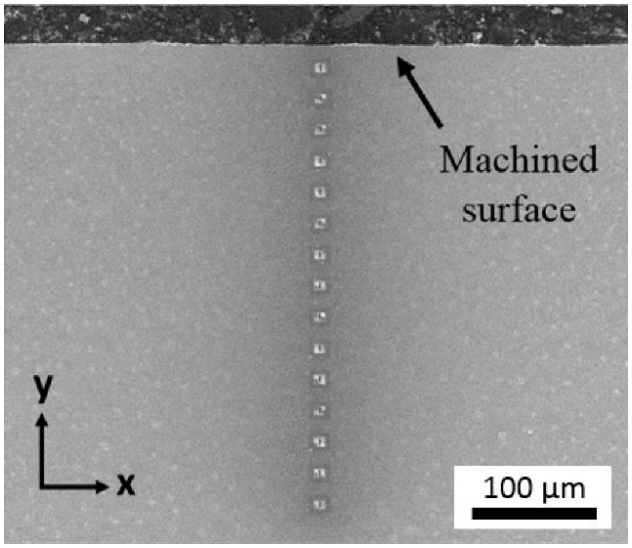

Figure 6. A series of patterns and slots milled as a function of distance below low-stress machined sample surface. Sequential slots in a series were spaced approximately 25 µm.

Three series of micro-slotting measurements were performed on each sample in order to capture the residual stress gradients despite variations in stress due to non-uniformity of surface processing or grain-to-grain variations in stress due to local anisotropy in the material. Measurements taken at equivalent depths below the sample surface were spaced approximately 100 μm. All measurements were made near the center of the samples in order to avoid any stress relaxation effects near the sectioned edges.

2.5 SENSITIVITY ANALYSIS OF SLOT GEOMETRY UNCERTAINTIES

Quantification of slot geometry uncertainties was of great interest in this study, since the sensitivity of the results to slot dimension variations was unknown. A virtual sensitivity study was carried out in order to quantify this effect. First, an average displacement value, U_x, for the $5 \times 1 \times 7$ μm^3 control slot size was determined by identifying the points within the surface point-grid that corresponded with the area of the milled pattern and then averaging those displacements to get a single value. FE models were created for 0.25 and 0.50 μm changes in the slot length, width, and depth, and an FE model was created with fillet edges on the surface of the slot to better replicate the actual milled geometry. All FE models were created using a consistent surface point-grid and a uniform compressive stress of 1000 MPa perpendicular to the slot length. U_x was then calculated for each slot parameter variation and compared to the U_x value for the control slot size to calculate the percent difference. Under the pure elastic assumptions, the estimated percent difference in the U_x values is equal to the estimated percent difference in the residual stress. Thus, the near-linear relationships between the slot parameter

variations and the effects on the residual stress measurements could be established for the DIC point-grid used in this study (Figure 7).

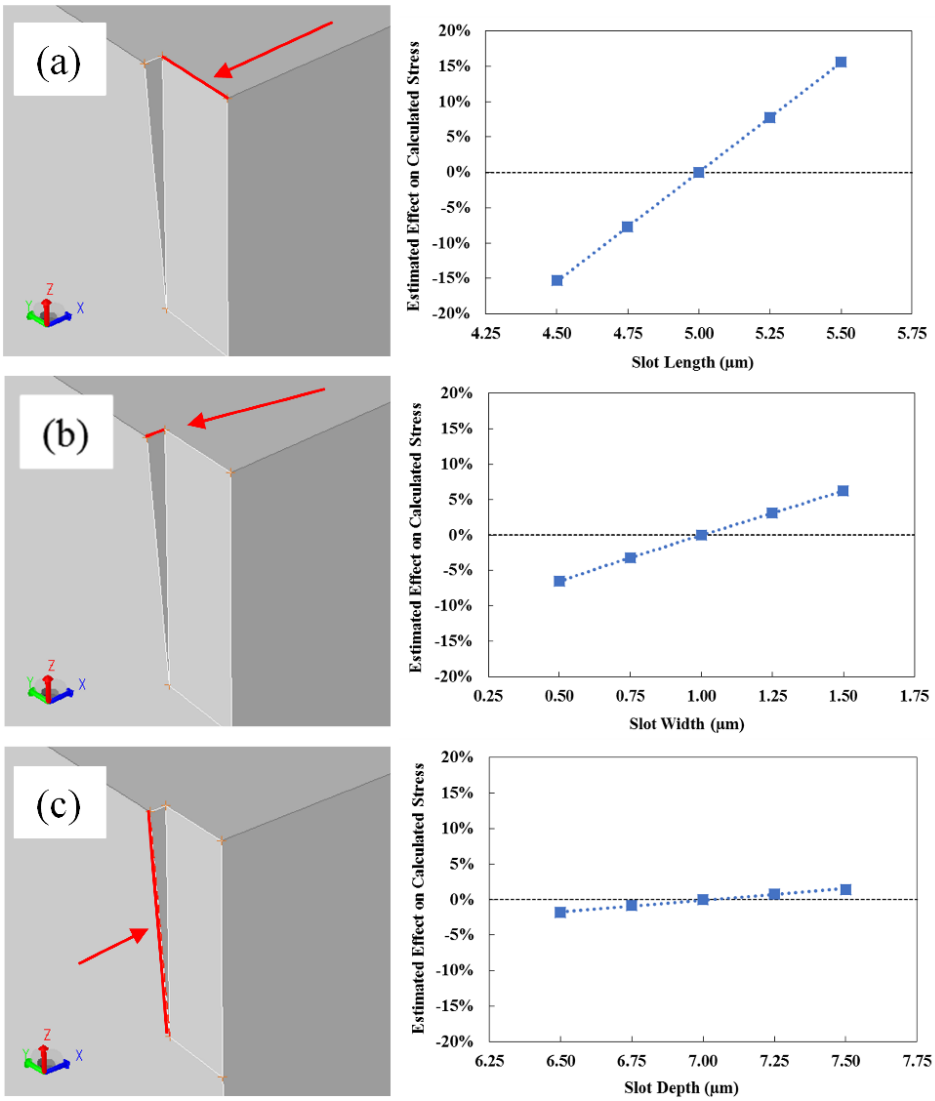

Figure 7. Quarter symmetry FE models of milled slots indicate adjusted slot parameters of (a) length, (b) width, and (c) depth. Plots show near-linear relationships between actual milled slot dimensions and corresponding effects on residual stress calculations, estimated by calculating changes in the average displacement value, U_x. Negative effects indicate underestimation of residual stress, while positive effects indicate overestimation. Uncertainties for milled slot parameters in this study can be interpolated from these relationships.

If the size of the actual milled slot is larger than that of the FE model that is used by the MATLAB DIC software for stress calculation, the resulting displacements around the slot are larger, and the residual stress in the local region is overestimated. Likewise, smaller slot dimensions result in an underestimation of the residual stress.

Uncertainties in the milled slot dimensions for this study were determined by estimating the slot parameters observed in the electron images (Figure 8). Slot length and width variations were estimated by the MATLAB DIC software, which uses image thresholding to identify the location of the slot relative to the milled grid points. Cleaning cross-sections were milled in order to obtain images of the slot profiles, and the measurement feature in the SEM user software was used to estimate the slot depths. Image analysis software was used to estimate the radii of the rounded slot edges, which are created by the ion beam during milling.

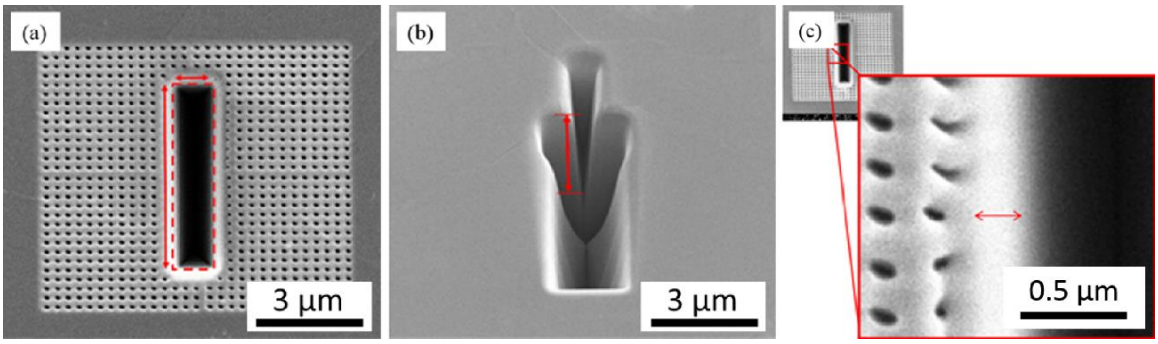

Figure 8. Example electron images used for determining slot parameter variations. (a) Slot lengths and widths were estimated at slot surface by MATLAB DIC program. (b) Slot depths were made visible by milling cleaning cross-sections and were estimated by user during SEM operation. (c) Radii of rounded slot edges were estimated using image analysis.

3. RESULTS AND DISCUSSION

This section first reviews the slot geometry uncertainties that were estimated for the micro-slotting measurements performed in this study. Next, the residual stress measurements obtained using both the XRD and micro-slotting methods on the shot peened and low-stress surface-machined Ti-6Al-4V samples are discussed. Disagreements in the estimated residual stress profiles are assessed in view of differences between the two measurement methods.

3.1 SLOT GEOMETRY UNCERTAINTIES

The maximum and minimum parameters estimated for the slots milled in this study are shown in Table 1. The effects on the residual stress calculations were interpolated using the relationships shown in Figure 7.

Table 1. Maximum effects of slot parameter variations on the residual stress measurements presented in this study.

Milled Slot Parameter	Measured Dimension (μm)	Residual Stress Outcome	Effect on Calculated Residual Stress
Length	4.77	Underestimated	-7.6%
	5.00	Nominal	0.0%
	5.10	Overestimated	+2.5%
Width	0.87	Underestimated	-1.7%
	1.00	Nominal	0.0%
	1.20	Overestimated	+2.5%
Depth	6.80	Underestimated	-0.7%
	7.00	Nominal	0.0%
	7.20	Overestimated	+0.6%
Fillet edges	0.00	Nominal	0.0%
	0.25	Overestimated	+0.3%

The variations in the slot length were shown to have the greatest effect on the calculated residual stress states. A residual stress underestimation of ~7.6% approaches the measurement standard deviation for residual stress magnitudes of ~350 MPa. Therefore, the residual stress measurements were adjusted based on the estimated slot lengths. Uncertainties due to the other slot parameters were determined to be very small and were therefore considered insignificant with regard to the results of this study.

3.2 RESIDUAL STRESS MEASUREMENTS

The three series of micro-slotting measurements show the residual stress data to be in good agreement with the XRD results on the shot peened sample (Figure 9). The XRD residual stress data show a deep compressive stress extending below the surface to an estimated depth of 250 μm, and the measurements are consistent in the three ϕ directions. Cross-plotting the three series of micro-slotting measurements shows a significant amount of scatter within the stress profile. This outcome can be explained by the local characteristic of the micro-slotting method. Each XRD residual stress measurement is both an average of the residual stress measured within the irradiated area and an exponentially weighted average over a specific penetration depth beneath the exposed surface of the material [27]. Thus, the measurement volume of XRD is on the order of millimeters, while the measurement volume of each micro-slot is on the order of microns. In regions where local residual stress variations occur due to surface processing or microstructural effects, the small measurement volume of the micro-slotting method is capable of capturing this variability. This is observed at a depth of 240-280 μm below the surface of the shot peened

sample. Micro-slotting measurements capture residual stresses in the range of ±250 MPa at approximately the same depth where XRD estimates 0 MPa.

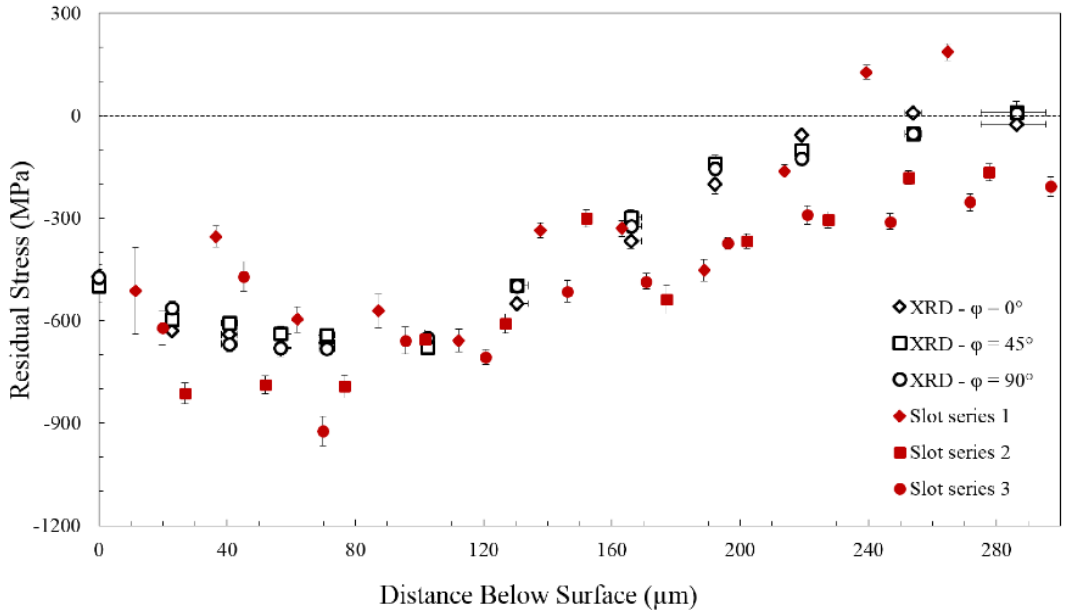

Figure 9. Comparison of XRD and micro-slotting results for the shot peened residual stress profile. XRD measurements are consistent in the three ϕ directions. Residual stress distribution captured by the three series of micro-slotting measurements is in good agreement with the XRD results. Scatter among micro-slotting measurements is attributed to the local characteristic of the method.

The XRD and micro-slotting results for the low-stress machined sample (Figure 10) did not agree as well as those of the shot peened sample, and this can also be explained by the local characteristic of the micro-slotting method. The XRD measurements, consistent in the three ϕ directions, show a very shallow stress profile with a maximum

compressive stress of ~380 MPa at the surface. The micro-slotting measurements indicate a higher compressive stress of ~650 MPa just below the surface.

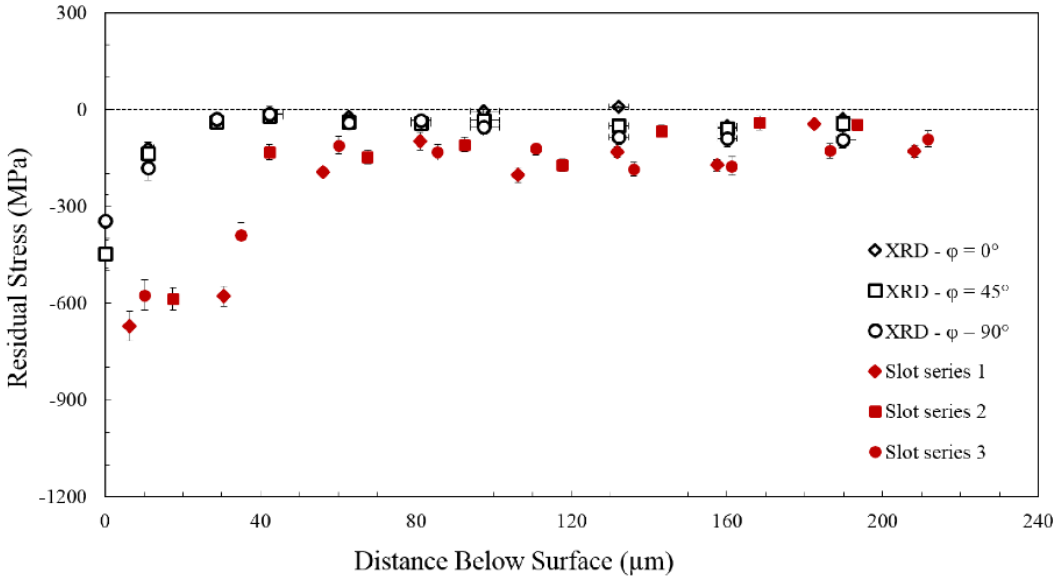

Figure 10. Comparison of XRD and micro-slotting results for the low-stress machined residual stress profile. XRD measurements are again consistent in the three ϕ directions. Measured near-surface residual stresses differ for the two methods, indicating that smaller measurement volumes may be more suitable for capturing shallow stress profiles with steep gradients.

The distinct differences in the near-surface measurements indicate that the larger measurement volume of XRD may not be well-suited for measuring shallow or rapidly changing stress profiles. The micron-sized measurement volume of the micro-slotting method may be more reliable for characterizing this type of surface modification process.

3.3 DISCUSSION OF ERROR SOURCES IN MICRO-SLOTTING METHOD

Many error sources have an effect on the micro-slotting method and should be addressed when interpreting the results. In this study, sample sectioning was required in order to access the sub-surface residual stresses induced by the surface machining and shot peening processes. The cross-section preparation of the samples was assumed to result in complete relief of the out-of-plane residual stress, which modifies the in-plane stress state due to introduction of the free surface. This effect was not accounted for in this study and therefore presents a source of error. FE simulation should be used to accurately estimate the extent of the modified stress state prior to incorporating the data into models or simulations.

Since the micro-slotting method is a surface analysis technique, it is very sensitive to any near-surface stresses that may be induced during the sectioning and polishing procedures. In this study, significant stresses were not observed in areas where low stresses were expected. Thus, the influence of the sample preparation procedure on the residual stress measurements was assumed to be negligible.

Sources of error can also originate from insufficient SEM calibration, resulting in image artifacts that are captured by DIC and cause incorrect measurement of displacements around the slots. No effects of image rotation or shifts on the resulting displacements were observed in this study. Therefore, the effects of systematic errors originating from the SEM were presumed to be negligible.

It is well known that FIB use causes damage to the sample due to implanted Ga ions [28]. Previous work suggests that ion implantation generates a compressive stress due to volume expansion in the ion-implanted area [29], and this compressive stress is

dependent on the ion species and energy [30] that are used for milling. In order to determine if the compressive stress induced during FIB pattern milling had a significant effect on the results of this study, the authors compared micro-slotting residual stress measurements employing FIB-milled patterns with measurements employing electron beam Pt deposited patterns. Five measurements were performed for each patterning technique. All measurements were taken at equivalent depths below the surface of a chem-milled sample that did not undergo a surface modification process. An average stress of -36.5 ± 26.2 MPa was calculated from the FIB-milled pattern measurements, while an average stress of -13.1 ± 31.7 MPa was calculated from the measurements employing the Pt deposition patterns. The difference between these two averages is not significant with regard to the residual stresses measured in this study. The most likely explanation for this is the size of the ion-implanted volume in relation to the volume of the slot. Sample geometries with a high ratio of FIB-milled surface to the overall volume are more likely to be affected by ion implantation [31]. Although FIB milling may be inducing a compressive surface residual stress in the local patterned area, the depth of the affected region is shallow in comparison to the 7 μm slot depth and does not have a significant effect on the displacements.

The use of isotropic elastic constants presents an additional source of error for the micro-slotting technique. The maximum effects of local anisotropy on the micro-slotting measurements presented in this study can be estimated using the single-crystal elastic properties of the hexagonal α phase [32]. If a micro-slot is milled in a single α grain with the maximum-stiffness grain orientation perpendicular to the slot length, the elastic property assumptions used in this study would result in ~25% underestimation of the residual stress magnitude. With the minimum-stiffness grain orientation perpendicular to

the slot length, the chosen elastic properties would result in ~8% overestimation of the residual stress magnitude. The assumption that only anisotropy in the α phase is influential on the residual stress results is reasonable, since the alloy microstructure was observed to be primarily α-Ti. However, the individual α grains are constrained in the complex two-phase microstructure and may not exhibit single-crystal elastic behavior. Precise microstructural information should be obtained for each measurement region in order to observe and quantify these effects. Such an analysis will be presented in a future study.

4. CONCLUSION

Residual stress profiles in planar Ti-6Al-4V samples were successfully measured using the micro-slotting method. The micro-slotting measurements on the shot peened sample agreed very well with the XRD measurements, and the observed scatter in the predicted stress profile was attributed to the local characteristic of the micro-slotting method. Differences between the near-surface XRD and micro-slotting measurements on the low-stress surface-machined sample suggest that the micro-slotting method may be a more ideal choice for capturing shallow residual stress profiles with steep stress gradients. The larger measurement volume of XRD becomes a limitation when measuring these types of profiles.

Prior to performing the micro-slotting measurements, FE models were used to determine the necessary spacing between sequentially milled slots and neighboring series of measurements to ensure < 1% error. This spacing was evaluated as a function of slot length, L, and depth, D. A minimum spacing of 3L + D was determined for sequential slots in a series, and a minimum spacing of 8L + 4D was determined for neighboring series of

measurements. A virtual sensitivity study using FEA was also performed in order to quantify the effect of slot geometry uncertainties on the residual stress measurements presented in this study. Slot length was observed to have the greatest effect on the residual stress calculations, and so the measurements were adjusted in order to account for these variations.

The successful application of the micro-slotting procedure used in this study establishes the micro-slotting method as a reliable near-surface residual stress measurement technique and promotes the implementation of micro-slotting residual stress measurements for fatigue life models and crack growth simulations. The demonstrated use of FE models for optimizing the procedure and quantifying uncertainties shows the robustness of the micro-slotting technique, and the results of this study validate the measurement procedure for capturing local residual stresses in complex-shaped Ti-6Al-4V components where conventional XRD methods are not capable of measuring residual stress.

ACKNOWLEDGMENTS

This project was supported by the Air Force Research Lab (AFRL)-managed Metals Affordability Initiative (MAI). This work is a collaborative research effort of Boeing and Missouri S&T and was made possible by Boeing's presence on the Missouri S&T campus in Rolla, MO. The authors wish to acknowledge Matt Watkins from Engineering Software Research & Development, Inc. (ESRD) and Ioannis Violatos for their technical expertise, along with the technical staff at Missouri S&T's Materials Research Center.

REFERENCES

[1] Withers PJ and Bhadeshia HKDH. Overview – residual stress part 2 – Nature and origins. *Mater Sci Technol* 2001; 17(4): 366-375.

[2] Withers PJ. Residual stress and its role in failure. *Rep Prog Phys* 2007; 70: 2211-2264.

[3] Schajer GS. *Practical residual stress measurement methods*. Chichester: John Wiley & Sons, Ltd, 2013, pp.18-24.

[4] Noyan IC and Cohen JB. *Residual stress: measurement by diffraction and interpretation*. New York: Springer-Verlag, 1987, pp.117-130.

[5] Cullity BD and Stock SR. *Elements of X-ray diffraction.* 3rd ed. Upper Saddle River, NJ: Prentice Hall, 2001, pp.435-442.

[6] Sabate N. Residual stress measurement on a MEMS structure with high-spatial resolution. *J Microelectromech S* 2007; 17: 365-372.

[7] Korsunsky AM, Sebastiani M and Bemporad E. Focused ion beam ring drilling for residual stress evaluation. *Mater Lett* 2009; 63: 1961-1963.

[8] Lunt A, Salvati E, Ma L, et al. Full in-plane strain tensor analysis using the microscale ring-core FIB milling and DIC approach. *J. Mech. Phys. Solids* 2016; 94: 47-67.

[9] Kang KJ, Yao N, He MY, et al. A method for in situ measurement of the residual stress in thin films by using the focused ion beam. *Thin Solid Films* 2003; 443: 71-77.

[10] Prime MB. Residual stress measurement by successive extension of a slot: the crack compliance method. *Appl Mech Rev* 1999; 52: 75-96.

[11] Sabate N, Vogel D, Gollhardt A, et al. Digital image correlation of nanoscale deformation fields for local stress measurement in thin films. *Nanotechnol* 2006; 17: 5624-5270.

[12] Winiarski B, Langford R, Tian J, et al. Mapping residual stress distributions at the micron scale in amorphous materials. *Metall Mater Trans A* 2010; 41: 1743-1751.

[13] Kang KJ, Darzens S and Choi GS. Effect of geometry and materials on residual stress measurement in thin films by using the focused ion beam. *J Eng Mater Technol* 2004; 126: 457-464.

[14] Violatos I, Thomas M, Castle JB, et al. Sub-surface plastic and elastic strain fields and fatigue performance of drilled titanium plates. In: *Proceedings of the 13th world conference on titanium* (eds V Venkatesh, AL Pilchak, JE Allison, et al.), San Diego, CA, 16-20 August 2015, pp.1035-1040. Somerset, NJ: Wiley-TMS.

[15] Winiarski B, Gholinia A, Tian J, et al. Submicron-scale depth profiling of residual stress in amorphous materials by incremental focused ion beam slotting. *Acta Mater* 2012; 60: 2337-2349.

[16] Mansilla C, Martinez-Martinez D, Ocelik V, et al. On the determination of local residual stress gradients by the slit milling method. *J Mater Sci* 2015; 50: 3646-3655.

[17] Lunt A, Baimpas N, Salvati E, et al. A state-of-the-art review of micron-scale spatially resolved residual stress analysis by FIB-DIC ring-core milling and other techniques. *J Strain Anal Eng Des* 2015; 50: 426-444.

[18] Lunt A and Korsunsky AM. A review of micro-scale focused ion beam milling and digital image correlation analysis for residual stress evaluation and error estimation. *Surf Coat Technol* 2015; 283: 373-388.

[19] Winiarski B, Benedetti M. Fontanari V, et al. Comparative analysis of shot-peened residual stresses using micro-hole drilling, micro-slot cutting, X-ray diffraction methods and finite element modeling. In: Bossuyt S, Schajer G and Carpinteri A (eds) *Residual stress, thermomechanics & infrared imaging, hybrid techniques and inverse problems*, vol. 9. New York: Springer, pp.215-223.

[20] Salvati E, Sui T and Korsunsky AM. Uncertainty quantification of residual stress evaluation by the FIB-DIC ring-core method due to elastic anisotropy effects. *Int J Solids Struct* 2016; 87: 61-69.

[21] Basu I, Ocelik V and De Hosson JTM. Experimental determination and theoretical analysis of local residual stress at grain scale. In: *WIT transactions on engineering sciences*, vol. 116 (eds D Northwood, T Rang, J De Hosson, et al.) Southampton, England: WIT Press, 2017.

[22] ASTM B265-15. Standard specification for titanium and titanium alloy strip, sheet and plate.

[23] AMS2431:2017. Peening media, cast steel shot, regular hardness.

[24] SAE. *Residual stress measurement by X-ray diffraction.* SAE J784a, August 1971. Warrendale, PA: SAE.

[25] Winiarski B, Schajer GS and Withers PJ. Surface decoration for improving the accuracy of displacement measurements by digital image correlation in SEM. *Exp Mech* 2012; 52: 793-804.

[26] Blaber J, Adair B and Antoniou A. Ncorr: open-source 2D digital image correlation MATLAB software. *Exp Mech* 2015; 55: 1105-1122.

[27] Prevey PS. X-ray diffraction residual stress techniques. In: Mills K (ed.) *Metals handbook*, vol. 10, 9th ed. Metals Park, OH: American Society for Metals, 1986, pp.380-392.

[28] Nastasi M and Mayer JW. *Ion implantation and synthesis of materials*. Berlin: Springer Verlag, 2006.

[29] Kang TJ, Kim JG, Lee JS, et al. Low-thermal-budget and selective relaxation of stress gradients in gold micro-cantilever beams using ion implantation. *J Micromech Microeng* 2005; 15: 2469-2478.

[30] Dahmen K, Giesen M, Ikonomov J, et al. Steady-state surface stress induced in noble gas sputtering. *Thin Solid Films* 2003; 428: 6-10.

[31] McCaffrey JP, Phaneuf MW and Madsen LD. Surface damage formation during ion-beam thinning of samples for transmission electron microscopy. *Ultramicroscopy* 2001; 87: 97-104.

[32] Tromans D. Elastic anisotropy of HCP metal crystals and polycrystals. *Int J Res Rev Appl Sci* 2011; 6: 462-483.

II. MICRO-SLOTTING RESIDUAL STRESS MEASUREMENT TECHNIQUE FOR UNDERSTANDING FATIGUE PERFORMANCE OF OPEN-HOLE Ti-6Al-4V SAMPLES

Elizabeth Burns[1,2], Joseph Newkirk[1], James Castle[2], and Jennifer Creamer[2]

[1]Department of Materials Science and Engineering

Missouri University of Science and Technology

Rolla, MO, USA

[2]Boeing Research and Technology

St. Louis, MO, USA

Submitted for publication in *Journal of Materials Engineering and Performance*

ABSTRACT

Micro-slotting, a micro-scale relaxation residual stress measurement technique, has been shown in recent years to be a reliable method for measuring local residual stresses in metallic materials. This study demonstrates the unique application of the micro-slotting residual stress measurement technique for measuring near-edge tangential residual stresses around cold-expanded holes in Ti-6Al-4V plates. Knowledge of the near-edge elastic strains induced by the hole processing, in combination with plastic strain information obtained using electron backscatter diffraction, allowed for interpretation of fatigue life differences and crack growth behavior between the as-drilled and cold-expanded conditions. The similar crack initiation lives of the as-drilled and cold-expanded open-hole coupons were attributed to the similar elastic and plastic strains present at the hole edges. The subsequent crack growth resistance observed for the cold-expanded holes was a result of the large compressive residual stress region induced by cold expansion.

1. INTRODUCTION

Reliable measurement of near-edge residual stresses around fastener holes plays a significant role in successful fatigue life prediction of metallic airframe structures. Fastener holes act as sites of stress concentration and are prone to fatigue cracking in aging aircraft [1]. Furthermore, the complexity of the drilling process results in numerous parameters that can affect fatigue performance [2]. The process of cold expansion [3] is a widely used method for extending the fatigue life of fastener holes. The improvement in fatigue life is a result of the compressive tangential residual stress region around the hole that is

introduced by the cold expansion process [4]. The use of this process in the design stage, however, is limited by the ability to accurately measure this resultant residual stress distribution at the hole edge.

Established residual stress measurement techniques are limited with regards to measuring residual stress around holes. X-ray diffraction (XRD) and neutron diffraction are non-destructive methods that can measure residual stress in two dimensions [5], yet both techniques are unable to resolve steep stress gradients close to the hole edge since resolution is limited by the averaging effect of the beam [6-9]. The contour method [10] is the most commonly used destructive technique for measuring residual stress around holes and can provide two-dimensional maps of the tangential residual stress distributions [11]. However, contour method results are understood to be uncertain near the edges of the cut, and this region of uncertainty can extend up to 0.500 mm from the part or hole edge [12].

While established measurement techniques can successfully capture the more macro-scale residual stress state, supplemental data obtained via micro-scale residual stress measurement techniques could be obtained for increased accuracy in fatigue life prediction. The combination of small gauge volume and improved spatial resolution makes these techniques ideal for measuring residual stress in close proximity to the edge of holes. The micro-slotting technique was first proposed by Kang et al. for measuring residual stresses in thin films [13] and relies on the combined imaging and milling capabilities of a scanning electron microscope-focused ion beam (SEM-FIB) system. The FIB is used to mill a series of micron-sized slots, resulting in localized residual stress relief. Electron beam images of the local regions are taken before and after the slots are milled, and digital image correlation

(DIC) is used to measure the resulting displacement of the material. The residual stress in each local region can then be interpolated using finite element solutions.

The micro-slotting technique was recently demonstrated to be a reliable method for measuring local residual stress in Ti-6Al-4V by comparing the measurement results to data obtained using a standard XRD depth profiling technique on shot peened and surface-machined planar coupons [14]. Prior to performing the measurements, the measurement procedure was verified through the use of finite-element (FE) models for determining the appropriate spacing between sequential measurements and for quantifying uncertainties. The results of this previous work thus validated the use of the micro-slotting measurement procedure for use on more complex-shaped Ti-6Al-4V components.

The work presented here builds on a previous study in which the micro-slotting technique and electron backscatter diffraction (EBSD) were used to evaluate the elastic and plastic strain gradients, respectively, around drilled holes in Ti-6Al-4V plates [15]. Residual stresses are a result of permanent inelastic strains [16], which means that both the drilling and cold expansion processes induce a region of plastic strain that can provide intergranular crack initiation sites [2, 17]. It is therefore important to evaluate the extent of this plastic deformation region prior to making any conclusions with regards to fatigue behavior. The use of EBSD allows for high-resolution assessment of such deformed regions. The image quality parameters of band contrast (BC) and band slope (BS) are collected at each measurement point in an EBSD scan and quantify the quality of each acquired electron backscatter pattern (EBSP). BC values describe the brightness level of the detected diffraction bands, while BS values indicate the intensity gradient at the edge of the bands [18]. BC and BS values are known to decrease with increased plastic strain

[19, 20]. Thus, evaluation of these image quality parameters over a sample region of interest can provide qualitative information regarding the distribution of strain in the material [21].

The primary goal of the presented study is to demonstrate the unique application of the micro-slotting technique for measuring near-edge tangential residual stresses around cold-expanded holes in order to interpret differences in fatigue behavior between the as-drilled and cold-expanded conditions. Low-cycle fatigue (LCF) testing was performed on as-drilled and cold-expanded open-hole Ti-6Al-4V coupons, and crack growth data was obtained. Micro-slotting residual stress measurements were performed as a function of distance from the hole edge on both an as-drilled and a cold-expanded hole. Semi-quantitative measurements of the plastic deformation depth associated with the drilling and cold expansion processes were obtained using EBSD. The elastic and plastic strain gradients were then compared for each sample and used to draw conclusions regarding differences in fatigue life and crack growth behavior.

2. MATERIALS AND METHODS

2.1 SAMPLE MATERIAL AND PREPARATION

A total of 10 samples were fabricated from mill-annealed Ti-6Al-4V (ASTM Grade 5 [22]) plates that were stress-relief annealed and chem-milled prior to machining. The bulk microstructure was determined to be equiaxed α-phase with intergranular β-phase.

The samples used in this study were open-hole fatigue coupons (Figure 1) with a thickness of 6.35 mm, a width of 46.0 mm, and a length of 295 mm. All holes were pre-drilled using a speed of 425 r/min and a feed rate of 0.064 mm/rev. Cold expansion was

performed on the holes in half of the coupons using a split mandrel to give 4.2% interference, where interference is quantified as the measured increase in hole diameter divided by the initial hole diameter. All holes were then reamed to a final diameter of 6.35 mm using a speed of 200 r/min and a feed rate of 0.152 mm/rev.

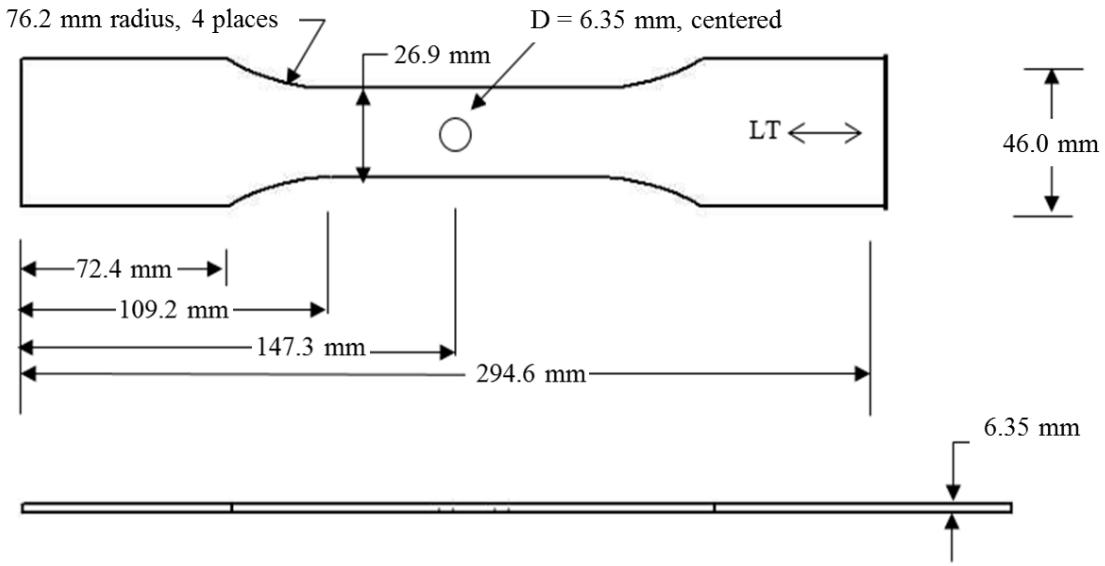

Figure 1. Open-hole specimen geometry for both the as-drilled and cold-expanded holes. Half of the specimens received 4.2% cold expansion using a split mandrel. All specimens were then reamed to a final diameter of 6.35 mm.

Samples were prepared for EBSD and residual stress measurements by sectioning a 20-mm x 15-mm piece from each fatigue coupon to include the as-drilled or cold-expanded hole. The pieces were then mounted in a thermosetting bakelite resin with carbon filler for use in the SEM (Figure 2a). The surfaces of the samples were prepared by grinding to a 9 μm finish with a diamond suspension and then polishing with colloidal silica for approximately 30 minutes using the lowest force setting in order to minimize any

deformation induced during the grinding steps. Approximately 1 mm of material was removed from the sample surface during the initial grinding step. All residual stress measurements were therefore assumed to be representative of the stress state in the bore section. The effects of the cold expansion process on the residual stress present at the entrance and exit sides of the hole were not investigated in this study.

2.2 MICRO-SLOTTING RESIDUAL STRESS MEASUREMENTS

A series of micro-slotting measurements was performed on each sample as a function of distance from the hole edge (Figure 2b) in order to capture the tangential residual stress distributions induced by the drilling and cold expansion processes. The micro-slotting measurements were performed using the measurement procedure that was established as part of a previous study [14].

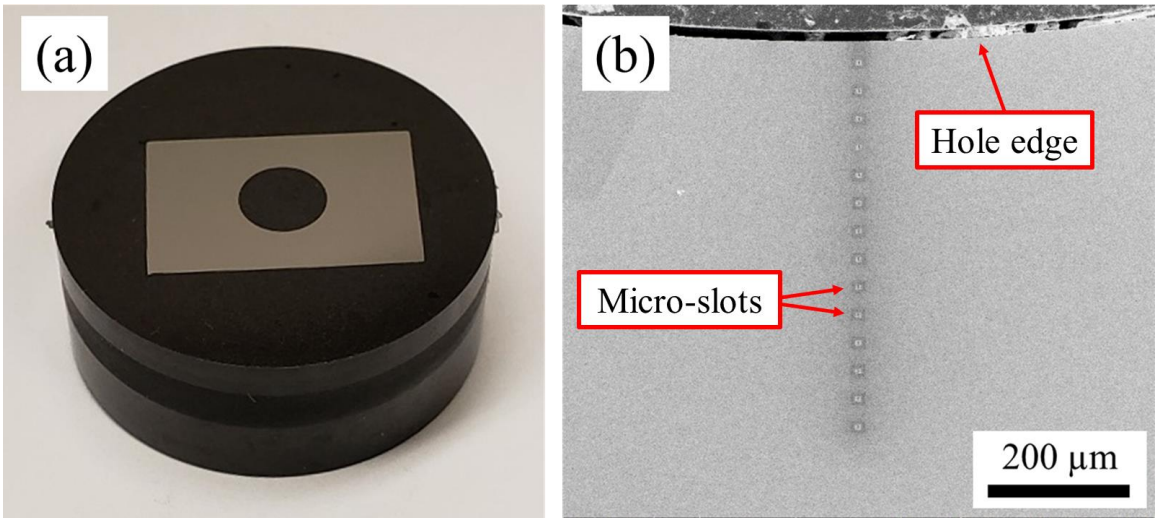

Figure 2. An as-drilled sample and a cold-expanded sample were set aside for micro-slotting residual stress measurements and EBSD. (a) Each hole sample was sectioned from a fatigue specimen and prepared for SEM. (b) A series of micro-slots was milled as a function of distance from the edge of each hole. Image is from as-drilled hole sample.

A Helios NanoLab 600 SEM-FIB was used to perform milling and imaging of the measurement regions. The colloidal silica polishing procedure used in this study resulted in a scratch-free surface finish that lacked sufficient surface features required for reliable DIC. Therefore, artificial patterns of small surface dots, approximately 70 nm in depth, were created on the sample using the FIB. Series of patterns were milled using a voltage of 30 kV and a current of 28 pA, and the corresponding series of $5 \times 1 \times 7$ μm^3 micro-slots were milled using a current of 0.92 nA. Electron beam images of the patterned regions were taken at 0° stage tilt before and after milling the micro-slots using a voltage of 5 kV and a beam current of 43 pA (Figure 3). Imaging was performed with the integration filter using a scan speed of 3 µs on 8 frames. Image resolution was 1024 × 884 pixels.

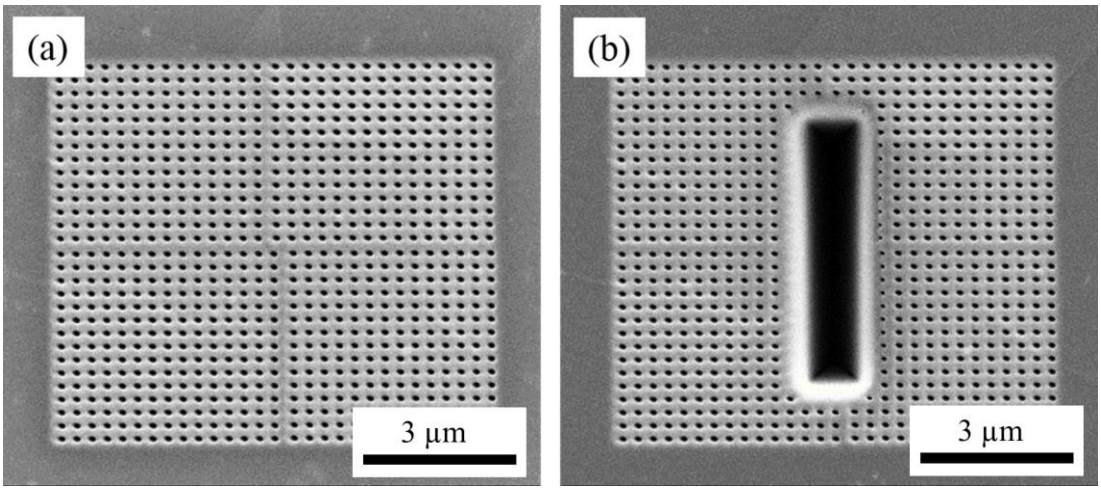

Figure 3. Electron images of each FIB-milled pattern were taken (a) before and (b) after milling the $5 \times 1 \times 7$ μm^3 micro-slots. Images were then imported into a MATLAB DIC program to measure the displacement of each grid point due to local residual stress relaxation.

A MATLAB DIC code was created to determine the displacement field around each micro-slot. A 3D FE model in StressCheck® with a uniform compressive stress of 1000 MPa, quarter symmetry, fixed boundary conditions, and isotropic elastic properties (E = 110.3 GPa, v = 0.31) was used for calculation of the reference displacement field. The displacement field for each measurement region was then interpolated on the FE displacement field in order to determine the original stress state of each measurement region.

In accordance with the previous study [14], a minimum distance of 22 μm between subsequently milled slots was determined to be necessary for <1% change in grid-point displacements due to overlapping strain relaxation fields.

The use of isotropic elastic constants presents a source of error for the micro-slotting technique. Previous work with this technique emphasizes the importance of obtaining precise microstructural information with EBSD in order to accurately calculate the residual stress magnitude in each measurement region. Due to the qualitative nature of the residual stress analysis in this study, no attempt will be made to adjust the residual stress measurements for anisotropy effects.

2.3 SEMI-QUANTITATIVE MEASUREMENT OF PLASTIC DEFORMATION

Plastic deformation induced by the drilling and cold expansion processes was characterized using EBSD. Data was collected using a Nordlys detector situated within the FIB/FESEM system. An EBSD map of a region near the hole edge was acquired on each sample using an electron beam acceleration voltage of 20 kV, a current of 11 nA, and a step size of 0.5 μm. The data was analyzed using Channel5 software.

The depth of plastic deformation for each sample was quantified by extracting image quality parameters from the EBSD scans. An image quality gradient was created for each sample by averaging the BC and BS values obtained at each 0.5 μm step away from the hole edge. These average image quality values produce a gradient that goes from low quality to high quality as the image quality values are extracted from regions of high strain to regions of low strain with increasing distance from the hole edge. The depth of this gradient thus gives a semi-quantitative measurement of the plastic deformation region present at the edge of each hole sample.

2.4 FATIGUE TESTING AND CRACK GROWTH DETECTION

Low cycle fatigue tests were performed on the remaining 8 open-hole coupons in accordance with ASTM E466 using a maximum stress of 275 MPa. The LCF loadings were conducted under a strain ratio of R = 0.02 for 500 cycles, followed by R = 0.50 for 50 cycles. A combination of optical microscopy and eddy current scans were used to detect crack initiation and to provide crack growth data for each coupon. Initiation was noted when a crack reached a size of approximately 0.25 mm × 0.25 mm. Fracture surface images were acquired using a digital optical microscope from both an as-drilled and a cold-expanded hole sample in order to make additional observations.

3. RESULTS AND DISCUSSION

3.1 MICRO-SLOTTING RESIDUAL STRESS MEASUREMENTS

The micro-slotting residual stress measurements for the as-drilled hole sample are shown in Figure 4. The measurements show that a very shallow residual stress distribution

is induced by the drilling process. A tensile residual stress is detected at the edge of the hole, followed by a low-magnitude compressive stress region that extends 150-200 µm from the hole edge. The maximum compressive stress measured in this region was approximately 300 MPa in magnitude. The measured residual stress distribution decays to zero at approximately 200 µm from the hole edge.

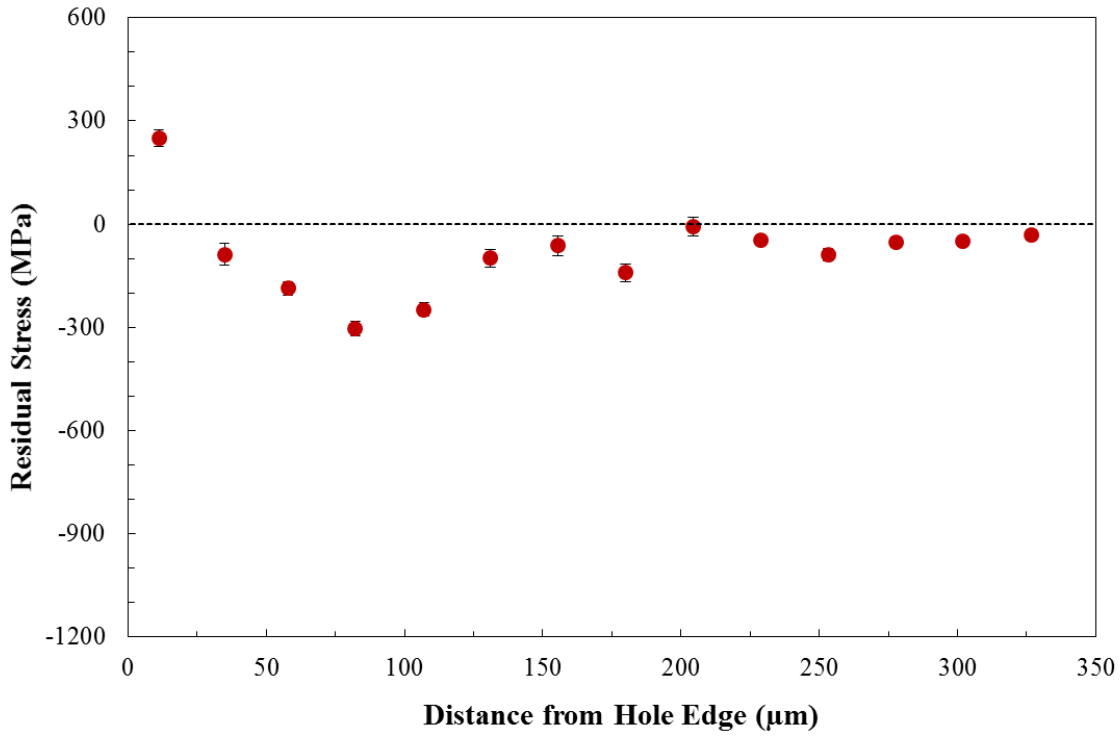

Figure 4. Micro-slotting results for the as-drilled hole sample show a very shallow tensile residual stress, followed by a compressive stress region that extends 150-200 µm from the hole edge.

Figure 5 shows the micro-slotting results for the cold-expanded hole. A tensile residual stress of 300 MPa is detected at the hole edge, followed by a large region of compressive residual stress that is 400-500 MPa in magnitude.

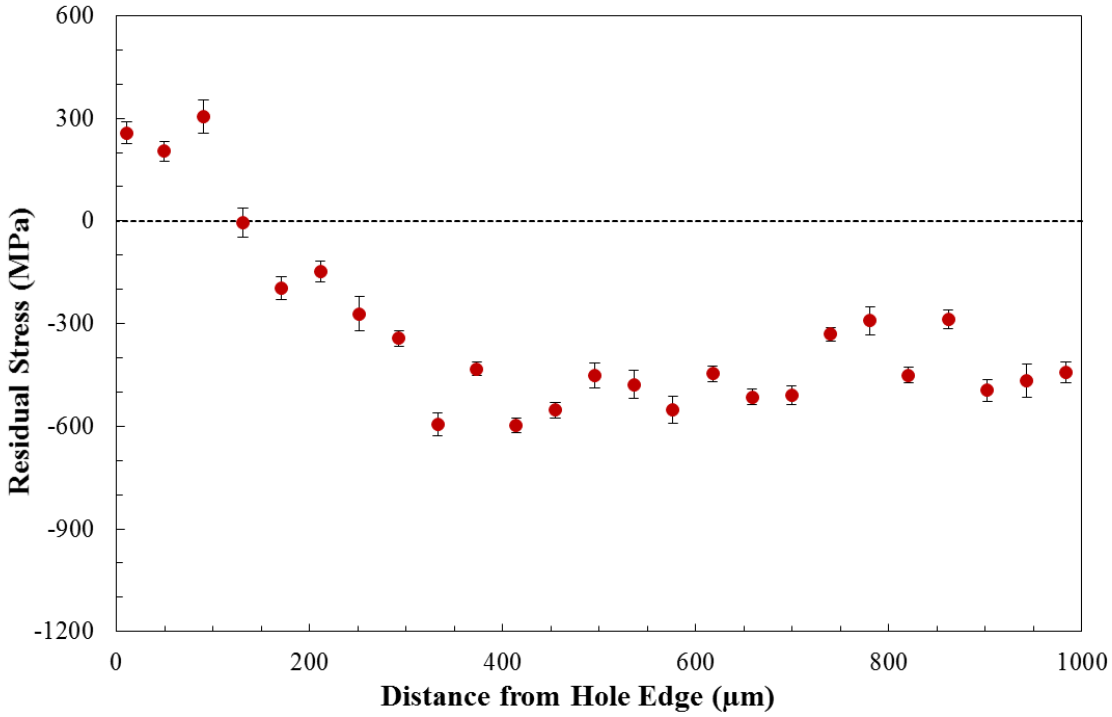

Figure 5. Micro-slotting results for the cold-expanded hole show a shallow tensile residual stress at the hole edge, followed by a large compressive stress zone. The tensile stress at the hole edge was investigated to be a result of the final reaming step.

The series of micro-slotting measurements on the cold-expanded hole sample was continued to a maximum distance of ~1000 µm from the hole edge, and it is clear that the compressive residual stress region induced by cold expansion extends beyond this distance. As expected, the compressive residual stress region induced by cold expansion is of higher magnitude and extends much farther from the hole edge than the compressive stress region induced by the drilling process alone.

The tensile residual stress observed at the edge of the cold-expanded hole was not expected and was thus investigated further. Both the as-drilled and cold-expanded hole samples received a final reaming step prior to fatigue testing. Therefore, the reaming step

was investigated as the source of the tensile residual stress. This was carried out by preparing an additional cold-expanded sample without a final reaming step and performing a series of micro-slotting measurements as a function of distance from the hole edge (Figure 6).

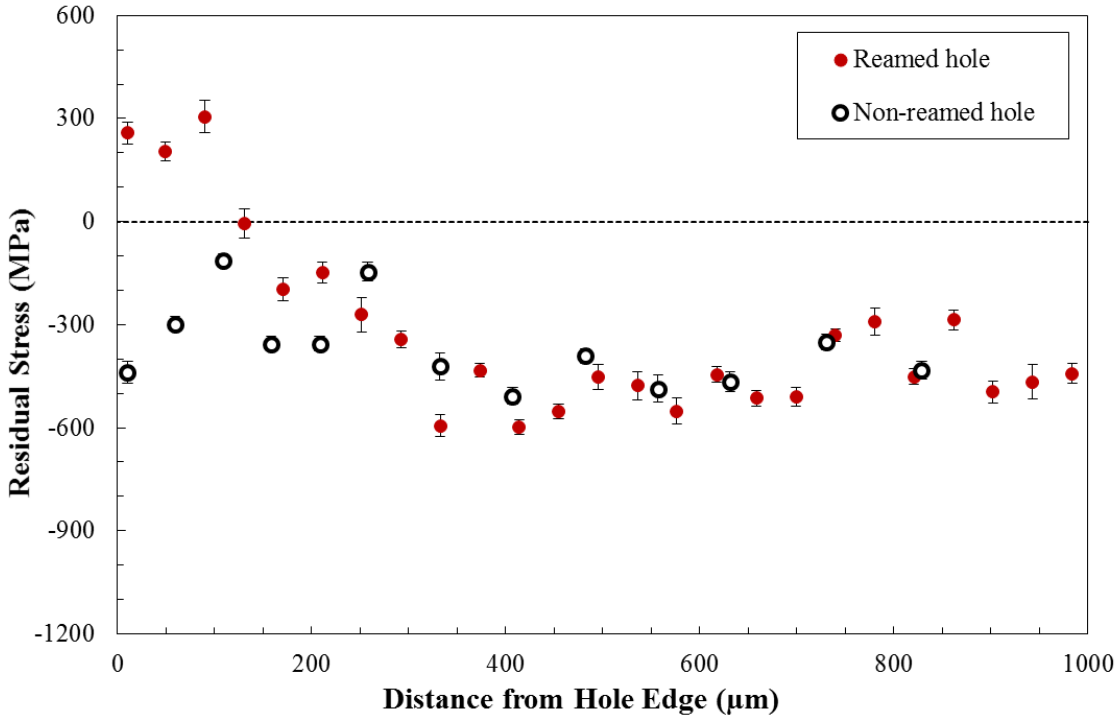

Figure 6. Series of micro-slotting measurements on the cold-expanded hole with no final reaming step plotted against the measurements for the reamed cold-expanded hole. Results show a compressive residual stress at the hole edge. No tensile residual stress was detected, which indicates that the tensile stress measured on the reamed cold-expanded hole sample is due to the final reaming step.

The micro-slotting measurements on the non-reamed cold-expanded hole show a compressive residual stress region that is very similar to the compressive residual stress region measured on the reamed cold-expanded hole. However, no tensile residual stress

was detected near the hole edge. This indicates that the small tensile residual stress on the reamed cold-expanded hole sample was most likely induced by the reaming step. All of the open-hole fatigue coupons received a final reaming step prior to fatigue testing. Consequently, all of the cold-expanded coupons were assumed to have a shallow tensile residual stress present at the hole edge.

3.2 SEMI-QUANTITATIVE MEASUREMENT OF PLASTIC DEFORMATION USING EBSD

The elastic-plastic strain relationships for the as-drilled and cold-expanded hole samples were observed by overlaying the image quality gradients obtained using EBSD and the residual stress measurements obtained using the micro-slotting technique (Figure 7). The image quality plots for each sample show low normalized BC and BS values at the hole edge, indicating regions of high strain. These values increase as data are collected at increasing distances from the hole edges and continue to increase until they reach nominal low-strain values. The depth of plastic deformation on each sample was estimated by observing the distance from the hole edge at which the normalized BC and BS values reach these nominal values.

For the as-drilled hole, both the depth of plastic deformation and peak compressive residual stress lie ~75 μm from the edge of the hole. This trend correlates with the work done by I. Violatos et al. [15] in which the peak compressive residual stress was observed to be within 10 μm of the plastic deformation depth for drilled holes in Ti-6Al-4V. However, this trend is not observed for the cold-expanded hole. Although the depth of plastic deformation on the cold-expanded hole also appears to be ~75 μm, the compressive

residual stress region induced by cold expansion extends much farther away from the hole edge.

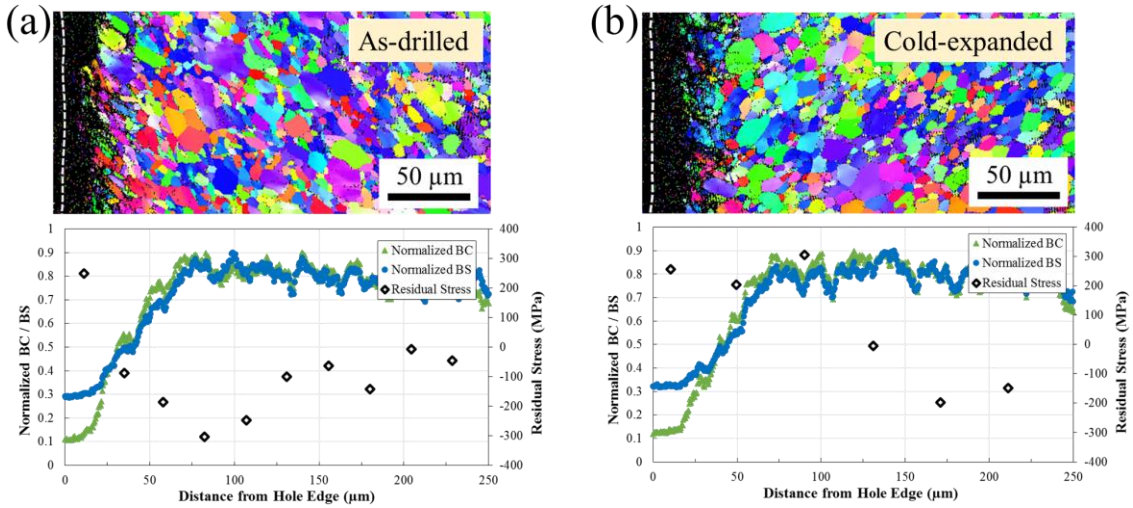

Figure 7. EBSD orientation maps taken at the edge of each hole (top images) and corresponding semi-quantitative image quality gradients extracted from the EBSPs (bottom plots). (a) As-drilled hole plot shows that the plastic deformation depth correlates with the peak compressive residual stress measured by the micro-slotting technique. (b) Cold-expanded hole plot shows a similar plastic deformation depth, but the data does not follow this same trend.

While additional work hardening is understood to be induced during the cold expansion process, the results show no significant difference between the plastic deformation depths for the two hole processing conditions. The image quality gradients for the two samples both reach nominal values at ~75 µm from the hole edge. In other words, the depth of plastic deformation at the edge of the hole was not significantly affected by the cold expansion process.

3.3 FATIGUE TESTING AND CRACK GROWTH RESULTS

Low cycle fatigue tests were performed on the 8 remaining open-hole coupons. As expected, the results (Figure 8) show a dramatic increase in fatigue life for the cold-expanded holes.

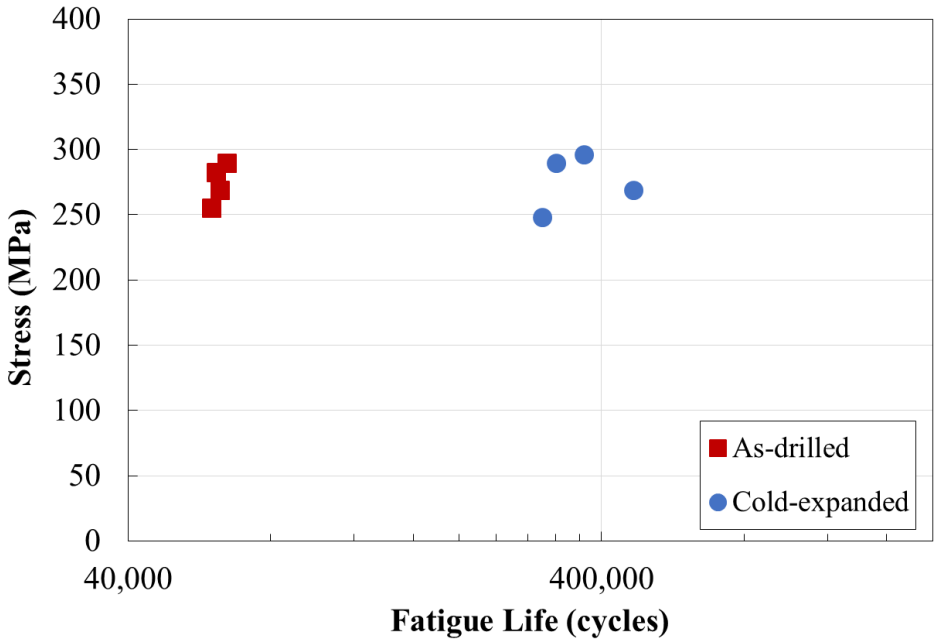

Figure 8. Fatigue life results show two distinct groups. Cold working process significantly increased fatigue life of open-hole coupons.

A combination of optical microscopy and eddy current scans were used to detect crack initiation and to provide crack growth data for a single crack on each sample. The crack growth plot (Figure 9) shows that the crack initiation lives are very similar for the two sample groups. This can be attributed to the tensile residual stresses measured at the edges of both the as-drilled and cold-expanded hole samples and the similar depths of

plastic deformation indicated by EBSD. Upon close observation of the data, the cold expansion process appears to provide a small benefit in crack initiation life of 20,000-50,000 cycles. However, it is not clear if this trend is due to the additional work hardening that takes place at the hole edge during cold expansion or to measurement error resulting from the minimum flaw size required for eddy current detection of crack initiation. Investigation of this effect is outside the scope of this study.

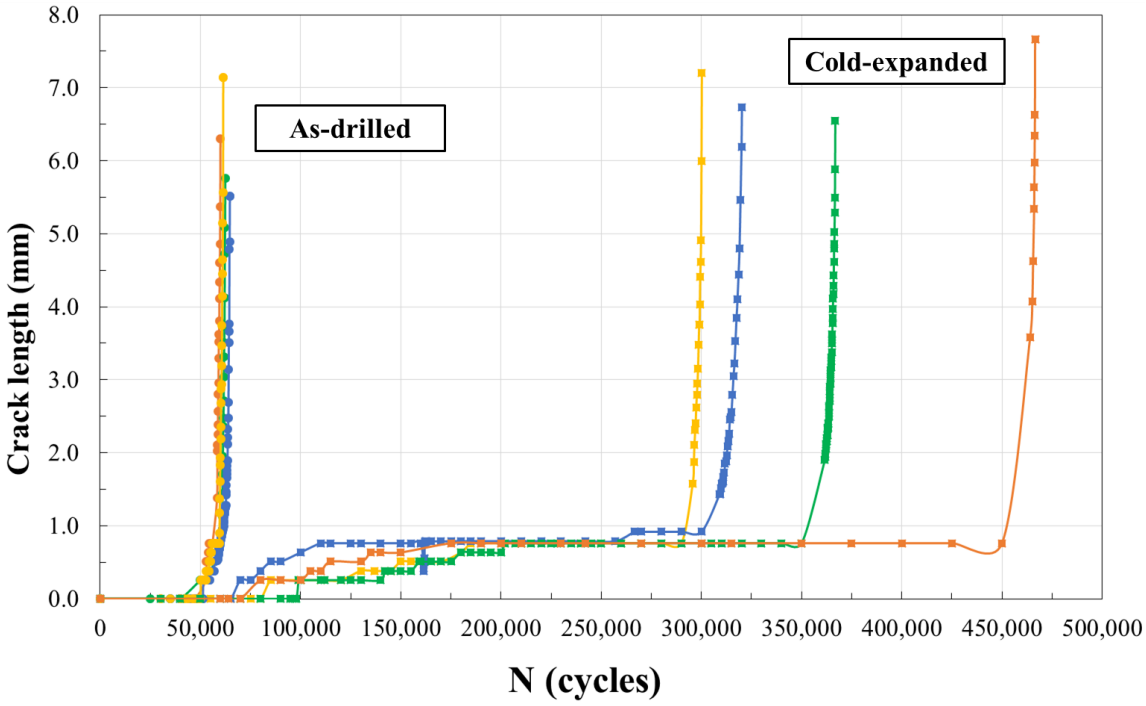

Figure 9. Crack growth measurements show similar crack initiation lives for the low-stress drilled and cold worked holes, which was attributed to the similar elastic and plastic strains observed at the hole edges. Crack growth was significantly affected by the cold working process as a result of the large compressive residual stress region.

Crack growth, on the other hand, is significantly affected by the cold expansion process. Crack growth occurred very slowly at first, followed by a period of arrest. This period of

crack growth resistance can be attributed to the large compressive residual stress region induced by the cold expansion process. The cracks on the cold-expanded holes then continued to grow at the same speed as those detected on the as-drilled holes.

Further analysis on a sample from each group was conducted via fractography. The fracture surface images shown in Figure 10 revealed a single initiation site on the as-drilled hole sample. Multiple crack initiation sites were observed on the cold-expanded hole sample, with a majority of the cracks initiating in the bore section.

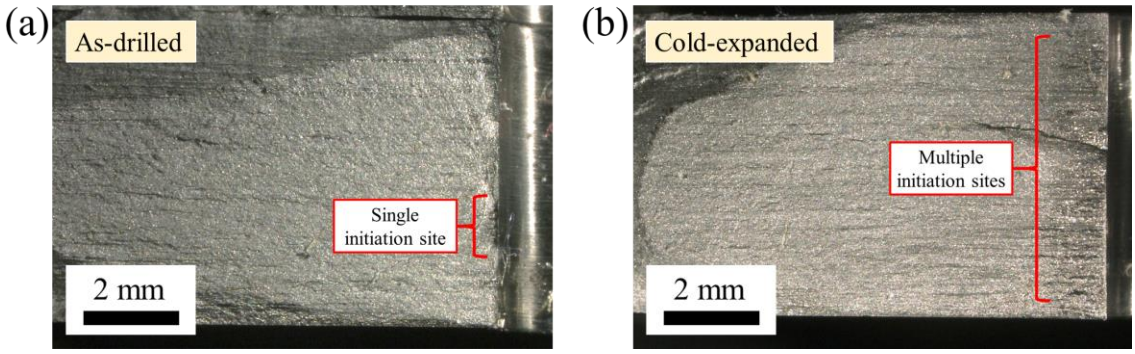

Figure 10. Fracture surface images show (a) a single crack initiation site in the bore section of the as-drilled hole sample and (b) multiple crack initiation sites in the bore section of the cold-expanded hole sample. Accumulation of crack initiation sites most likely occurred during the period of crack growth resistance.

The presence of multiple crack initiation sites on the cold-expanded hole confirms the near-edge residual stress distribution measured by the micro-slotting technique. The small tensile residual stress at the edge of the hole most likely promoted crack initiation, thus allowing an accumulation of crack initiation sites to occur during the period of crack

growth resistance that occurred as a result of the large compressive residual stress region induced by cold expansion.

4. CONCLUSION

This study demonstrated the unique application of the micro-slotting residual stress measurement technique for measuring near-edge tangential residual stresses around cold-expanded holes. In comparison with more established measurement methods, the improved spatial resolution of the micro-slotting technique allows for residual stress measurement within micron-range of hole edges. The micro-slotting procedure used in this study therefore allowed for accurate characterization of the near-edge residual stress state on both an as-drilled hole and a cold-expanded hole. Knowledge of these near-edge elastic strains, in combination with plastic strain information obtained from EBSD, allowed for interpretation of fatigue life differences and crack growth behavior.

The micro-slotting residual stress measurements detected a shallow, low-magnitude tangential residual stress distribution on the as-drilled hole sample, with a tensile stress present at the hole edge, while a much larger compressive residual stress region of higher magnitude was detected on the cold-expanded hole. The measurements also suggested that a small tensile residual stress was introduced at the edge of the cold-expanded holes by the final reaming step performed prior to fatigue testing. The depth of plastic deformation present on each hole sample was semi-quantitatively characterized using image quality parameters from EBSD, and the results indicated that the cold-expansion process did not have a significant effect on the depth of the plastic deformation region induced by drilling. The similar crack initiation lives of the as-drilled and cold-

expanded open-hole coupons were thus attributed to the similar elastic and plastic strains present at the hole edges. The subsequent crack growth resistance observed for the cold-expanded holes was a result of the large compressive residual stress region induced by cold expansion.

ACKNOWLEDGMENTS

This project was supported by the Air Force Research Lab (AFRL)-managed Metals Affordability Initiative (MAI). This work is a collaborative research effort of Boeing and Missouri S&T and was made possible by Boeing's presence on the Missouri S&T campus in Rolla, MO.

REFERENCES

[1] D.L. Rich and L.F. Impellizzeri, Fatigue analysis of cold worked and interference fit fastener holes, cyclic stress-strain and plastic deformation aspect of fatigue crack growth. American Society for Testing and Materials, ASTM STP, 1977, 637, p 153-175

[2] J. Castle, "Drilling Induced Fatigue Damage in Ti-6Al-4V," Ph.D. Thesis, Washington University in St. Louis, 2010.

[3] T.N. Chakherlou and J. Vogwell, The effect of cold expansion on improving the fatigue life of fastener holes, Eng. Failure Anal., 2003, 10, p 133-24

[4] J.L. Phillips, "Sleeve Coldworking Fastener Holes," Tech. Rep. AFML-TR-74-10, Air Force Mat. Lab., Wright-Patterson AFB, 1974

[5] I.C. Noyan and J.B. Cohen, Residual stress: measurement by diffraction and interpretation, 1987, New York: Springer-Verlag, p 117-130

[6] G. Dietrich and J.M. Potter, Stress measurements on cold-worked fastener holes, Adv. X-Ray Anal., 1977, 20, p 321-328

[7] R. Cook and P. Holdway, Residual stresses induced by hole cold expansion, Computer Methods and Experimental Measurements for Surface Treatment Effects, M.H. Aliabadi and C.A. Brebbia, Eds., Computational Mechanics Publications, 1993, p 91-100

[8] L. Edwards and D.Q. Wang, Neutron diffraction determination of the complete 3D residual stress distribution surrounding a cold-expanded hole, Proc. 4th European Conference on Residual Stresses, Vol. 2, S. Denis, Ed., 1996 (Bourgogne, France), Société Francaise de Métallurgie et de Matériaux, 1998, p 619-626

[9] R. Hermann, Three-dimensional stress distribution around cold expanded holes in aluminium alloys, Eng. Fract. Mech., 1994, 48 (6), p 819-835

[10] M. Prime, Cross-sectional mapping of residual stresses by measuring the surface contour after a cut, J. Eng. Mater. Technol., 2001, 123, p 162-168

[11] Y. Zhang, M. Fitzpatrick, and L. Edwards, Measurement of the residual stresses around a cold expanded hole in an EN8 steel plate using the contour method, Mater. Sci. Forum, 2002, 404-407, p 527-534

[12] G. Schajer, Practical Residual Stress Measurement Methods, 2013, Chichester: John Wiley & Sons, Ltd, p 109-138

[13] K.J. Kang, N. Yao, M.Y. He, and A.G. Evans, A method for in situ measurement of the residual stress in thin films by using the focused ion beam, Thin Solid Films, 2003, 443, p 71-77

[14] E. Burns, J. Newkirk, and J. Castle, Micro-slotting technique for reliable measurement of sub-surface residual stress in Ti-6Al-4V, J. Strain Anal. Eng. Des., 2018, 53(6), p 389-399

[15] I. Violatos, M. Thomas, J.B. Castle, and B.P. Wynne, Sub-surface plastic and elastic strain fields and fatigue performance of drilled titanium plates, Proceedings of the 13th World Conference on Titanium, V. Venkatesh, A.L. Pilchak, J.E. Allison, S. Ankem, R. Boyer, J. Christodoulou, H.L. Fraser, M.A. Imam, Y. Kosaka, H.J. Rack, A. Chatterjee, and A. Woodfield, Eds., 2015 (San Diego, CA), Wiley-TMS, 2016, p 1035-1040

[16] A. Korsunsky, A Teaching Essay on Residual Stresses and Eigenstrains, 2017, Butterworth-Heinemann

[17] L. Reid, Incorporating hole cold expansion to meet durability and damage tolerance airworthiness objectives, SAE International, 1997, SAE Paper No. 972624

[18] T. Maitland and S. Sitzman, Chapter 2: Electron Backscatter Diffraction (EBSD) Technique and Materials Characterization, In: Scanning Microscopy for Nanotechnology, W. Zhou and Z.L. Wang, Eds., 2007, Springer, p 41-75

[19] A.J. Wilkinson and D.J. Dingley, Quantitative deformation studies using electron back scatter patterns, Acta Metall. Mater., 1991, 39(12), p 3047-3055

[20] N.C. Krieger Lassen, D. Juul Jensen, and K. Conradsen, Automatic recognition of deformed and recrystallized regions in partly recrystallized samples using electron back scattering patterns, Mater. Sci. Forum, 1994, 157-162, p 149-158

[21] S.I. Wright, M.M. Nowell, and D.P. Field, A review of strain analysis using electron backscatter diffraction, Microsc. Microanal., 2011, 17, p 316-329

[22] "Standard Specification for Titanium and Titanium Alloy Strip, Sheet and Plate," ASTM B265-15, ASTM International, 2015

III. QUALITATIVE EVALUATION OF LOCAL MICROSTRUCTURE EFFECTS ON MICRO-SLOTTING RESIDUAL STRESS MEASUREMENTS IN Ti-6Al-4V

Elizabeth Burns[1,2], Joseph Newkirk[1], and James Castle[2]

[1]Department of Materials Science and Engineering

Missouri University of Science and Technology

Rolla, MO, USA

[2]Boeing Research and Technology

St. Louis, MO, USA

To be submitted for publication in *Materials and Design*

ABSTRACT

A thorough understanding of both macroscopic and microscopic residual stresses is critical for reliable prediction of fatigue behavior in metallic materials. Recent works have demonstrated that micro-scale relaxation residual stress measurement techniques are capable of capturing residual stresses at both the macro- and micro-scales on a variety of metallic materials due to their micron-sized gauge volumes and high spatial resolution. However, studies that aim to identify and quantify the specific sources of microscopic stresses are limited. The goal of the presented study is to explore the use of the micro-slotting technique for understanding residual stress distribution at the microstructural level. A grid of $2 \times 0.2 \times 3$ μm^3 micro-slotting measurements was milled in a high magnitude compressive residual stress region below the surface of a shot peened Ti-6Al-4V sample. Micro-slots were milled both perpendicular and parallel to the shot peened surface, and averaging the measurements allowed for estimation of the macroscopic residual stress state. For each micro-slotting measurement, data plots of both the measured displacement magnitudes and the interpolated residual stress values were overlaid to scale with a local microstructure map obtained using electron backscatter diffraction. This analysis allowed for novel qualitative observations regarding residual stress orientation and microstructure effects on the local residual stress relaxation, which were used to explain deviations between the measurements and the predicted macroscopic stress state. These effects included changes in residual stress approaching grain boundaries, elastic modulus differences in neighboring α grains, and constrained relaxation due to local phase distribution.

1. INTRODUCTION

A thorough understanding of residual stress distribution at both the macroscopic and microscopic scales is critical for accurate prediction of fatigue behavior in metallic components [1]. Induced by nearly all manufacturing processes, residual stresses are an elastic response to inhomogeneous plastic strains [2] and can be categorized by the length scale over which they equilibrate [3, 4].

Macroscopic residual stresses are long range stresses that equilibrate over the scale of the structure or component and are measured using conventional residual stress measurement techniques [5]. These techniques include both stress relaxation measurement methods [6] and diffraction methods [7]. Microscopic residual stresses vary over grain scale and nearly always exist in polycrystalline materials as a result of differences in neighboring grain orientations or phase distribution [8]. Measurement techniques that are capable of measuring these intergranular stresses are limited since they require micron-scale gauge volumes and high spatial resolution. Such techniques include micro-focus synchrotron X-ray diffraction [9, 10], high resolution-electron backscatter diffraction [11], and the more recently established micro-scale stress relaxation measurement methods [12]. These methods employ the combined imaging and milling capabilities of a scanning electron microscope-focused ion beam (SEM-FIB) dual-beam system to scale down the geometries of established stress relaxation techniques to micron-sized gauge volumes. Milling geometry selection is based on the desired residual stress information. The micro-slotting technique [13] provides measurement of the single stress component perpendicular to the slot, while the micro-hole drilling [14] and micro-scale ring-core [15, 16] methods are capable of providing the full in-plane stress tensor.

The micro-slotting technique was first proposed by Kang et al. [13] for measuring residual stresses in thin films and involves using the FIB to mill a narrow rectangular slot. Relaxation of the surrounding material results in relief of the in-plane residual stress component that lies perpendicular to the slot. Displacement of the material is measured by taking electron beam images of the local region before and after the slot is milled and using digital image correlation (DIC) to resolve the displacements between the two images. The residual stress in the measurement region is then interpolated using analytic or finite element (FE) solutions and assuming pure elastic relaxation. Numerous advances with this technique have been made in recent years, and those most relevant to the measurement procedure used in this study include the use of shorter length micro-slots in combination with FE modeling for increased spatial resolution [17] and the use of FE modeling for creating a reliable micro-slotting measurement procedure [18].

Other recent works employing micro-scale methods have investigated the ability of these techniques to capture both the macroscopic and microscopic residual stress states. A study by J. Everaerts et al. involved using the micro ring-core technique in combination with eigenstrain modeling to separate the macroscopic and microscopic stresses in a bimodal Ti-6Al-4V bar following plastic four-point bending [19]. However, when the separate contributions of the macroscopic and microscopic residual stresses are unknown, a significant amount of scatter can be observed in the measurement results [16, 20]. A separate study by J. Everaerts et al. [21] saw good agreement between micro ring-core measurements and high-energy synchrotron X-ray strain data on a laser shock-peened Ti-6Al-4V sample, yet decreasing the gauge volume of the micro ring-core measurements resulted in strong deviations from the X-ray results due to the presence of microscopic

residual stresses. While these recent works aimed to quantify microscopic residual stresses, studies that serve to identify the specific sources of these stresses are limited. One such study performed by I. Basu et al. [22] employed a micro-slotting methodology to measure spatially resolved residual stress profiles in the vicinity of grain boundaries in commercially pure titanium.

The main goal of the presented study is to explore the use of the micro-slotting technique for understanding residual stress distribution and sources of microscopic residual stresses at the microstructural level. First, a laboratory X-ray diffraction (XRD) depth profiling technique is used to measure the sub-surface residual stress profile induced by shot peening in order to identify a sub-surface region of high magnitude residual stress on a shot peened Ti-6Al-4V sample. A grid of micro-slotting measurements is then milled in the sub-surface region with slots oriented both perpendicular and parallel to the shot peened surface for measurement of the σ_x and σ_z residual stress components, respectively. Electron backscatter diffraction (EBSD) is then used to obtain local microstructural information in the micro-slot measurement regions. Data plots of the displacement magnitudes measured by DIC and the interpolated residual stresses are overlaid to-scale with the local microstructure EBSD maps, thus presenting a novel approach for evaluating local microstructure effects on residual stress relaxation at the micro-scale. Select measurement regions are shown and discussed to summarize consistencies in the qualitative observations.

2. MATERIALS AND METHODS

2.1 SAMPLE MATERIAL AND PREPARATION

Samples were prepared from a mill-annealed Ti-6Al-4V (ASTM Grade 5 [23]) plate of 6.0 mm thickness that was stress relief annealed and chem-milled prior to surface processing. The resulting bulk microstructure, shown in Figure 1, was determined to be equiaxed α phase with intergranular β phase.

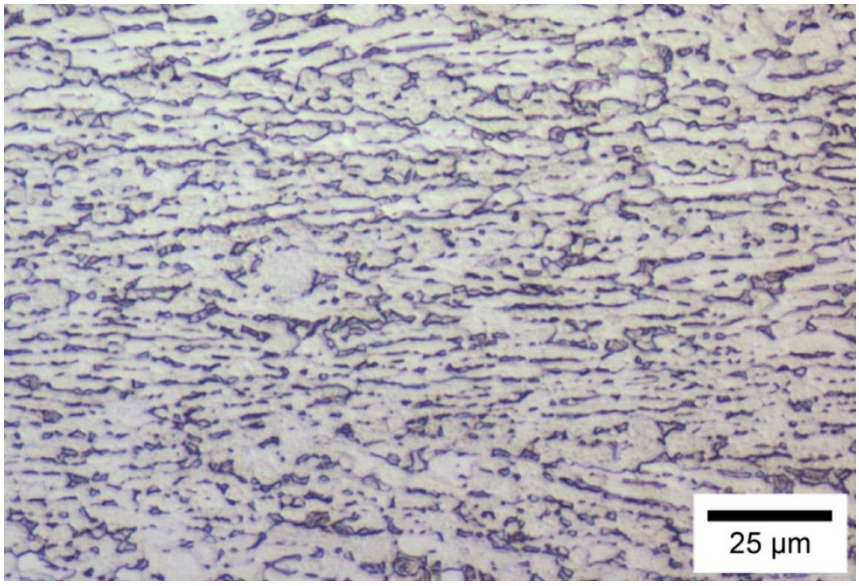

Figure 1. Optical micrograph of mill-annealed Ti-6Al-4V plate. Etched microstructure revealed equiaxed α phase with intergranular β phase.

The plate was shot peened to an Almen intensity of 0.32 mm A with 200% coverage using a robotic shot peening setup and cast steel shot of size S230 [24]. A sample with dimensions of approximately 75 mm × 100 mm was sectioned from the plate for XRD residual stress

measurements using a band saw, while a 20 mm × 10 mm piece was sectioned from the plate using a water jet cutter and set aside for micro-slotting residual stress measurements.

2.2 XRD RESIDUAL STRESS MEASUREMENTS

XRD residual stress measurements were performed in order to identify a high magnitude compressive residual stress below the shot peened surface of the sample for micro-slotting measurements. A Philips X'Pert Materials Research Diffractometer was used to carry out the XRD residual stress measurements, and the $\sin^2\Psi$ method was applied using the diffraction of Cu Kα radiation from the {213} lattice planes of the α phase. Measurements were taken on the surface of the sample and in increments of 10-35 μm below the surface. Electrolytic polishing was used for localized material removal on a 15 mm-diameter region in the middle of the coupon. The amount of material removed between measurements was estimated by using micrometers to measure the sample thickness in the polished region before and after each polishing step. The size of the measurement region was limited by a collimator to a 2 mm × 2 mm area. The effect of localized electrolytic polishing on residual stress relaxation was determined to be negligible using a StressCheck® FE model.

2.3 MICRO-SLOTTING METHOD

The 20 mm × 10 mm piece sectioned from the plate was mounted in a thermosetting bakelite resin with carbon filler for use in the SEM. The surface of the sample cross-section was prepared by grinding to a 9 μm finish with a diamond suspension and polishing with

colloidal silica. The sample was polished for 30 minutes using the lowest force setting in order to minimize any deformation induced during the grinding steps.

A Helios NanoLab 600 SEM-FIB was used to perform the micro-slotting measurements. Local artificial patterns of small surface dots were milled into the polished sample surface using the FIB. The patterns were milled using a voltage of 30 kV and a current of 9.7 pA, resulting in surface dots approximately 4 nm in depth. The corresponding $2 \times 0.2 \times 3\ \mu m^3$ slots were milled using a current of 28 pA. Electron beam images of the patterned regions before and after milling the micro-slots (Figure 2) were imported into MATLAB DIC software in order to determine the displacements of the grid points around each slot. All imaging was performed with the integration filter using a scan speed of 1 µs on 8 frames. Image resolution was 1024 × 884 pixels.

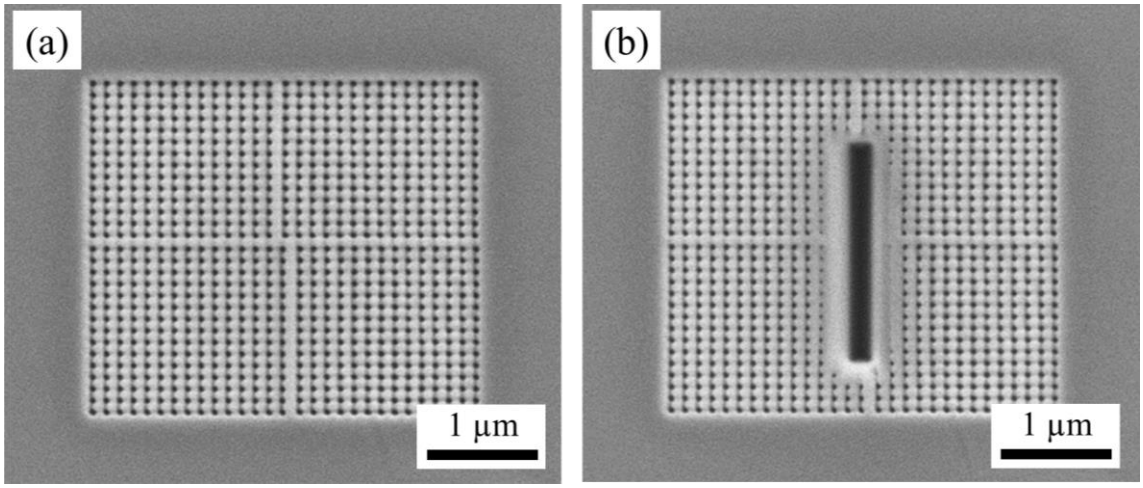

Figure 2. Electron beam images of each milled pattern were taken (a) before and (b) after milling each $2 \times 0.2 \times 3\ \mu m^3$ slot. Images were then imported into MATLAB DIC program for measurement of grid point displacements around each slot due to local residual stress relaxation.

The MATLAB DIC code used in this study employed the cpcorr function to resolve the displacements of the grid points. Surface displacements from a reference stress FE model were then used to interpolate a residual stress value from the displacement of each grid point. The reference displacement field was calculated using a 3D FE model of a 2 × 0.2 × 3 μm^3 slot in a finite body created in StressCheck®. The 3D FE model was created using quarter symmetry, fixed boundary conditions, and a uniform compressive stress of 1000 MPa perpendicular to the slot length. Isotropic elastic properties for the finite body (E = 112.6 GPa, v = 0.34) were chosen in order to agree with the elastic constant used in the XRD analysis [25]. A grid of points was created on the surface of the body, and a text file of the grid point coordinates and corresponding displacement values were extracted from the FE results for input into the MATLAB DIC software.

For each micro-slot, a residual stress value was interpolated for each milled grid point on either side of the slot, and the average of these values was determined to be the average residual stress in the local region. Therefore, a residual stress value and a standard deviation were reported for each measurement location. Grid points within 0.5 μm of the slot edges exhibited extremely large displacements and were therefore removed prior to residual stress calculation. Points above and below the slot ends were also removed due to the small displacements in these regions and to increase consistency between measurements. All of the remaining points in the grids were used to calculate an average residual stress value and a standard deviation for each micro-slot. No outlier data points were removed in this study.

A grid of 25 micro-slotting measurements was performed on the prepared sample cross-section, as shown in Figure 3. The orientation of the micro-slot lengths relative to the

shot peened surface was alternated between perpendicular and parallel in order to measure the σ_x and σ_z residual stress components, respectively. The micro-slots were spaced approximately 10 µm apart in both the x- and y-directions. The grid was placed so that the micro-slotting measurements captured the residual stress at a range of 50-90 µm below the shot peened surface, as the XRD results indicated high magnitude residual stresses in this region. FE analysis was used, according to a previous study [16], to determine the percent change in the grid point displacements due to overlapping strain fields for subsequently milled micro-slots. For the 10 µm spacing used in this study, the average percent error due to this effect was estimated to be ~6%.

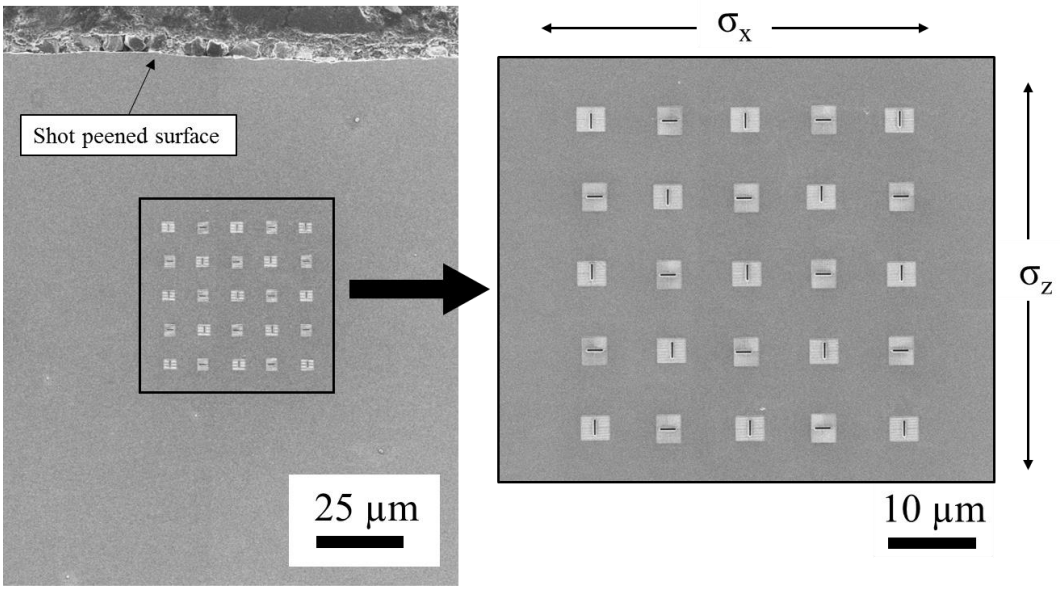

Figure 3. Micro-slotting residual stress measurements were performed in a grid pattern on polished sample cross-section. Slots were spaced ~10 µm in both the vertical and horizontal directions and were oriented both perpendicular and parallel to the shot peened surface, resulting in measurements of the σ_x and σ_z residual stress components, respectively.

2.4 EVALUATION OF MICROSTRUCTURE IN MICRO-SLOT MEASUREMENT REGIONS

EBSD was used to collect microstructural information in the micro-slotting measurement regions. Data was collected using a Nordlys detector situated within the SEM-FIB system. Electron backscatter patterns (EBSPs) were acquired using an electron beam acceleration voltage of 20 kV, a current of 11 nA, and a step size of 0.1 μm. The EBSD microstructural maps were created using AzTec software.

Due to the effects of the ion beam on the near-surface region during pattern milling, EBSPs were unable to be collected from the milled pattern regions surrounding each micro-slot. Therefore, the sample was polished for 3 minutes using colloidal silica to remove the ion beam-affected area so that EBSPs could be collected in the patterned regions and a local microstructural map could be acquired for each micro-slot measurement. The amount of material removed during this polishing step was estimated to be < 1 μm [26]. Plots of both the displacement magnitude measured at each grid point and the residual stress interpolated at each grid point using the isotropic FE model were then compared to the local microstructure maps. This allowed for observation of microstructural effects on local residual stress relaxation.

2.5 EFFECTS OF LOCAL ELASTIC PROPERTIES ON MICRO-SLOTTING MEASUREMENTS

The use of isotropic elastic constants presents a prominent source of error for the micro-slotting technique. The high anisotropy of the Ti α phase [27] adds error at the micron scale where residual stress relaxation is dominated by local elastic properties. The Ti-6Al-4V microstructure of the sample used in this study was observed to primarily

consist of the hexagonal α phase. Therefore, the maximum effects of anisotropy on the micro-slotting measurements can be estimated using the single-crystal elastic properties of the α phase [28]. With the maximum-stiffness α grain direction oriented perpendicular to the slot length, the use of the isotropic FE model would result in ~25% underestimation of the residual stress magnitude. The minimum stiffness direction oriented perpendicular to the slot length would result in ~8% overestimation of the residual stress magnitude.

The effect of grain orientation on the residual stress interpolated around each slot could be more accurately estimated by obtaining the Euler angles of the α grains in each measurement region with EBSD and then calculating the directional elastic modulus using the single crystal elastic properties [29]. While this calculation is rather simple for micro-slots that are milled in single α grains, it is much more difficult for complex microstructural regions containing multiple α grains or both the α and β phases. Therefore, no attempt was made to correct the micro-slotting residual stress measurements for local elastic property variation in this study. However, potential effects of anisotropy are still discussed for the micro-slot measurement regions evaluated in the next section.

The microstructure below the exposed surface will also significantly contribute to the displacement of the material around each slot and will further complicate data correction. An incremental milling procedure can be used to evaluate the microstructure in the local region throughout the measurement gauge volume. This was performed as part of a recent study by F. Archie et al. in which the micro ring-core method was used to measure residual stress distribution in lath martensite [30]. Due to the large number of micro-slotting measurements performed in this study, observations were solely based on the microstructure information collected from the exposed surface.

2.6 OTHER POTENTIAL ERROR SOURCES IN MICRO-SLOTTING METHOD

The cross-section preparation of the sample prior to performing the micro-slotting measurements was assumed to result in complete relief of the out-of plane σy residual stress component, and introduction of this free surface via sectioning affects the in-plane stress state. Correction via mathematical approach [16] or FE modeling should be used to accurately estimate the extent of the modified stress state prior to incorporating the data into design practices. The measurements presented in this study were not corrected for this effect.

Use of the FIB for pattern milling is understood to affect the near-surface region of the sample due to implantation of Ga ions [31]. Previous research suggests that ion implantation may result in the creation of an amorphous layer at the surface [32] or may induce a compressive residual stress due to volume expansion in the ion-implanted region [33, 34]. In accordance with a previous study [18], the depth of the affected region was assumed to be shallow in comparison to the slot depth and any potential effects on the residual stress measurements presented in this study were assumed to be insignificant.

Other potential sources of error include near-surface stresses induced during the polishing procedure and DIC errors resulting from image artifacts caused by insufficient SEM calibration. No consistent effects were observed in the measured displacements and the corresponding residual stress magnitudes. Thus, effects of these errors on the micro-slotting measurements presented in this study were presumed to be negligible.

3. RESULTS

3.1 RESIDUAL STRESS MEASUREMENTS

Figure 4 shows the micro-slotting measurements of the sub-surface σ_x residual stress component in the grid region plotted against the XRD residual stress measurements. The XRD measurements show the typical sub-surface residual stress profile that is induced by shot peening. The significant scatter that is observed among the micro-slotting data points is expected due to the local nature of the technique. The XRD measurements average the residual stress over a 2 mm × 2 mm area at each depth, thus providing measurements of the macroscopic residual stress state. On the other hand, the residual stresses measured by the micron-scale gauge volume of the micro-slotting technique are dominated by local microscopic residual stresses. While the compressive residual stress magnitudes measured by the micro-slotting technique vary significantly from ~300 MPa to ~900 MPa, the average of the data points within the grid approaches the residual stress magnitude that is measured by XRD. XRD measures a compressive residual stress of ~650 MPa at a depth of ~70 MPa, while the grid of micro-slots measures an average compressive residual stress of ~590 MPa. Averaging the micro-slotting measurements presents a simulated residual stress value resulting from a larger measurement volume. Since this average value is comparable to the residual stress measured by XRD, an assumption can be made that the individual micro-slotting measurements are accurate summations of the macroscopic and microscopic residual stresses present in the sample. In other words, the deviations between the micro-slotting measurements and the macroscopic stress state estimated by XRD can be attributed to local microstructure effects.

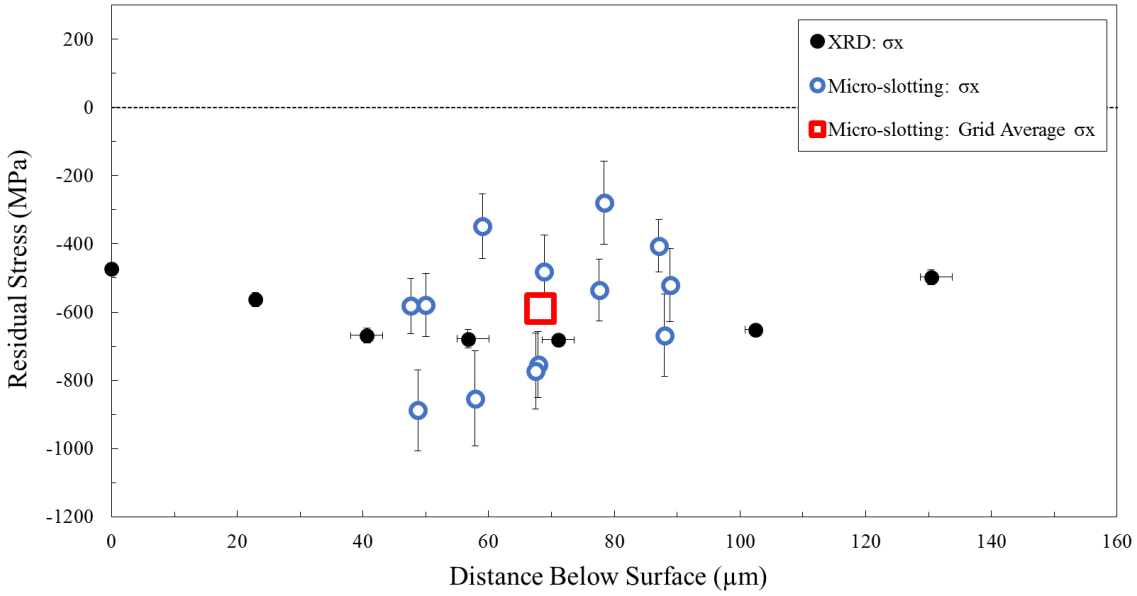

Figure 4. XRD and micro-slotting results measuring sub-surface σ_x residual stress component. Micro-slotting measurements are dominated by microscopic residual stresses and show expected scatter. Average of σ_x measurements within the grid approaches residual stress magnitude measured by XRD.

Figure 5 shows the micro-slotting measurements of the sub-surface σ_z residual stress component in the grid region. Again, the micro-slotting measurements show expected scatter as a result of the local nature of the technique. Higher magnitude σ_z residual stresses are detected in the upper portion of the grid region at a depth of 50-60 µm below the shot peened surface, and this most likely indicates the presence of a σ_z gradient within the grid region. The average σ_z value for the grid region was calculated to be a compressive residual stress with a magnitude of ~210 MPa.

While the average σ_z residual stress component for the grid region is of considerably low magnitude relative to the calculated average σ_x residual stress component, the consistent measurement of non-zero values throughout the grid region

indicates the presence of a shear stress component σ_{xz} below the sample surface. In order to determine the direction and magnitude of this component, two additional micro-slotting measurements were performed with the slot lengths oriented 45° relative to the shot peened surface. Averaging the two measurements allowed for a σ_{xz} estimation of +90 MPa. Thus, the two sub-surface principal residual stress components and corresponding rotation could be calculated. These values were determined as σ_1 = -610 MPa, σ_2 = -190 MPa, and Θ = 13°, with Θ being a counter-clockwise rotation.

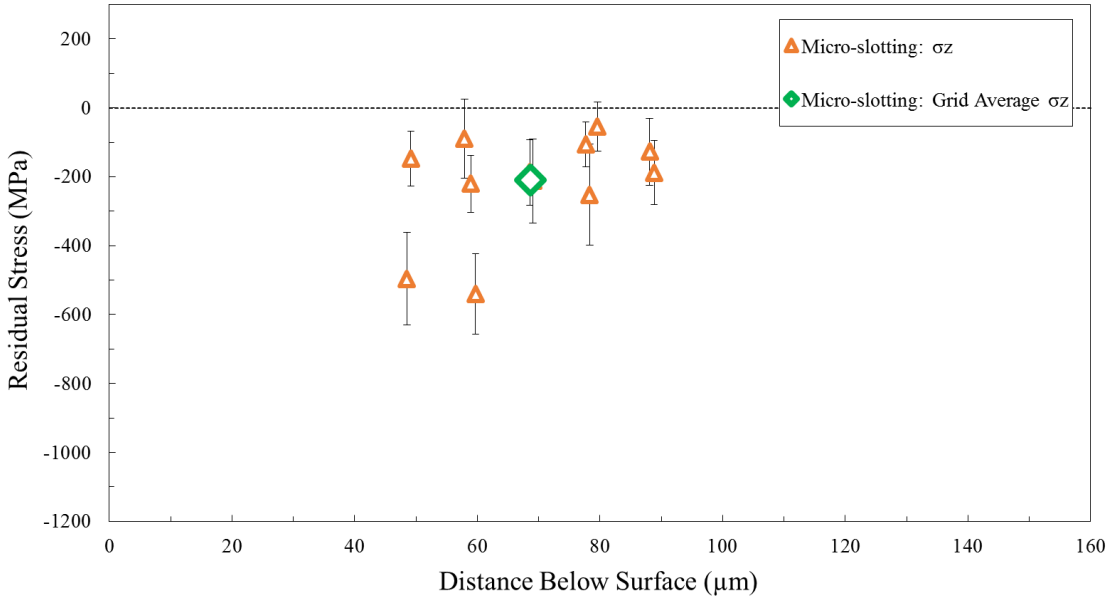

Figure 5. Micro-slotting results measuring sub-surface σ_z residual stress component. Measurements again show considerable scatter due to local nature of technique. Significant magnitudes of σ_z measurements indicate presence of σ_{xz} residual stress component.

3.2 OBSERVATIONS OF LOCAL MICROSTRUCTURE EFFECTS

Qualitative observations of microstructure effects on each micro-slotting residual stress measurement performed in this study were made by overlaying the data plots of the displacement magnitudes measured at each grid point and the local microstructure images created using the EBSD software. Plots of the residual stress interpolated at each grid point were also overlaid with the local microstructure images in order to more clearly see distinct differences in residual stress within the grids. The residual stress at each grid point was interpolated using the isotropic FE model described in the previous section.

The data plots and microstructure images were evaluated for all measurement locations and showed several consistencies related to stress direction, elastic modulus differences in neighboring grains, and local phase distribution. The measurement regions selected for this section summarize the consistencies that were made in these observations. Results are shown and described for six micro-slots in total. Four of the micro-slots shown in this section were oriented perpendicular to the shot peened surface for measurement of the σ_x residual stress component, while the other two micro-slots were oriented parallel to the shot peened surface for measurement of the σ_z residual stress component.

Figure 6 shows the displacement magnitude and residual stress plots for a micro-slot that was milled perpendicular to the shot peened surface and in a single α grain region. This measurement provided a σ_x compressive residual stress value of ~750 MPa at a depth of ~70 μm below the shot peened surface, which is similar to the residual stress magnitude measured by XRD.

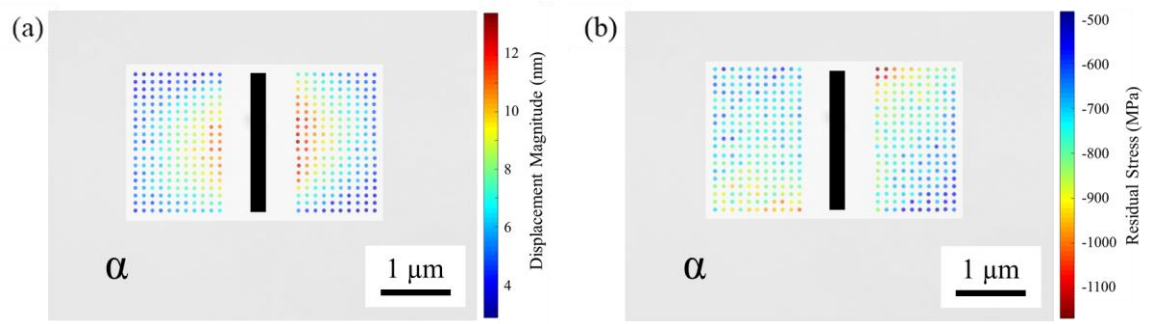

Figure 6. Data plots for a σ_x micro-slot measurement in single α grain region. (a) Displacement magnitude plot shows near-symmetric strain distribution with slight counter-clockwise rotation of the residual stress component perpendicular to slot length. (b) Residual stress plot indicates resultant errors in residual stress interpolation due to use of FE model.

The near-symmetric strain plot for this micro-slotting measurement (Figure 6a) indicates a small counter-clockwise rotation of the residual stress component perpendicular to the slot length. The FE model used to interpolate a residual stress value at each grid point assumes a residual stress component that is perfectly perpendicular to the slot length. The use of this model therefore results in residual stress interpolation errors, with the most significant errors occurring at the grid points closest to the slot ends. These errors are evident in the residual stress plot (Figure 6b).

Figure 7 shows the displacement magnitude and residual stress plots for a micro-slot that was milled in a more complex microstructural region. This slot was also milled perpendicular to the shot peened surface for measurement of the σ_x residual stress component, resulting in a compressive residual stress measurement of ~890 MPa at a depth of ~50 μm below the shot peened surface.

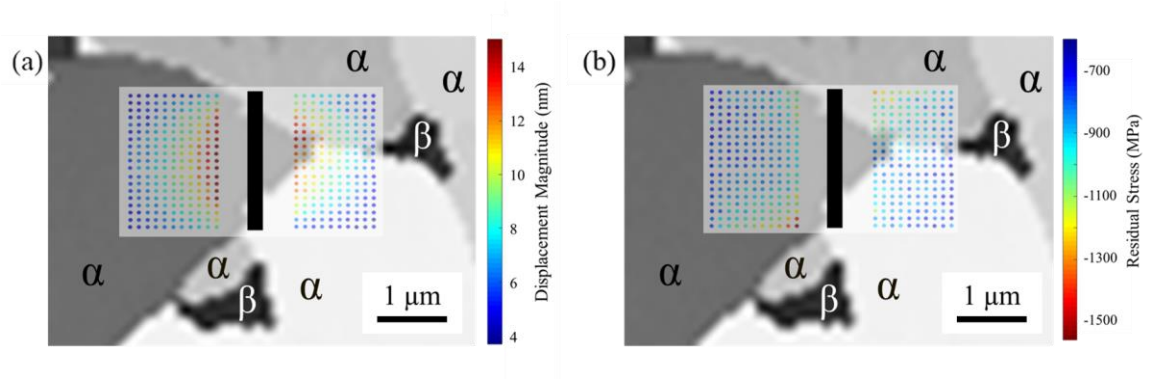

Figure 7. Data plots for a σ_x micro-slot measurement in more complex microstructural region. (a) Displacement magnitudes near slot edges indicate slight rotation of residual stress component perpendicular to the slot. (b) Residual stress plot shows high magnitude stresses interpolated at some grid points. Possible explanations include stress rotation and presence of β phase. Interpolated stresses also appear to increase approaching grain boundary regions.

The displacement plot for this micro-slot (Figure 7a) is very symmetric, yet close observation of the displacements measured near the slot edges suggests a small counter-clockwise rotation of the residual stress component that lies perpendicular to the slot. The increased complexity of the microstructural region is apparent in the residual stress plot for this measurement location (Figure 7b). Residual stresses of very high magnitude (~1400 MPa) were detected on the left side of the slot close to the slot edge. The presence of the β grain towards the bottom of the microstructure image serves as a possible explanation for this, since the lower elastic modulus of the β phase would result in overestimation of the residual stresses interpolated using the FE model. The β phase region in the microstructure image may extend into the region below the exposed surface. Additional β phase may also be present at the α grain boundaries in this region.

The residual stress plot overlaid with the microstructure in Figure 7b also suggests that the interpolated residual stress magnitudes increase approaching grain boundary regions. The grid points on the left side of the slot that measure a residual stress magnitude of ~1000 MPa appear to follow the grain boundaries of the α grain, while the residual stress magnitude detected toward the middle of the grain is ~800 MPa. The same trend is observed on the right side of the slot, although not as clearly.

The slight rotation of the residual stress component perpendicular to the slot length suggested by the displacement plot would result in additional errors in the residual stress plot, similar to those shown in Figure 6b. However, separating these errors from the microstructure-related effects is difficult. Improved analysis of the microscopic residual stress sources shown in this measurement region, including grain boundary presence and local phase distribution, would most likely be accomplished using a smaller micro-slot gauge volume.

Figure 8 shows the displacement magnitude and residual stress plot for another micro-slot that was milled in a complex microstructural region. The slot was milled perpendicular to the shot peened surface to give a σ_x compressive residual stress magnitude of ~850 MPa at a depth of ~60 μm below the shot peened surface. Unlike the displacement plots shown in Figures 6 and 7, the displacement plot for this micro-slot (Figure 8a) is not symmetric. A large range of displacement magnitudes are measured on the left side of the slot, and this variance correlates to interpolated residual stress values that range from -500 MPa to -1100 MPa, as shown in the residual stress plot (Figure 8b).

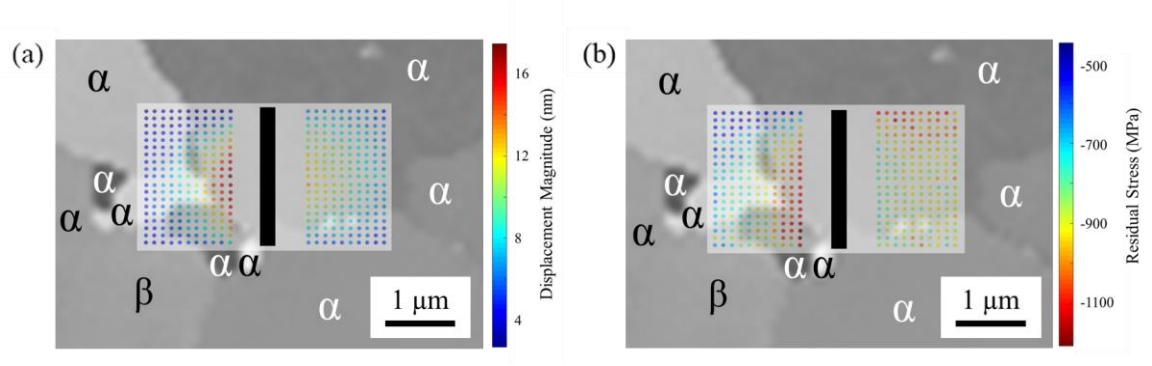

Figure 8. (a) Displacement magnitude and (b) residual stress plots for additional σ_x micro-slot measurement in complex microstructural region. Plots show large range of measured displacements and interpolated residual stress values on left side of slot. Assuming β grain extends toward slot below exposed surface, lower elastic modulus would cause larger displacements near slot edge, and stress relaxation would be constrained by surrounding α grains.

The local microstructure image shows several α grains and a single β grain in the lower left corner. The presence of this β grain offers a possible explanation for the larger range of displacements observed on the left side of the slot. Assuming that the β grain extends toward the slot below the patterned region, the lower elastic modulus of the β phase would result in significantly larger grid point displacements. The residual stress relaxation in the β phase region would then be constrained by the surrounding α grains.

The source of the high magnitude stresses on the right side of the slot is not clear. The stresses appear to increase toward the top edge of the slot, and this may be measurement error associated with the rotated stress direction. The other residual stress magnitudes measured on the right side of the slot are significantly higher than the residual stress magnitude measured by XRD and may be a result of different elastic properties in this measurement region. However, determining which specific grains are influential on the residual stress relaxation is difficult due to the complex microstructure.

Figure 9 shows the displacement magnitude and residual stress grid outputs for an additional micro-slotting measurement location. This slot was milled perpendicular to the shot peened surface for measurement of the σ_x residual stress component, resulting in a compressive residual stress magnitude of ~480 MPa at a depth of ~70 μm below the shot peened surface.

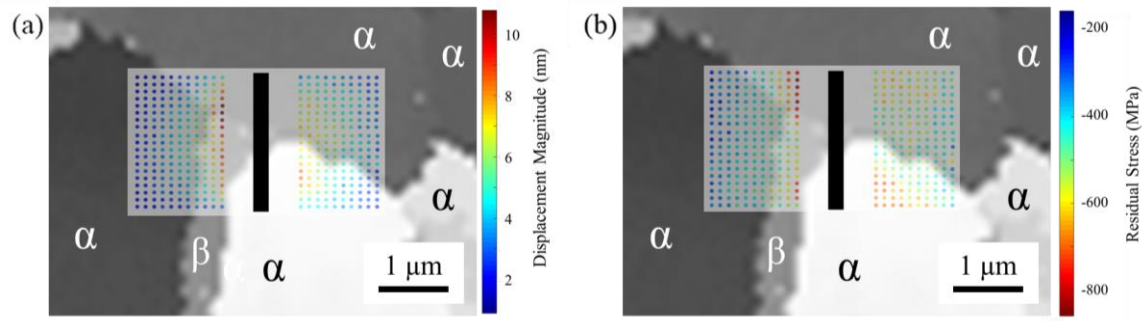

Figure 9. Data plots for additional σ_x micro-slot measurement region. (a) Displacement magnitude plot indicates near-symmetric strain distribution around slot, with larger range of displacements measured on left side. (b) Residual stress plot suggests that β grain presence is responsible for larger residual stresses detected near slot edge and that distinct differences in interpolated residual stress magnitudes on right side of slot are result of different elastic moduli in corresponding α grains.

The displacement magnitude plot for this slot (Figure 9a) shows a larger range of measured displacement magnitudes on the left side of the slot, in comparison to those measured on the right side of the slot. The residual stress plot (Figure 9b) shows the corresponding range of interpolated residual stresses on the left side of the slot, which range from ~800 MPa in magnitude near the slot edge to ~300 MPa at the left edge of the grid. The higher magnitude residual stresses detected near the slot edge are most likely due to the presence of the β grain in the lower left region of the grid. Assuming the β grain extends toward the slot

below the exposed surface, significantly larger displacements would be expected due to the lower elastic modulus of the β phase. Similar to the observations made for Figure 8, the residual stress relaxation in the β phase is then constrained by the neighboring α grains.

The residual stress plot also reveals a region of residual stress on the right side of the slot that is ~700 MPa in magnitude while the other grid points on the right side of the slot measure residual stress magnitudes of 400-600 MPa. The microstructure image suggests that this difference is a result of the different elastic moduli of the corresponding α grains.

Figures 10 and 11 show the displacement magnitude and residual stress plots for micro-slots that were milled parallel to the shot peened surface in order to measure the σ_z residual stress component. Figure 10 shows the plots for a micro-slotting measurement that was milled in a single α grain region and resulted in a compressive residual stress magnitude of ~210 MPa at a depth of ~70 μm below the shot peened surface, which is equivalent to the average σ_z value calculated for the measurement grid region.

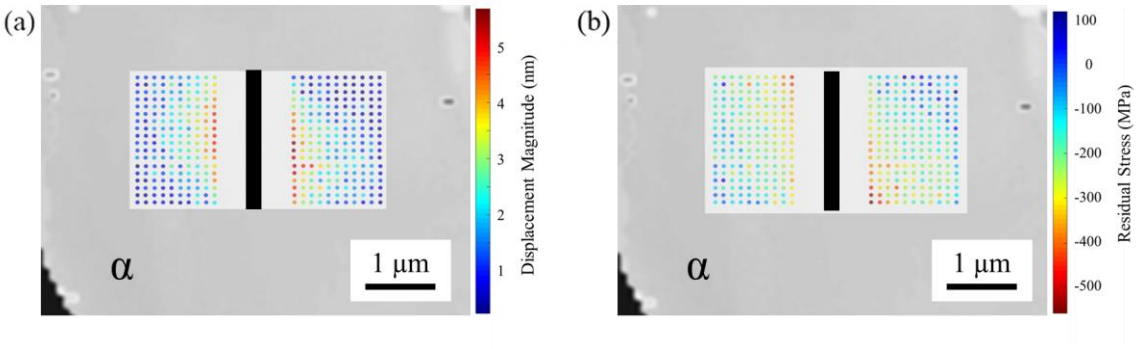

Figure 10. Data plots for σ_z micro-slot measurement in single α grain region. (a) Displacement magnitude plot indicates that stress relaxation is dominated by higher magnitude principal residual stress component. (b) Residual stress plot shows corresponding errors in residual stress interpolation due to use of FE model.

Most evident in this displacement plot (Figure 10a) is the rotation of the residual stress relaxation, which appears to be dominated by the higher magnitude principal residual stress component σ_1 that was calculated in the previous section. This rotation then correlates to errors in the residual stress plot (Figure 10b) due to the use of the FE model.

Figure 11 shows plots for a micro-slotting measurement that was milled in a more complex microstructural region and gave a compressive residual stress magnitude of ~250 MPa at a depth of ~80 µm below the shot peened surface.

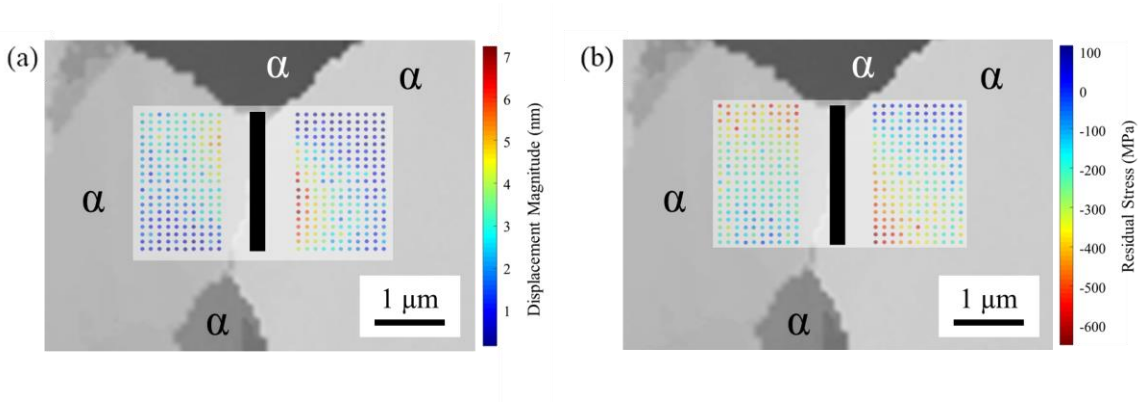

Figure 11. Data plots for σ_z micro-slot measurement in complex microstructural region. (a) Displacement plot again indicates that stress relaxation is dominated by σ_1 principal residual stress component. (b) Residual stress plot shows corresponding errors in residual stress interpolation due to use of FE model.

Again, the most evident feature in the displacement magnitude plot (Figure 11a) is the rotation of the stress component. The direction of residual stress relaxation correlates with the rotation that was calculated for the σ_1 principal residual stress component and resembles the rotation that was observed for the previous micro-slot measurement shown in Figure 10. The corresponding errors associated with using the FE model are shown in the residual

stress plot (Figure 11b) and appear as both higher and lower magnitude residual stresses at the top and bottom of the grid.

4. DISCUSSION

The slot size chosen for this study was small relative to the grain sizes observed in the local EBSD maps, and the residual stress relaxation observed around the slots milled in complex microstructure regions was therefore dominated by microscopic stresses. Micro-slots milled in single α grain regions gave residual stress values closest to the macroscopic residual stress values predicted by XRD and by averaging the micro-slotting measurements over the entire grid region. Furthermore, no microstructural effects were visible in the strain plots for these measurement regions. On the other hand, micro-slots milled in complex microstructure regions gave residual stress values that deviated from the macroscopic residual stress value, and the corresponding displacement magnitude and interpolated residual stress plots allowed for evaluation of these effects relative to the microstructure. However, convolution of these effects, combined with errors resulting from the rotated stress direction, limited the observations in this study to those of a qualitative nature. Improved analysis and quantification of the microscopic residual stresses that result from the phenomena observed in this study may be accomplished by decreasing the gauge volume of the micro-slotting measurements.

The results of this work therefore suggest that the micro-slotting technique could be modified to measure macroscopic or microscopic residual stresses by changing the slot size relative to the grain size of the material. This is similar to an observation made for the micro ring-core method in a previous study performed by J. Everearts et al. [21]. Increasing

the micro-slot gauge volume would allow the microstructure in the measurement region to become more representative of the bulk material. As a result, measurement errors due to local anisotropy, grain boundary presence, and local phase distribution would be minimized. The comparison of the micro-slotting and XRD residual stress measurements presented in this study provides an illustration of this effect. By averaging the micro-slotting measurements, the effective volume of the measurement technique is increased, and the average residual stress value approaches the macroscopic residual stress measured by XRD. This also suggests that an ideal measurement volume exists relative to the grain size of the material that will minimize the effects of microscopic residual stresses on micro-slotting measurements of the macroscopic residual stress state.

5. CONCLUSION

In this study, a grid of $2 \times 0.2 \times 3\ \mu m^3$ gauge volume micro-slotting residual stress measurements were performed in a high compressive residual stress sub-surface region of a shot peened Ti-6Al-4V sample. Micro-slots were milled both perpendicular and parallel to the shot peened surface for measurement of the σ_x and σ_z residual stress components, respectively. The macroscopic residual stress state in the grid region was estimated by averaging the micro-slotting measurements, and the average σ_x value was found to be in close agreement with the macroscopic residual stress measured by XRD. Thus, the micro-slotting residual stress measurements were assumed to be accurate summations of the macroscopic and microscopic residual stresses present in the grid region. Additional measurements were performed near the grid region in order to measure the σ_{xz} residual stress component, and the principal residual stress components and corresponding rotation

were then calculated. The presence of this rotation was confirmed by the displacement magnitude plots for the micro-slotting measurements.

In addition to local measurement of residual stress, the micro-slotting strain outputs provided information regarding residual stress direction and local microstructure effects. For each measurement region, plots of the displacement magnitudes and interpolated residual stresses were overlaid with local microstructure maps obtained using EBSD. This novel approach allowed for evaluation of microstructure effects on local residual stress relaxation and the corresponding errors in the residual stress interpolation using an isotropic FE model. These effects included changes in residual stress approaching grain boundaries, elastic modulus differences in neighboring α grains, and constrained relaxation due to local phase distribution. However, the convolution of these effects in complex microstructure measurement regions limited the ability to quantitatively analyze the sources of the local residual stress variations. A smaller micro-slot gauge volume would be ideal for isolation and accurate quantification of these effects. The results of this study also suggest that the use of a larger micro-slot gauge volume, relative to the grain size of the material, would allow for minimized influence of microscopic residual stresses on measurement of the macroscopic residual stress state.

ACKNOWLEDGMENTS

This project was supported by the Air Force Research Lab (AFRL)-managed Metals Affordability Initiative (MAI). This work is a collaborative research effort of Boeing and Missouri S&T and was made possible by Boeing's presence on the Missouri S&T campus in Rolla, MO.

REFERENCES

[1] M.N. James, Residual stress influences on structural reliability, Eng. Failure Anal. 18 (2011) 1909-1920. https://doi.org/10.1016/j.engfailanal.2011.06.005.

[2] A. Korsunsky, A Teaching Essay on Residual Stresses and Eigenstrains, Butterworth-Heinemann, Oxford, 2017.

[3] P.J. Withers, H.K.D.H. Bhadeshia, Residual stress: Part 1 – Measurement techniques, Mater. Sci. Technol. 17 (2001) 355-365. https://doi.org/10.1179/026708301101509980.

[4] P.J. Withers, H.K.D.H. Bhadeshia, Residual stress: Part 2 – Nature and origins, Mater. Sci. Technol. 17 (2001) 366-375. https://doi.org/10.1179/026708301101510087.

[5] G.Schajer, Practical Residual Stress Measurement Methods, John Wiley & Sons, Chichester, 2013.

[6] G.S. Schajer, Relaxation methods for measuring residual stresses: Techniques and opportunities. Experimental Mechanics 50 (2010) 1117-1127. https://doi.org/10.1007/s11340-010-9386-7

[7] I.C. Noyan, J.B. Cohen, Residual stress: measurement by diffraction and interpretation, Springer-Verlag, New York, 1987.

[8] E. Macherauch, Residual stresses, in: G.C. Sih, E. Sommer, and W. Dahl (Eds.), Application of Fracture Mechanics to Materials and Structures, Springer Netherlands, Dordrecht, 1984, pp. 157-192. https://doi.org/10.1007/978-94-009-6146-3_7

[9] A.J.G. Lunt, N. Baimpas, E. Salvati, I.P. Dolbya, T. Sui, S. Ying. H. Zhang, A.K. Kleppe, J. Dluhos, A.M. Korsunsky, A state-of-the-art review of micron-scale spatially resolved residual stress analysis by FIB-DIC ring-core milling and other techniques, J. Strain Anal. Eng. Des. 50 (2015) 426-444. https://doi.org/10.1177/0309324715596700

[10] J.S. Chung, G.E. Ice, Automated indexing for texture and strain measurement with broad-bandpass x-ray microbeans, J. Appl. Phys. 86 (1999) 5249-5255. https://doi.org/10.1063/1.371507

[11] A.J. Wilkinson, G. Meaden, D.J. Dingley, High-resolution elastic strain measurement from electron backscatter diffraction patterns: New levels of sensitivity, Ultramicroscopy 106 (2006) 307-313. https://doi.org/10.1016/j.ultramic.2005.10.001

[12] A. Lunt, A.M. Korsunsky, A review of micro-scale focused ion beam milling and digital image correlation analysis for residual stress evaluation and error estimation, Surf. Coat. Technol. 283 (2015) 373-388. https://doi.org/10.1016/j.surfcoat.2015.10.049

[13] K.J. Kang, N. Yao, M.Y. He, A.G. Evans, A method for in situ measurement of the residual stress in thin films by using the focused ion beam, Thin Solid Films 443 (2003) 71-77. https://doi.org/10.1016/S0040-6090(03)00946-5

[14] N. Sabate, D. Vogel, A. Gollhardt, J. Keller, C. Cane, I. Gracia, J.R. Morante, B. Michel, Residual stress measurement on a MEMS structure with high-spatial resolution. J. Microelectromech. Syst. 17 (2007) 365-372. 10.1109/JMEMS.2006.879701

[15] A.M. Korsunsky, M. Sebastiani, E. Bemporad, Focused ion beam ring drilling for residual stress evaluation, Mater. Lett. 63 (2009) 1961-1963. https://doi.org/10.1016/j.matlet.2009.06.020

[16] A. Lunt, E. Salvati, L. Ma, I.P. Dolbnya, T.K. Neo, A.M. Korsunsky, Full in-plane strain tensor analysis using the microscale ring-core FIB milling and DIC approach, J. Mech. Phys. Solids 94 (2016) 47-67. https://doi.org/10.1016/j.jmps.2016.03.013

[17] I. Violatos, M. Thomas, J.B. Castle, B.P. Wynne, Sub-surface plastic and elastic strain fields and fatigue performance of drilled titanium plates, in: V. Venkatesh, A.L. Pilchak, J.E. Allison, S. Ankem, R.R. Boyer, J. Christodoulou, H.L. Fraser, M.A. Imam, Y. Kosaka, H.J. Rack, A. Chatterjee, A. Woodfield (Eds.), Proceedings of the 13th World Conference on Titanium, Wiley-TMS, New Jersey, 2015, pp. 1035-1040.

[18] E. Burns, J. Newkirk, J. Castle, Micro-slotting technique for reliable measurement of sub-surface residual stress in Ti-6Al-4V, J. Strain Anal. Eng. Des. 53 (2018) 389-399. https://doi.org/10.1177/0309324718778225

[19] J. Everaerts, E. Salvati, F. Uzun, L.R. Brandt, H. Zhang, A.M. Korsunsky, Separating macro- (Type I) and micro- (Type II+III) residual stresses by ring-core FIB-DIC milling and eigenstrain modelling of a plastically bent titanium alloy bar, Acta Mater. 156 (2018) 43-51. https://doi.org/10.1016/j.actamat.2018.06.035

[20] E. Salvati, A.M. Korsunsky, An analysis of macro- and micro-scale residual stresses of Type I, II and III using FIB-DIC micro-ring-core milling and crystal plasticity FE modelling, Int. J. Plast. 98 (2017) 123-138. https://doi.org/10.1016/j.ijplas.2017.07.004

[21] J. Everaerts, X. Song, B. Nagarajan, A.M. Korsunsky, Evaluation of macro- and microscopic residual stresses in laser shock-peened titanium alloy by FIB-DIC ring-core milling with different core diameters, Surf. Coat. Technol. 349 (2018) 719-724. https://doi.org/10.1016/j.surfcoat.2018.06.043

[22] I. Basu, V. Ocelik, J.T.M. De Hosson, Experimental determination and theoretical analysis of local residual stress at grain scale, in: D. Northwood, T. Rang, J. De Hosson, C.A. Brebbia (Eds.), WIT Transactions in Engineering Sciences, Vol. 116, WIT Press, Southampton, England, 2017, pp. 3-14. 10.2495/MC170011

[23] ASTM B265-15. Standard specification for titanium and titanium alloy strip, sheet and plate.

[24] AMS2431:2017. Peening media, cast steel shot, regular hardness.

[25] B.D. Cullity. Elements of X-ray Diffraction, second ed., Addison-Wesley, Reading, MA, 1978.

[26] S. Babu, Advances in Chemical Mechanical Planarization, Woodhead Publishing, Cambridge, 2016.

[27] G. Lütjering, J.C. Williams, Titanium, Springer-Verlag, Berlin, 2007.

[28] D. Tromans, Elastic anisotropy of HCP metal crystals and polycrystals. Int. J. Res. Rev. Appl. Sci. 6 (2011) 462-483.

[29] A.S. Norwick, B.S. Berry, Anelastic Relaxation in Crystalline Solids, Academic Press, New York, 1972.

[30] F. Archie, M.Z. Mughal, M. Sebastiani, E. Bemporad, S. Zaefferer, Anisotropic distribution of the micro residual stresses in lath martensite revealed by FIB ring-core milling technique, Acta Mater. 150 (2018) 327-338. https://doi.org/10.1016/j.actamat.2018.03.030

[31] M. Nastasi, J.W. Mayer, Ion Implantation and Synthesis of Materials, Springer-Verlag, Berlin, 2006.

[32] S. Prussin, D.I. Margolese, R.N. Tauber, Formation of amorphous layers by ion implantation. J. Appl. Phys. 57, 180 (1985) 180-185. https://doi.org/10.1063/1.334840

[33] T.J. Kang, J.G. Kim, J.S. Lee, J.H. Lee, J.H. Hahn, H.Y. Lee, Y.H. Kim, Low-thermal-budget and selective relaxation of stress gradients in gold micro-cantilever beams using ion implantation. J. Micromech. Microeng. 15 (2005) 2469-2478. https://doi.org/10.1088/0960-1317/15/12/032

[34] K. Dahmen, M. Giesen, J. Ikonomov, K. Starbova, H. Ibach, Steady-state surface stress induced in noble gas sputtering. Thin Solid Films 428 (2003) 6-10. https://doi.org/10.1016/S0040-6090(02)01182-3

IV. MICRO-SCALE RESIDUAL STRESS MEASUREMENTS ACROSS INTERFACES IN AN LFMT Ti-6Al-4V BUILD

Elizabeth Burns[1,2], Joseph Newkirk[1], and James Castle[2]

[1]Department of Materials Science and Engineering

Missouri University of Science and Technology

Rolla, MO, USA

[2]Boeing Research and Technology

St. Louis, MO, USA

To be submitted for publication in *Additive Manufacturing*

ABSTRACT

Residual stress build-up in additive manufacturing can negatively impact mechanical properties or result in distortion of the finished parts. Recent developments in micro-scale stress relaxation measurement techniques have shown them to be capable of providing spatially resolved residual stress data in complex geometries and suggest the use of these techniques for understanding residual stress origins in additive manufacturing processes. This study therefore demonstrates the use of the micro-slotting technique for measurement of local residual stress in additive manufactured (AM) components. Micro-slotting residual stress measurements were performed across two different interfaces in samples sectioned from a complex Ti-6Al-4V geometry built with laser freeform manufacturing technology (LFMT). The build consisted of a large oval-shaped thin wall structure and support stiffeners deposited on a baseplate of the same alloy. The first sample was acquired from a baseplate-build wall interface region, and the second sample was acquired from a build wall-stiffener interface region near the top of the build. The micro-slots were oriented to capture the residual hoop stress in the thin wall. Post-measurement optical microscopy allowed for verification of the measurement locations relative to the interfaces and for analysis of the residual stress data at the microstructural level.

1. INTRODUCTION

Laser freeform manufacturing technology (LFMT) is a direct laser deposition process in which metal powder is introduced into the focused beam of a high-power laser, thus allowing for deposition of complex near-net-shape metal components [1]. The

movement of the laser causes repeated localized melting and rapid cooling, which leads to thermal expansion and contraction of the material. The resultant permanent inelastic strains [2] can give rise to significant residual stresses in the finished builds.

Residual stress in additive manufactured (AM) parts can have a negative impact on mechanical properties and may result in distortion upon part removal from the baseplate or during subsequent machining processes. Moreover, residual stress accumulation during deposition of large parts can result in significant distortion prior to completion of the build [3, 4]. Accurate estimation of residual stress accumulation during AM processes is accomplished using computational models [5-7], which allow for design-based approaches to residual stress mitigation. However, the accuracy of these models relies on validation using experimental data.

Numerous attempts have been made in recent years to quantify residual stresses in AM parts, and a variety of measurement techniques have been used, including x-ray diffraction [8], neutron diffraction [9], and the contour method [10]. These techniques, however, are limited with regards to spatial resolution and measurement accuracy in complex geometry components [11]. As a result, many previous studies have focused on characterizing the distribution of residual stress in simple build geometries [12-14] and using simple build geometries to investigate effects of process parameters on the residual stress state. Such process parameters include dwell time [15], exposure strategy [16], and laser power and travel speed [17, 18].

In recent years, the development of micro-scale stress relaxation measurement techniques [19-21] has allowed for high-spatial resolution residual stress measurements on complex-shaped components where conventional measurement techniques are not capable

of measuring residual stress. These techniques employ a scanning electron microscope-focused ion beam (SEM-FIB) dual-beam system to mill away micron-scale volumes of material and to acquire electron images of the local regions before and after milling. Digital image correlation (DIC) is then used to resolve the material displacements in the local measurement regions from the electron images, and the original residual stress state in each measurement region is interpolated using analytical or finite element (FE) solutions. Sequential milling of these micro-scale geometries [22] allows for spatially resolved residual stress measurements within micron-range of specific features or locations in a part [23-25].

More recent works demonstrate the capability of these techniques for capturing local residual stress variations that occur as a result of microscopic stresses [23, 26-28]. These stresses are inherent to polycrystalline materials due to the presence of grain boundaries, grain orientation differences in neighboring grains, and changes in local phase distribution. Microscopic residual stresses therefore vary on the order of grain size, while macroscopic residual stresses vary over large distances, most often over the scale of the component. [29]

While the data provided by macroscopic residual stress measurement techniques is ideal for validating distortion predictions, the micro-scale measurement gauge volumes of these new techniques can allow for targeted residual stress measurements in AM parts [30]. This study therefore seeks to demonstrate the use of the micro-slotting technique for measurement of local residual stress in AM components by acquiring residual stress data across two different interfaces in a complex LFMT Ti-6Al-4V build. Two interface regions were sectioned from a large representative geometry consisting of a Ti-6Al-4V oval-shaped

thin wall structure and support stiffeners that was deposited on a baseplate of the same alloy. The first sample was acquired from a baseplate-build wall region, while the second was sectioned from the top of the build in a build wall-stiffener interface region. A series of micro-slotting residual stress measurements was then performed across the interface of interest on each sample, and optical microscopy was used to verify the micro-slotting measurement locations relative to the sample interfaces.

2. MATERIALS AND METHODS

2.1 SAMPLE PREPARATION

A laser-deposited Ti-6Al-4V (ASTM Grade 5 [31]) representative geometry was fabricated onto a 50-mm thick mill-annealed Ti-6Al-4V baseplate using the LFMT process. Process conditions included a laser power of 860 W and a powder feed rate of 6 g/min. The finished build consisted of an oval-shaped thin wall surrounded by eight support stiffeners. Significant distortion was observed in the finished build as a result of internal residual stress.

The first deposited layers of the oval-shaped geometry and surrounding stiffeners were 0.25 mm thick and were built using a contour and hatch approach. The gauge thicknesses of the wall and stiffeners were then incrementally decreased with each layer until the hatch approach was no longer needed, and a contour approach was used to build the remaining thin wall portion. This thin wall was ~2.0 mm wide and consisted of deposited layers with 0.50-mm thickness.

An 18.5 mm × 11.0 mm block containing a portion of the build wall, an attached stiffener, and the underneath portion of the baseplate was sectioned from the original

geometry using a band saw. The two samples of interest for this study, Samples A and B, were then sectioned from this block (Figure 1) using electrical discharge machining (EDM). Distortion was observed in the parts after each sectioning step, indicating relaxation of the macroscopic residual stress state that was present in the original build.

Sample A was sectioned from the baseplate-build wall interface to give approximate dimensions of 19 mm (x) × 11 mm (y) × 25 mm (z). The sample height (z) included ~14 mm of the baseplate. The x-z cross-section surface of the sample was then prepared for micro-slotting measurements.

Sample B was sectioned from the build wall-stiffener interface located ~14 mm below the top of the block that was removed from the original geometry (Figure 1b). The final sample consisted of ~27 mm of the build wall and ~18 mm of the attached support stiffener. Micro-slotting measurements were taken on the cross-sectioned x-y plane.

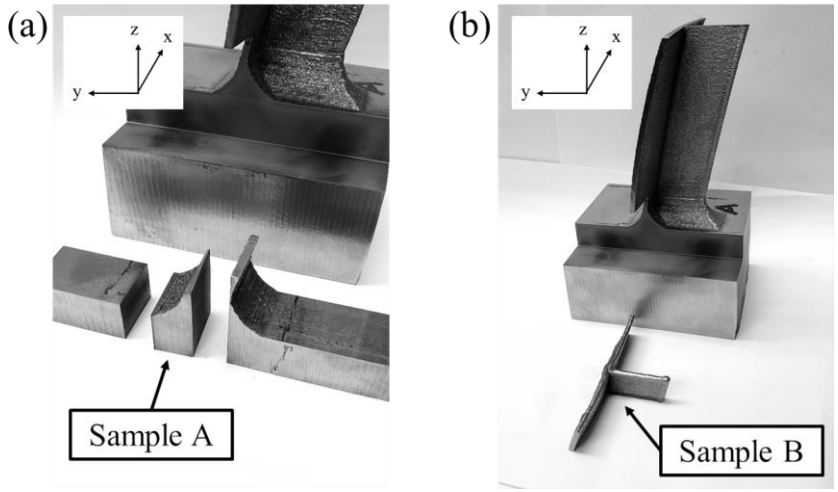

Figure 1. A block containing the build wall, attached stiffener, and baseplate was sectioned from original build geometry using a band saw. (a) Sample A was sectioned from the baseplate-build wall interface, while (b) Sample B was sectioned from the top of the build to include the build wall-stiffener interface. Both samples were sectioned using EDM.

Distortion was observed after most of the sectioning steps that were performed for sample preparation. This indicated relaxation of the macroscopic residual stress state that was present in the original build. For this study, residual stress relaxation due to sectioning was assumed to result in lower magnitudes of residual stress measured in the two samples. The microscopic residual stresses and the distribution of the compressive and tensile residual stresses at the interfaces were assumed to not be affected.

2.2 Ti-6Al-4V MICROSTRUCTURE

A sample with a mirror cross-section to Sample A was sectioned from the block via EDM. This sample was prepared metallographically and etched with Kroll's reagent in order to acquire optical images of the microstructure in both the baseplate and the build wall (Figure 2).

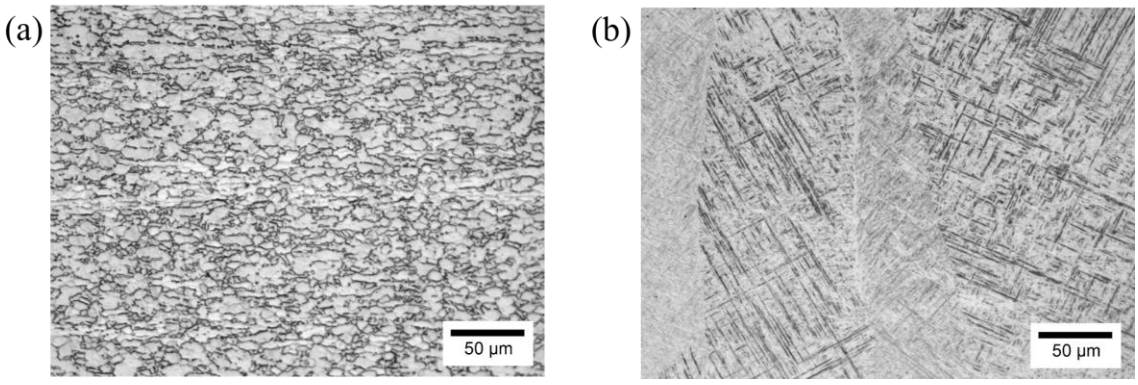

Figure 2. Additional sample was sectioned from the sample block and etched to reveal the baseplate and build microstructure. (a) Mill-annealed microstructure of baseplate consisted of equiaxed α with intergranular β. (b) Microstructure of build wall shows large columnar prior β grains of Widmanstätten α.

The mill-annealed microstructure of the Ti-6Al-4V baseplate (Figure 2a) was determined to consist of equiaxed α with intergranular β. The microstructure of the build wall consists of large columnar prior β grains of basketweave Widmanstätten α laths.

2.3 MICRO-SLOTTING RESIDUAL STRESS MEASUREMENTS

The cross-sectioned surface of interest on each sample was prepared for micro-slotting residual stress measurements by mounting the sample in a conductive bakelite resin and grinding the surface to a 9 μm finish with a diamond suspension. Final polishing was performed for at least 30 minutes using colloidal silica and the lowest force setting in order to minimize any deformation induced during the grinding steps.

A Helios NanoLab 600 focused ion beam/field emission scanning electron microscope (FIB/FESEEM) was used to carry out the micro-slotting procedure. First, the FIB was used to mill local artificial patterns in the measurement regions. The patterns consisted of small surface dots, approximately 100 nm in depth, and were created using a voltage of 30 kV and a current of 93 pA. The corresponding series of $5 \times 0.5 \times 7$ μm^3 micro-slots were then milled using a current of 0.46 nA. Electron beam images of the patterned regions (Figure 3) were taken at 0° stage tilt before and after milling the micro-slots, and these images were acquired using a voltage of 5 kV and a beam current of 0.17 nA. Imaging was performed with the integration filter using a scan speed of 1 μs on 8 frames. Image resolution was 1024 × 884 pixels. A sequential milling procedure was established for this study using the FE analysis approach described in a previous study [23].

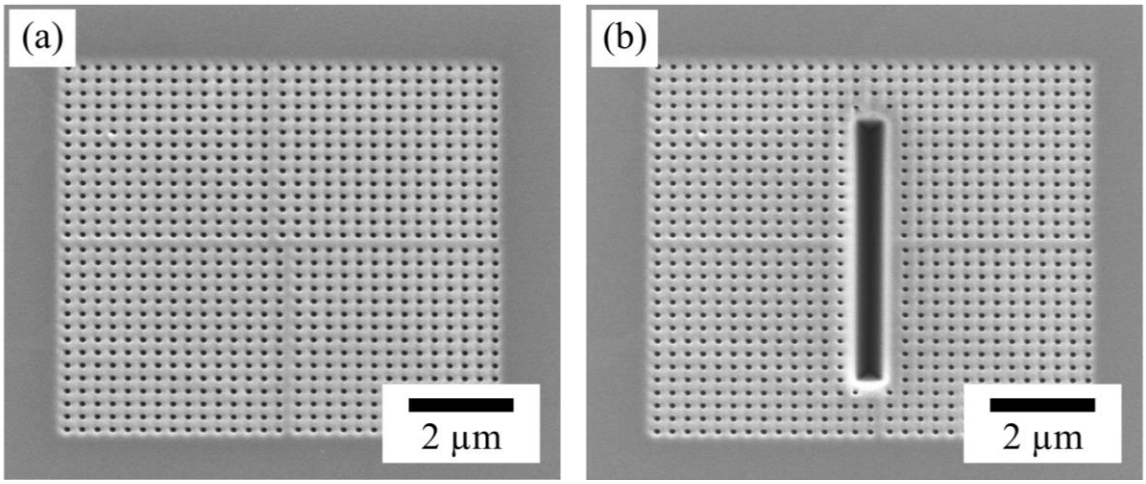

Figure 3. Electron images imported into MATLAB DIC program for measurement of grid point displacements. Images were taken in each patterned region (a) before and (b) after the corresponding 5 × 0.5 × 7 μm^3 micro-slot was milled.

A MATLAB DIC code employing the cpcorr function was used to resolve the displacements of the grid points between the two electron images for each measurement location. The MATLAB code was then used to linearly interpolate a residual stress value from the displacement of each grid point using the surface displacements from a reference stress FE model created in StressCheck®. The 3D FE model employed quarter symmetry, isotropic properties (E = 110 GPa, v = 0.31 [32]), and a uniform compressive stress of 1000 MPa perpendicular to the slot length. For each micro-slotting measurement, a residual stress value was interpolated for each milled grid point on either side of the slot, resulting in an average residual stress value and a standard deviation for each measurement. An outlier removal procedure identical to one used in a previous study [23] was then performed. Each measurement reported in this study was therefore determined using a minimum 60% of the points in the corresponding grid.

A series of micro-slotting measurements was performed on each sample in order to capture the residual stress profile across the specified interface. The micro-slotting measurements were taken towards the middle of each sample in order to avoid regions of significant residual stress relaxation near the sectioned edges. On Sample A, a series of 45 micro-slots was performed in the x-z plane of the build with the slot lengths oriented perpendicular to the baseplate to allow for measurement of the residual stress in the x-direction (Figure 4).

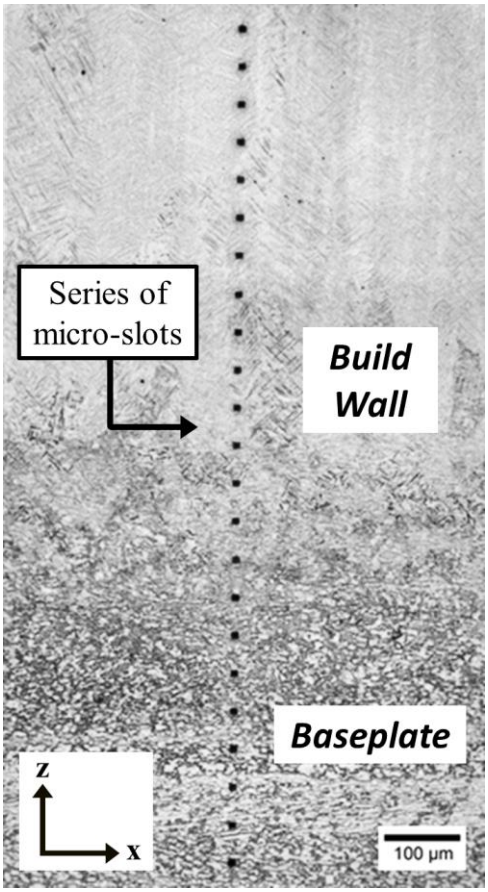

Figure 4. Optical microscope image of micro-slotting measurements performed across baseplate-build wall interface. Micro-slots were performed on cross-sectioned x-z plane and were oriented to measure residual stress in x-direction as a function of z. Etched microstructure allowed for verification of measurement locations relative to interface.

The x-direction corresponds to the residual hoop stress in the oval-shaped thin wall structure of the original build geometry. The spacing between the measurements was approximately 50 µm.

On Sample B, a series of 31 micro-slotting measurements was performed in the x-y plane of the build with the slot lengths oriented parallel to the support stiffener to allow for measurement of the residual stress in the x-direction (Figure 5). Again, the x-direction corresponds to the residual hoop stress in the oval-shaped thin wall structure of the original geometry. The micro-slotting measurements on this sample were also spaced ~50 µm apart.

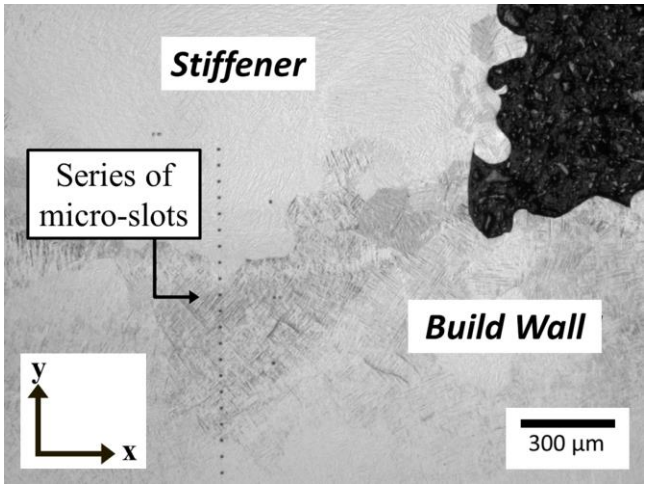

Figure 5. Optical microscope image of micro-slotting measurements performed across build wall-stiffener interface. Micro-slots were performed on cross-sectioned x-y plane and were oriented to measure residual stress in x-direction.

The first measurement was taken ~300 µm away from the inner radius of the oval-shaped thin wall. Subsequent measurements were then performed as a function of increasing y to allow for measurement of the residual stress distribution from the build wall into the

support stiffener. After the residual stress measurements were completed, optical microscopy of the sample allowed for verification of the measurement locations relative to the build wall-stiffener interface. The transition point between the build wall and the stiffener was identified by observing the two corners where the build wall joins the stiffener and then connecting the two corners with a line perpendicular to the series of micro-slotting measurements.

3. RESULTS AND DISCUSSION

3.1 MICRO-SLOTTING RESIDUAL STRESS MEASUREMENTS

The micro-slotting residual stress results for Samples A and B are shown in Figures 6 and 7, respectively. The residual stress profile measured on Sample A (Figure 6) shows compressive residual stress in the baseplate with a magnitude of ~50 MPa. The residual stress profile goes to zero at a depth of 0.7-0.8 mm below the top of the baseplate and becomes a tensile residual stress that is ~50 MPa in magnitude. This tensile residual stress then continues with increasing z into the build wall. The data points in the compressive residual stress region show a significant amount of scatter from one measurement to the next, and this is expected due to the local nature of the micro-slotting technique. The micron-sized gauge volume is strongly affected by microscopic residual stresses, which are understood to be present in the measurement data as variations from the macroscopic stress state.

The amount of scatter observed in this plot resembles the data presented in a previous study in which micro-slotting residual stress measurements of similar gauge volume were used to capture a sub-surface residual stress profile on a shot peened, mill-

annealed Ti-6Al-4V plate [23]. Therefore, the increased scatter observed in the compressive residual stress region may suggest increased microscopic residual stresses in the baseplate due to the characteristic microstructure. However, the plot also indicates that a significant portion of the tensile residual stress region lies within the baseplate. The entire tensile residual stress region shows considerably less scatter among the micro-slotting measurements than the compressive residual stress region. This suggests that the differences observed in the measurement scatter may not be solely related to the microstructure present in the measurement regions.

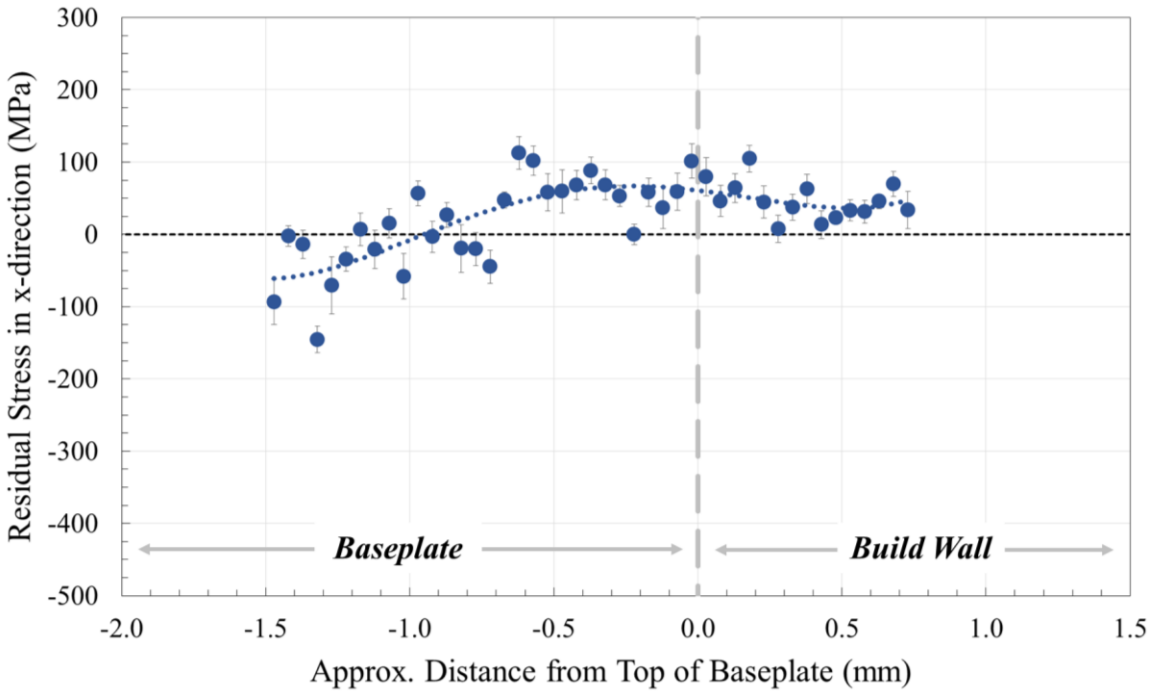

Figure 6. Micro-slotting residual stress measurements for Sample A reveal compressive residual stress region in baseplate that becomes tensile residual stress below top of baseplate. More scatter is observed among measurements in compressive region than among those in tensile region, which may be a result of microscopic stresses in plate material.

The residual stress profile measured on Sample B is displayed in Figure 7 and shows a compressive residual stress in the build wall with a maximum magnitude of ~140 MPa. The magnitude of this compressive residual stress region decreases as the measurements approach the build wall-stiffener interface, and tensile residual stresses are measured in the sampled portion of the support stiffener.

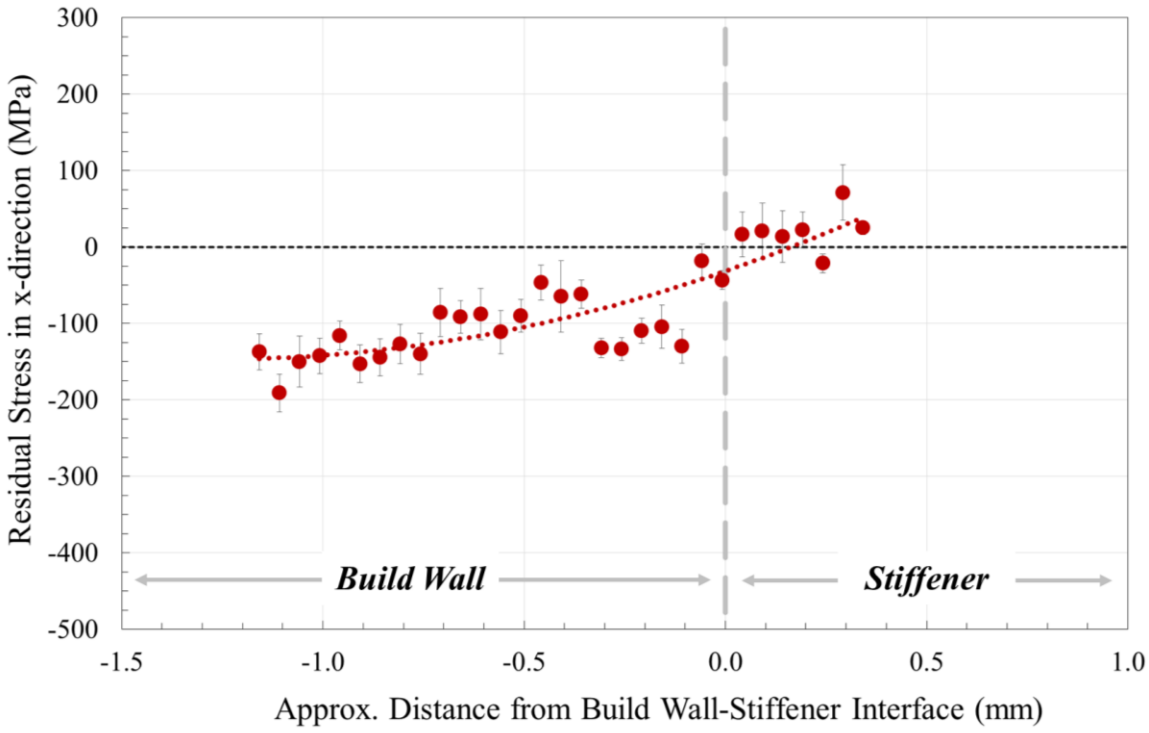

Figure 7. Micro-slotting residual stress results for Sample B show compressive residual stress region in build wall that is balanced by tensile residual stress region in support stiffener. Transition between compressive and tensile regions occurs precisely at interface.

The measurement results for Sample B indicate a transition between the compressive residual stress region and tensile residual stress region that occurs precisely at the build

wall-stiffener interface. The compressive residual hoop stresses in the build wall are evidently balanced by a tensile residual stress in the support stiffener. The scatter among the data points in this plot resembles the reduced scatter observed between adjacent data points in the tensile residual stress region of the plot shown in Figure 6. This is expected, since the measurements shown here in Figure 7 were also taken in a sampled section of the build.

The measurements performed on Sample A show a tensile residual stress in the x-z plane near the bottom of the build, while the measurements for Sample B show a compressive residual stress in the x-y plane near the top of the build. This discrepancy was assumed to be indicative of the original macroscopic residual stress distribution in the build wall. Measurement of this distribution was not within the scope of this study.

3.2 LIMITATIONS OF THE MICRO-SLOTTING TECHNIQUE

The primary disadvantage of the micro-slotting technique in this study was the associated limitation on sample size. Sample size was restricted by the SEM chamber, and it was therefore necessary to section small samples away from the original geometry in order to measure local residual stresses at the interfaces of interest. An assumption was made that the residual stress distributions present at these interfaces was not affected by the stress relief that occurred during sectioning. However, this assumption was not validated, and future studies should avoid sectioning, if possible.

Cross-section preparation of the samples was required in order to perform the measurements in the desired locations. This was assumed to result in complete relief of the out-of-plane residual stress component, thereby affecting the in-plane residual stress state.

Mathematical corrections [33] or FE analysis can be used to estimate the original residual stress present in the sample. The measurements presented in this study were not corrected for this effect.

An additional source of error in this study is the use of isotropic elastic constants for interpolation of residual stress in the micro-slot measurement regions. Correction for local modulus effects of the highly anisotropic Ti α phase [34] can be accomplished by performing EBSD in the micro-slot measurement regions to acquire grain orientation information [35]. Such data correction was not performed in this study due to the large number of micro-slotting measurements performed on each sample. However, the maximum effects of local anisotropy in the Ti α phase can be estimated using the single-crystal elastic properties [36]. The resultant error in the interpolated residual stress magnitudes, relative to the elastic properties used in this study, would range from ~25% underestimation to ~8% overestimation.

4. CONCLUSION

This study demonstrated the use of the micro-slotting technique for measurement of local residual stress in AM components. Spatially resolved residual stress data was acquired across two different interfaces in samples sectioned from a complex LFMT Ti-6Al-4V build. The build consisted of an oval-shaped thin wall structure and support stiffeners deposited on a baseplate of the same alloy. A series of micro-slotting residual stress measurements was performed across the desired interface on each sample, and the micro-slots were oriented to capture the residual hoop stress present in the thin wall. Post-measurement optical microscopy allowed for verification of the measurement locations

relative to the sample interfaces and analysis of the residual stress data at the microstructural level. The results of this study therefore emphasize the use of the micro-slotting technique for future studies that aim to understand residual stress origins in AM parts.

The first sample was acquired from the baseplate-build wall interface region. The micro-slotting measurements revealed a compressive residual stress region in the baseplate that transitioned to a tensile residual stress region at a depth of 0.7-0.8 mm below the top of the baseplate. Considerably less scatter was observed among the data points in the tensile portion of the residual stress profile, and a possible explanations for this observation is the increased microscopic residual stresses in the inherent baseplate microstructure. The second sample was a build wall-stiffener interface region that was acquired near the top of the build wall. The micro-slotting residual stress measurements revealed a compressive residual stress region in the build wall that was balanced by a region of tensile residual stress in the support stiffener. The transition between the compressive and tensile regions was shown to occur precisely at the build wall-stiffener interface.

ACKNOWLEDGMENTS

This work was funded by Boeing Research & Technology and is a collaborative research effort of Boeing and Missouri S&T. The authors wish to acknowledge both Nathan Ashmore and Justin L'Hote of Boeing Research & Technology for their guidance and for providing the samples used in this study.

REFERENCES

[1] RPM Innovations: Laser Freeform Manufacturing Technology (LFMT). http://www.rpm-innovations.com/laser_freeform_manufacturing_technology, 2014 (accessed 18 October 2018).

[2] T. DebRoy, H.L. Wei, J.S. Zuback, T. Mukherjee, J.W. Elmer, J.O. Milewski, A.M. Beese, A. Wilson-Heid, A. De, W. Zhang, Additive manufacturing of metallic components – Process, structure and properties, Prog Mater Sci 92 (2018) 112-224. https://doi.org/10.1016/j.pmatsci.2017.10.001

[3] E.R. Denlinger, P. Michaleris, Mitigation of distortion in large additive manufacturing parts, Proc. Inst. Mech. Eng. B J. Eng. Manuf. 231 (2015) 983-993. 10.1177/0954405415578580

[4] N.W. Klingbeil, J.L. Beuth, R.K. Chin, C.H. Amon, Residual stress-induced warping in direct metal solid freeform fabrication, Int. J. Mech. Sci. 44 (2002) 57-77. https://doi.org/10.1016/S0020-7403(01)00084-4

[5] T. Mukherjee, W. Zhang, T. DebRoy, An improved prediction of residual stresses and distortion in additive manufacturing, Comput. Mater. Sci. 126 (2017) 360-372. https://doi.org/10.1016/j.commatsci.2016.10.003

[6] S. Marimuthu, D. Clark, J. Allen, A.M. Kamara, P. Mativenga, L. Li, R. Scudamore, Finite element modelling of substrate thermal distortion in direct laser additive manufacture of an aero-engine component, Proc. Inst. Mech. Eng. C Mech. Eng. Sci. 227 (2013) 1987-1999. https://doi.org/10.1177/0954406212470363

[7] M.P. Mughal, H. Fawad, R.A. Mufti, Three-dimensional finite-element modelling of deformation in weld-based rapid prototyping, Proc. Inst. Mech. Eng. C Mech. Eng. Sci. 220 (2006) 875-885. https://doi.org/10.1243/09544062JMES164

[8] I.C. Noyan, J.B. Cohen, Residual stress: Measurement by Diffraction and Interpretation, Springer-Verlag, New York, 1987.

[9] M.T. Hutchings, P.J. Withers, T.M. Holden, T. Lorentzen, Introduction to the Characterization of Residual Stress by Neutron Diffraction, CRC Press, Boca Raton, FL, 2004.

[10] M.B. Prime, Cross-sectional mapping of residual stresses by measuring the surface contour after a cut. J. Eng. Mater. Technol. 123 (2001) 162-168. 10.1115/1.1345526

[11] G.S. Schajer, Practical residual stress measurement methods, John Wiley & Sons, Chichester, 2013.

[12] P. Rangaswamy, M.L. Griffith, M.B. Prime, T.M. Holden, R.B. Rogge, J.M. Edwards, R.J. Sebring, Residual stresses in LENS components using neutron diffraction and contour method. Mater. Sci. Eng. A Struct. Mater. 399 (2005) 72-83. https://doi.org/10.1016/j.msea.2005.02.019

[13] P. Rangaswamy, T.M. Holden, R.B. Rogge, M.L. Griffith, Residual stresses in components formed by the laser-engineered net shaping (LENS) process. J. Strain Anal. Eng. Des. 38 (2003) 519-527. https://doi.org/10.1243/030932403770735881

[14] B.A. Szost, S. Terzi, F. Martina, D. Boisselier, A. Prytuliak, T. Pirling, M. Hofmann, D.J. Jarvis, A comparative study of additive manufacturing techniques: Residual stress and microstructural analysis of CLAD and WAAM printed Ti-6Al-4V components. Mater. Des. 89 (2016) 559-567. https://doi.org/10.1016/j.matdes.2015.09.115

[15] E.R. Denlinger, J.C. Heigel, P. Michaleris, T.A. Palmer, Effect of inter-layer dwell time on distortion and residual stress in additive manufacturing of titanium and nickel alloys. J. Mater. Process. Technol. 215 (2015) 123-131. https://doi.org/10.1016/j.jmatprotec.2014.07.030

[16] P. Mercelis, J.P. Kruth, Residual stresses in selective laser sintering and selective laser melting. Rapid Prototyp. J. 12, 5 (2006) 254-265. https://doi.org/10.1108/13552540610707013

[17] R.J. Moat, A.J. Pinkerton, L. Li, P.J. Withers, M. Preuss, Residual stresses in laser direct metal deposited Waspaloy. Mater. Sci. Eng. A Struct. Mater. 528 (2011) 2288-2298. https://doi.org/10.1016/j.msea.2010.12.010

[18] L. Wang, S.D. Felicelli, P. Pratt, Residual stresses in LENS-deposited AISI 410 stainless steel plates. Mater. Sci. Eng. A Struct. Mater. 496 (2008) 234-241. https://doi.org/10.1016/j.msea.2008.05.044

[19] K.J. Kang, N. Yao, M.Y. He, A.G. Evans, A method for in situ measurement of the residual stress in thin films by using the focused ion beam, Thin Solid Films 443 (2003) 71-77. https://doi.org/10.1016/S0040-6090(03)00946-5

[20] N. Sabate, D. Vogel, A. Gollhardt, J. Keller, C. Cane, I. Gracia, J.R. Morante, B. Michel, Residual stress measurement on a MEMS structure with high-spatial resolution. J. Microelectromech. Syst. 17 (2007) 365-372. 10.1109/JMEMS.2006.879701

[21] A.M. Korsunsky, M. Sebastiani, E. Bemporad, Focused ion beam ring drilling for residual stress evaluation, Mater. Lett. 63 (2009) 1961-1963. https://doi.org/10.1016/j.matlet.2009.06.020

[22] A.J.G. Lunt, N. Baimpas, E. Salvati, I.P. Dolbya, T. Sui, S. Ying. H. Zhang, A.K. Kleppe, J. Dluhos, A.M. Korsunsky, A state-of-the-art review of micron-scale spatially resolved residual stress analysis by FIB-DIC ring-core milling and other techniques, J. Strain Anal. Eng. Des. 50 (2015) 426-444. https://doi.org/10.1177/0309324715596700

[23] E. Burns, J. Newkirk, J. Castle, Micro-slotting technique for reliable measurement of sub-surface residual stress in Ti-6Al-4V, J. Strain Anal. Eng. Des. 53 (2018) 389-399. https://doi.org/10.1177/0309324718778225

[24] I. Violatos, M. Thomas, J.B. Castle, B.P. Wynne, Sub-surface plastic and elastic strain fields and fatigue performance of drilled titanium plates, in: V. Venkatesh, A.L. Pilchak, J.E. Allison, S. Ankem, R.R. Boyer, J. Christodoulou, H.L. Fraser, M.A. Imam, Y. Kosaka, H.J. Rack, A. Chatterjee, A. Woodfield (Eds.), Proceedings of the 13th World Conference on Titanium, Wiley-TMS, New Jersey, 2015, pp. 1035-1040.

[25] B. Winiarski, M. Benedetti, V. Fontanari, et al. Comparative analysis of shot-peened residual stresses using micro-hole drilling, micro-slot cutting, X-ray diffraction methods and finite element modeling, in: S. Bossuyt, G. Schajer, A. Carpinteri (Eds.), Residual Stress, Thermomechanics & Infrared Imaging, Hybrid Techniques and Inverse Problems, Volume 9, Springer, New York, 2016, pp. 215-223. https://doi.org/10.1007/978-3-319-21765-9_27

[26] J. Everaerts, E. Salvati, F. Uzun, L.R. Brandt, H. Zhang, A.M. Korsunsky, Separating macro- (Type I) and micro- (Type II+III) residual stresses by ring-core FIB-DIC milling and eigenstrain modelling of a plastically bent titanium alloy bar, Acta Mater. 156 (2018) 43-51. https://doi.org/10.1016/j.actamat.2018.06.035

[27] E. Salvati, A.M. Korsunsky, An analysis of macro- and micro-scale residual stresses of Type I, II and III using FIB-DIC micro-ring-core milling and crystal plasticity FE modelling, Int. J. Plast. 98 (2017) 123-138. https://doi.org/10.1016/j.ijplas.2017.07.004

[28] J. Everaerts, X. Song, B. Nagarajan, A.M. Korsunsky, Evaluation of macro- and microscopic residual stresses in laser shock-peened titanium alloy by FIB-DIC ring-core milling with different core diameters, Surf. Coat. Technol. 349 (2018) 719-724. https://doi.org/10.1016/j.surfcoat.2018.06.043

[29] P.J. Withers, H.K.D.H. Bhadeshia, Residual stress: Part 1 – Measurement techniques, Mater. Sci. Technol. 17 (2001) 355-365. https://doi.org/10.1179/026708301101509980.

[30] E. Salvati, A.J.G. Lunt, S. Ying, T. Sui, H.J. Zhang, C. Heason, G. Baxter, A.M. Korsunsky, Eigenstrain reconstruction of residual strains in an additively manufactured and shot peened nickel superalloy compressor blade, Comput. Methods in Appl. Mech. Eng. 320 (2017) 335-351. https://doi.org/10.1016/j.cma.2017.03.005

[31] ASTM B265-15. Standard specification for titanium and titanium alloy strip, sheet and plate.

[32] MMPDS-12: Metallic Materials Properties Development and Standardization (MMPDS). Federal Aviation Administration, Washington, D.C., 2017.

[33] A. Lunt, E. Salvati, L. Ma, I.P. Dolbnya, T.K. Neo, A.M. Korsunsky, Full in-plane strain tensor analysis using the microscale ring-core FIB milling and DIC approach, J. Mech. Phys. Solids 94 (2016) 47-67. https://doi.org/10.1016/j.jmps.2016.03.013

[34] G. Lütjering, J.C. Williams, Titanium, Springer-Verlag, Berlin, 2007.

[35] E. Salvati, T. Sui, A.M. Korsunsky, Uncertainty quantification of residual stress evaluation by the FIB-DIC ring-core method due to elastic anisotropy effects. Int. J. Solids Struct. 87 (2016) 61–69. https://doi.org/10.1016/j.ijsolstr.2016.02.031

[36] D. Tromans, Elastic anisotropy of HCP metal crystals and polycrystals. Int. J. Res. Rev. Appl. Sci. 6 (2011) 462-483.

SECTION

3. CONCLUSIONS AND FUTURE WORK

In this research, a micro-slotting procedure was established and validated for capturing local residual stresses in complex-shaped Ti-6Al-4V components. First, FE models were used to determine the necessary spacing between sequentially milled slots and neighboring series of measurements to ensure minimal error, and this spacing was evaluated as a function of slot length and depth. A virtual sensitivity study using FE analysis was also performed in order to quantify the effect of slot geometry uncertainties on the residual stress measurements presented in this study. The established micro-slotting procedure was then used to measure sub-surface residual stresses on planar Ti-6Al-4V samples with both machined and shot peened surfaces. These measurements were compared to macro-scale XRD residual stress measurements, and discrepancies between the results were attributed to the more local nature of the micro-slotting technique. This successful application of the technique validated the established measurement procedure for use on more complex-shaped Ti-6Al-4V components where conventional XRD methods are not capable of measuring residual stress. The demonstrated use of FE models for optimizing the procedure and quantifying uncertainties showed the robustness of the technique, and such analyses can easily be repeated for altered slot sizes or different metallic alloys.

Next, the established procedure was used to demonstrate the unique application of the micro-slotting technique for measurement of near-edge tangential residual stresses around cold-expanded holes. The improved spatial resolution of the micro-slotting technique, in comparison to more established measurement methods, allowed for accurate

characterization of the near-edge residual stress state on both an as-drilled hole and a cold-expanded hole. Knowledge of these near-edge elastic strains induced by the hole processing, in combination with plastic strain information obtained from EBSD, allowed for interpretation of fatigue life differences and crack growth behavior between the as-drilled and cold-expanded conditions.

The effect of metallic microstructure on micro-slotting residual stress measurements was then addressed by milling a grid of smaller gauge volume micro-slots in a high magnitude residual stress sub-surface region of the shot peened planar Ti-6Al-4V sample. Micro-slots were milled both perpendicular and parallel to the shot peened surface for measurement of the two in-plane residual stress components. The macroscopic residual stress state in the grid region was estimated by averaging the micro-slotting measurements, and the average residual stress measured parallel to the shot peened surface was shown to be in close agreement with the macroscopic residual stress measured by XRD. Thus, the micro-slotting measurements were assumed to be accurate summations of the macroscopic and microscopic residual stresses present in the grid region. The presence of significant residual stress perpendicular to the shot peened surface suggested the presence of a shear stress component, and additional measurements were therefore performed in order to estimate the principal residual stress components and corresponding rotation within the grid region. The presence of this rotation was confirmed by the strain plots for the micro-slotting measurements. For each measurement region, plots of the displacement magnitudes and interpolated residual stresses were overlaid with local microstructure maps obtained using EBSD. This novel approach allowed for evaluation of microstructure effects on local residual stress relaxation and the corresponding errors in residual stress

interpolation associated with using the isotropic FE model. These effects included the calculated principal stress rotation as well as changes in residual stress approaching grain boundaries, elastic modulus differences in neighboring α grains, and constrained relaxation due to local phase distribution. However, the convolution of these effects in the complex microstructure measurement regions limited the observations in this study to those of a qualitative nature.

Finally, use of the micro-slotting technique was demonstrated for measuring local residual stress in AM components. Spatially resolved residual stress data was acquired across two different interfaces on samples sectioned from a complex LFMT Ti-6Al-4V build that consisted of an oval-shaped thin wall structure and support stiffeners deposited on a baseplate of the same alloy. The first sample was acquired from a baseplate-build wall interface region, and the second sample was acquired from a build wall-stiffener interface region near the top of the build. A series of measurements was performed across the desired interface on each sample with the micro-slots oriented to capture the residual hoop stress in the thin wall. Post-measurement optical microscopy allowed for verification of the measurement locations relative to the sample interfaces and analysis of the residual stress data at the microstructural level.

Overall, this research characterizes the micro-slotting technique as a valuable measurement capability for the metals and manufacturing community. This work meets the outlined objectives and thus establishes the micro-slotting technique as a robust and practical approach for measuring local residual stresses and providing supplemental data to conventional macro-scale techniques. Furthermore, this research successfully

demonstrates the use of the micro-slotting technique for metallic material applications for which there is a need for practical measurement of local residual stress.

Future work with the micro-slotting technique should investigate the relationship between metallic microstructure and measurement gauge volume for reliable measurement of both macroscopic and microscopic residual stresses. The results shown in this work illustrate the significant effects of microscopic residual stresses on micro-slotting measurements of the macroscopic residual stress state, and these effects appear as significant scatter in the data plots. However, averaging the measurements was shown to give an average value comparable to the macroscopic residual stress measured by XRD. This is understood to be a result of increasing the effective volume of the micro-slotting measurements. As the measurement gauge volume is increased, the elastic properties and characteristic microstructure of the measurement region approach those of the bulk material. Therefore, as the micro-slot gauge volume is increased, the microstructure effects on the measurement of the macroscopic residual stress state are minimized. This suggests the existence of an ideal slot size relative to the grain size of the metallic material. Alternatively, an effective volume approach could be employed in cases where the micro-slot volume is limited by the slot length in order to maintain high spatial resolution. Multiple measurements could be performed at a specific distance from the part surface or feature of interest, and a statistical average could be assumed to represent the macroscopic stress state. The total effective measurement volume would be the product of the chosen micro-slot gauge volume and the number of measurements, and this volume would correlate to the characteristic microstructure of the material. Investigating this relationship between metallic microstructure and micro-slotting measurement gauge volume may be

best accomplished using a variety of metallic alloys for increased range of grain size and phase distribution.

On the other hand, decreasing the gauge volume of the micro-slotting measurements relative to the grain size of the material may also prove useful. A smaller micro-slot gauge volume may be a more ideal approach for isolating and accurately quantifying the different sources of microscopic residual stresses in metallic materials. Application of smaller micro-slots to AM materials, for instance, may allow for characterization of residual stress distributions within tracks or layers as a function of build process parameters. Such analyses may provide an improved understanding of residual stress development in additive manufacturing processes.

BIBLIOGRAPHY

[1] P.J. Withers, "Residual stress and its role in failure," *Reports on Progress in Physics* 70 (2007) 2211-2264.

[2] G. Schajer, *Practical Residual Stress Measurement Methods*, John Wiley & Sons, Chichester (2013).

[3] K.J. Kang, N. Yao, M.Y. He, A.G. Evans, "A method for in situ measurement of the residual stress in thin films by using the focused ion beam," *Thin Solid Films* 443 (2003) 71-77.

[4] B. Winiarski, A. Gholinia, J. Tian, Y. Yokoyama, P.K. Liaw, P.J. Withers, "Submicron-scale depth profiling of residual stress in amorphous materials by incremental focused ion beam slotting," *Acta Materialia* 60 (2012) 2337-2349.

[5] B. Winiarski, M. Benedetti, V. Fontanari, M. Allahkarami, J.C. Hanan, G.S. Schajer, P.J. Withers, "Comparative analysis of shot-peened residual stresses using micro-hole drilling, micro-slot cutting, X-ray diffraction methods and finite-element modelling," In: S. Bossuyt, G. Schajer, A. Carpinteri (Eds.), *Residual Stress, Thermomechanics & Infrared Imaging, Hybrid Techniques and Inverse Problems, Volume 9*, Springer, New York (2016) 215-223.

[6] E. Salvati, T. Sui, A.M. Korsunsky, "Uncertainty quantification of residual stress evaluation by the FIB-DIC ring-core method due to elastic anisotropy effects," *International Journal of Solids and Structures* 87 (2016) 61-69.

[7] I. Violatos, M. Thomas, J.B. Castle, B.P. Wynne, "Sub-surface plastic and elastic strain fields and fatigue performance of drilled titanium plates," In: V. Venkatesh, A.L. Pilchak, J.E. Allison, S. Ankem, R.R. Boyer, J. Christodoulou, H.L. Fraser, M.A. Imam, Y. Kosaka, H.J. Rack, A. Chatterjee, A. Woodfield (Eds.), *Proceedings of the 13th World Conference on Titanium*, Wiley-TMS, New Jersey (2015) 1035-1040.

[8] D.L. Rich, L.F. Impellizzeri, "Fatigue analysis of cold worked and interference fit fastener holes, cyclic stress-strain and plastic deformation aspect of fatigue crack growth," *ASTM STP* 637, American Society for Testing and Materials (1977) 153-175.

[9] T.N. Chakherlou, J. Vogwell, "The effect of cold expansion on improving the fatigue life of fastener holes," *Engineering Failure Analysis* 10 (2003) 133-124.

[10] J.L. Phillips, "Sleeve Coldworking Fastener Holes," Tech. Rep. AFML-TR-74-10, Air Force Materials Lab, Wright-Patterson AFB (1974).

[11] J. Everaerts, E. Salvati, F. Uzun, L.R. Brandt, H. Zhang, A.M. Korsunsky, "Separating macro- (Type I) and micro- (Type II+III) residual stresses by ring-core FIB-DIC milling and eigenstrain modelling of a plastically bent titanium alloy bar," *Acta Materialia* 156 (2018) 43-51.

[12] J. Everaerts, X. Song, B. Nagarajan, A.M. Korsunsky, "Evaluation of macro- and microscopic residual stresses in laser shock-peened titanium alloy by FIB-DIC ring-core milling and different core diameters," *Surface and Coatings Technology* 349 (2018) 719-724.

[13] I. Basu, V. Ocelik, J.T.M. De Hosson, "Experimental determination and theoretical analysis of local residual stress at grain scale," In: D. Northwood, T. Rang, J. De Hosson, C.A. Brebbia (Eds.), *WIT Transactions in Engineering Sciences, Vol. 116*, WIT Press, Southampton (2017) 3-14.

[14] E. Salvati, A.M. Korsunsky, "An analysis of macro- and micro-scale residual stresses of Type I, II and III using FIB-DIC micro-ring-core milling and crystal plasticity FE modelling," *International Journal of Plasticity* 98 (2017) 123-138.

[15] E.R. Denlinger, P. Michaleris, "Mitigation of distortion in large additive manufacturing parts," *Proceedings of the Institution of Mechanical Engineers, Part B: Journal of Engineering Manufacture* 231 (2015) 983-993.

[16] P. Rangaswamy, M.L. Griffith, M.B. Prime, T.M. Holden, R.B. Rogge, J.M. Edwards, R.J. Sebring, "Residual stresses in LENS components using neutron diffraction and contour method," *Materials Science & Engineering A* 399 (2005) 72-83.

[17] P. Rangaswamy, T.M. Holden, R.B. Rogge, M.L. Griffith, "Residual stresses in components formed by the laser-engineered net shaping (LENS) process," *The Journal of Strain Analysis for Engineering Design* 38 (2003) 519-527.

[18] P.J. Withers, H.K.D.H. Bhadeshia, "Residual stress: Part 2 – Nature and origins," *Materials Science and Technology* 17 (2001) 366-375.

[19] A. Korsunsky, *A Teaching Essay on Residual Stresses and Eigenstrains*, Butterworth-Heinemann, Oxford (2017).

[20] P.J. Withers, H.K.D.H. Bhadeshia, "Residual stress: Part 1 – Measurement techniques," *Materials Science and Technology* 17 (2001) 355-365.

[21] E. Macherauch, "Residual stresses," In: G.C. Sih, E. Sommer, W. Dahl (Eds.) *Application of Fracture Mechanics to Materials and Structures*, Springer Netherlands, Dordrecht (1984) 157-192.

[22] S. Suresh, *Fatigue of Materials*, Cambridge University Press, Cambridge (1998).

[23] W. Schultz, "Shot peening of components to improve fatigue strength," *Proceedings of the Third International Conference on Shot Peening (ICSP-3),* Garmisch-Partenkichen, Germany (1987).

[24] M. Kobayashia, T. Matsuia, Y. Murakamib, "Mechanism of creation of compressive residual stress by shot peening," *International Journal of Fatigue* 20 (1998) 351-357.

[25] E.R. de los Rios, A. Walley, M.T. Milan, G. Hammersley, "Fatigue crack initiation and propagation on shot-peened surfaces in A316 stainless steel," *International Journal of Fatigue* 17 (1995) 493-499.

[26] A. Leon, "Benefits of split mandrel coldworking," *International Journal of Fatigue* 20 (1998) 1-8.

[27] D.L. Ball, D.R. Lowry, "Experimental investigation on the effects of cold expansion of fastener holes," *Fatigue & Fracture of Engineering Materials & Structures* 21 (1998) 17-34.

[28] A. Amrouche, G. Mesmacque, S. Garcia, A. Talha, "Cold expansion effect on the initiation and the propagation of the fatigue crack," *International Journal of Fatigue* 25 (2003) 949-954.

[29] J. Liu (Ed.), *Handbook of Measurement of Residual Stresses*, Society for Experimental Mechanics, USA (1996).

[30] G. Schajer, "Relaxation methods for measuring residual stresses: techniques and opportunities," *Experimental Mechanics* 50 (2010) 1117-1127.

[31] M. Prime, "Residual stress measurement by successive extension of a slot: the crack compliance method," *Applied Mechanics Reviews* 52 (1999) 75-96.

[32] I.F.W. Cheng, *Residual Stress Measurement and the Slitting Method*, Springer, New York (2007).

[33] J. Mathar, "Determination of initial stresses by measuring the deformations around drilled holes," *Transactions of ASME* 56 (1934) 249-254.

[34] R.V.W. Soete, "An industrial method for the determination of residual stresses," *Proceedings of SESA* 8 (1950) 17-28.

[35] N.J. Rendler, I. Vigness, "Hole-drilling strain-gage method of measuring residual stresses," *Experimental Mechanics* 6 (1966) 577-586.

[36] ASTM E837-13a, "Standard Test Method for Determining Residual Stresses by the Hole-Drilling Strain-Gage Method," ASTM International (2013).

[37] M. Prime, "Cross-sectional mapping of residual stresses by measuring the surface contour after a cut," *Journal of Engineering Materials and Technology* 123 (2001) 162-168.

[38] P. Pagliaro, M.B. Prime, H. Swenson, B. Zuccarello, "Measuring multiple residual-stress components using the contour method and multiple cuts," *Experimental Mechanics* 50 (2010) 187-194.

[39] B. Cullity, *Elements of X-ray Diffraction*, 3rd edition, Prentice Hall, New Jersey (2001).

[40] G.A. Webster, R.C. Wimpory, "Development of procedures for the measurement of residual stress by neutron diffraction," *Applied Physics A* 74 (2002) 1227-1229.

[41] M.T. Hutchings, P.J. Withers, T.M. Holden, T. Lorentzen, *Introduction to the Characterization of Residual Stress by Neutron Diffraction*, CRC Press, Boca Raton (2004).

[42] J.S. Chung, G.E. Ice, "Automated indexing for texture and strain measurement with broad-bandpass x-ray microbeams," *Journal of Applied Physics* 86 (1999) 5249-5255.

[43] A.J.G. Lunt, N. Baimpas, E. Salvati, I.P. Dolbnya, T. Sui, S. Ying, H. Zhang, A.K. Kleppe, J. Dluhos, A.M. Korsunsky, "A state-of-the-art review of micron-scale spatially resolved residual stress analysis by FIB-DIC ring-core milling and other techniques," *The Journal of Strain Analysis for Engineering Design* 50 (2015) 1-19.

[44] A.J. Wilkinson, G. Meaden, D.J. Dingley, "High-resolution elastic strain measurement from electron backscatter diffraction patterns: new levels of sensitivity," *Ultramicroscopy* 106 (2006) 307-313.

[45] A. Lunt, A. Korsunsky, "A review of micro-scale focused ion beam milling and digital image correlation analysis for residual stress evaluation and error estimation," *Surface and Coatings Technology* 283 (2015) 373-388.

[46] N. Sabate, D. Vogel, A. Gollhardt, J. Keller, C. Cane, I. Gracia, J.R. Morante, B. Michel, "Residual stress measurement on a MEMS structure with high-spatial resolution," *Journal of Microelectromechanical Systems* 17 (2007) 365-372.

[47] A.M. Korsunsky, M. Sebastiani, E. Bemporad, "Focused ion beam ring drilling for residual stress evaluation," *Materials Letters* 63 (2009) 1961-1963.

[48] A. Lunt, E. Salvati, L. Ma, I.P. Dolbnya, T.K. Neo, A.M. Korsunsky, "Full in-plane strain tensor analysis using the microscale ring-core FIB milling and DIC approach," *Journal of the Mechanics and Physics of Solids* 94 (2016) 47-67.

[49] N. Sabate, D. Vogel, A. Gollhardt, J. Marcos, I. Gracia, C. Cane, B. Michel, "Digital image correlation of nanoscale deformation fields for local stress measurement in thin films," *Nanotechnology* 17 (2006) 5264-5270.

[50] B. Winiarski, R.M. Langford, J. Tian, Y. Yokoyama, P.K. Liaw, P.J. Withers, "Mapping residual stress distributions at the micron scale in amorphous materials," *Metallurgical and Materials Transactions A* 41 (2010) 1743-1751.

[51] K.J. Kang, S. Darzens, G.S. Choi, "Effect of geometry and materials on residual stress measurement in thin films by using the focused ion beam," *Journal of Engineering Materials and Technology* 126 (2004) 457-464.

[52] B. Winiarski, A. Gholinia, J. Tian, Y. Yokoyama, P.K. Liaw, P.J. Withers, "Submicron-scale depth profiling of residual stress in amorphous materials by incremental focused ion beam slotting," *Acta Materialia* 60 (2012) 2337-2349.

[53] C. Mansilla, D. Martinez-Martinez, V. Ocelik, J. Th. M. De Hosson, "On the determination of local residual stress gradients by the slit milling method," *Journal of Materials Science* 50 (2015) 3646-3655.

[54] E. Burns, J. Newkirk, J. Castle, "Micro-slotting technique for reliable measurement of sub-surface residual stress in Ti-6Al-4V," *The Journal of Strain Analysis for Engineering Design* 53 (2018) 389-399.

[55] J. Castle, "Drilling Induced Fatigue Damage in Ti-6Al-4V," Ph.D. Thesis, Washington University in St. Louis (2010).

[56] L. Reid, "Incorporating hole cold expansion to meet durability and damage tolerance airworthiness objectives," SAE Paper No. 972624, SAE International (1997).

[57] I.C. Noyan, J.B. Cohen, *Residual Stress: Measurement by Diffraction and Interpretation*, Springer-Verlag, New York (1987).

[58] G. Dietrich, J.M. Potter, "Stress measurements on cold-worked fastener holes," *Advances in X-Ray Analysis* 20 (1977) 321-328.

[59] R. Cook, P. Holdway, "Residual stresses induced by hole cold expansion," In: M.H. Aliabadi, C.A. Brebbia (Eds.), *Computer Methods and Experimental Measurements for Surface Treatment Effects*, Computational Mechanics Publications (1993) 91-100.

[60] L. Edwards, D.Q. Wang, "Neutron diffraction determination of the complete 3D residual stress distribution surrounding a cold-expanded hole," In: S. Denis (Ed.), *Proceedings of the 4th European Conference on Residual Stresses, Vol. 2*, Societe Francaise de Metallurgie et de Materiaux, Bourgogne (1998) 619-626.

[61] R. Hermann, "Three-dimensional stress distribution around cold expanded holes in aluminium alloys," *Engineering Fracture Mechanics* 48 (1994) 819-835.

[62] Y. Zhang, M. Fitzpatrick, L. Edwards, "Measurement of the residual stresses around a cold expanded hole in an EN8 steel plate using the contour method," *Materials Science Forum* 404-407 (2002) 527-534.

[63] D. Herzog, V. Seyda, E. Wycisk, C. Emmelmann, "Additive manufacturing of metals," *Acta Materialia* (2016) 371-392.

[64] T. DebRoy, H.L. Wei, J.S. Zuback, T. Mukherjee, J.W. Elmer, J.O. Milewski, A.M. Beese, A. Wilson-Heid, A. De, W. Zhang, "Additive manufacturing of metallic components – process, structure and properties," *Progress in Materials Science* 92 (2018) 112-224.

[65] E.R. Denlinger, P. Michaleris, "Mitigation of distortion in large additive manufacturing parts," *Proceedings of the Institution of Mechanical Engineers, Part B: Journal of Engineering Manufacture* 231 (2015) 983-993.

[66] N.W. Klingbeil, J.L. Beuth, R.K. Chin, C.H. Amon, "Residual stress-induced warping in direct metal solid freeform fabrication," *International Journal of Mechanical Sciences* 44 (2002) 57-77.

[67] T. Mukherjee, W. Zhang, T. DebRoy, "An improved prediction of residual stresses and distortion in additive manufacturing," *Computational Materials Science* 126 (2017) 360-372.

[68] S. Marimuthu, D. Clark, J. Allen, A.M. Kamara, P. Mativenga, L. Li, R. Scudamore, "Finite element modelling of substrate thermal distortion in direct laser additive manufacture of an aero-engine component," *Proceedings of the Institution of Mechanical Engineers, Part C: Journal of Mechanical Engineering Science* 227 (2013) 1987-1999.

[69] M.P. Mughal, H. Fawad, R.A. Mufti, "Three-dimensional finite-element modelling of deformation in weld-based rapid prototyping," *Proceedings of the Institution of Mechanical Engineers, Part C: Journal of Mechanical Engineering Science* 220 (2006) 875-885.

[70] B.A. Szost, S. Terzi, F. Martina, D. Boisselier, A. Prytuliak, T. Pirling, M. Hofmann, D.J. Jarvis, "A comparative study of additive manufacturing techniques: residual stress and microstructural analysis of CLAD and WAAM printed Ti-6Al-4V components," *Materials and Design* 89 (2016) 559-567.

[71] E.R. Denlinger, J.C. Heigel, P. Michaleris, T.A. Palmer, "Effect of inter-layer dwell time on distortion and residual stress in additive manufacturing of titanium and nickel alloys," *Journal of Materials Processing Technology* 215 (2015) 123-131.

[72] P. Mercelis, J.P. Kruth, "Residual stresses in selective laser sintering and selective laser melting," *Rapid Prototyping Journal* 12 (2006) 254-265.

[73] J. Moat, A.J. Pinkerton, L. Li, P.J. Withers, M. Preuss, "Residual stresses in laser direct metal deposited Waspaloy," *Materials Science and Engineering A* 528 (2011) 2288-2298.

[74] L. Wang, S.D. Felicelli, P. Pratt, "Residual stresses in LENS-deposited AISI 410 stainless steel plates," *Materials Science and Engineering A* 496 (2008) 234-241.

[75] E. Salvati, A.J.G. Lunt, S. Ying, T. Sui, H.J. Zhang, C. Heason, G. Baxter, A.M. Korsunsky, "Eigenstrain reconstruction of residual strains in an additively manufactured and shot peened nickel superalloy compressor blade," *Computer Methods in Applied Mechanics and Engineering* 320 (2017) 335-351.

[76] V.A. Safronov, R.S. Khmyrov, D.V. Kotoban, A.V. Gusarov, "Distortions and residual stresses at layer-by-layer additive manufacturing by fusion," *Journal of Manufacturing Science and Engineering* 139 (2017) 031017-031017-6.

VITA

Elizabeth Anne Burns was born in 1993 in St. Louis, Missouri. After completing high school at St. Joseph's Academy in May 2011, she attended Missouri University of Science and Technology in Rolla, MO where she received her B.S. in Metallurgical Engineering in May 2015. Upon graduation, she continued her graduate studies at Missouri University of Science and Technology under joint government and industry funding through an Air Force Research Lab (AFRL)-managed Metals Affordability Initiative (MAI) consortium project awarded to Boeing Research & Technology. She received her Ph.D. in Metallurgical Engineering from Missouri University of Science and Technology in December 2018 under the advisement of Dr. Joseph Newkirk.